FECHNER DAY 2017

Conference Proceedings

The 33rd Annual Meeting of the International Society for Psychophysics

Sunday to Thursday, 22–26 October 2017

Kyōsō-kan and Hon-kan, Denki Building, Fukuoka, Japan

Organized by

Research Center for Applied Perceptual Science (ReCAPS)
Kyushu University

ReCAPS

Sponsored by

FCVB 公益財団法人 福岡観光コンベンションビューロー
Fukuoka Convention & Visitors Bureau

KYUSHU
UNIVERSITY

Proceedings of the 33rd Annual Meeting of the International Society for Psychophysics

Fechner Day 2017

Fukuoka, Japan
22–26 October 2017

How to cite this book: Kazuo Ueda, Hiroyuki Ito, Gerard B. Remijn, and Yoshitaka Nakajima (Eds.) *Fechner Day 2017: Proceedings of the 33rd Annual Meeting of the International Society for Psychophysics.* International Society for Psychophysics, Fukuoka, Japan, 2017.

Distribution: International Society for Psychophysics, c/o Kazuo Ueda, Department of Human Science, Kyushu University, 4-9-1 Shiobaru Minami-ku, Fukuoka 815-8540, Japan.

LaTeX typeset by Kazuo Ueda.

Printed by Kijima Printing Inc., 2-9-6 Shirogane, Chuo-ku, Fukuoka-shi, Fukuoka 810-0012, Japan.

Part XI
Free Talk Session 6

TEMPORAL ENSEMBLE CODING OF SUB-SECOND AUDITORY BEEPS: AN MEG STUDY

Lu Guo and Ming Bao
Key Laboratory of Noise and Vibration Research, Institute of Acoustics
Chinese Academy of Sciences, Beijing 100190, China
University of Chinese Academy of Sciences, Beijing 100049, China

Lihan Chen
School of Psychological and Cognitive Sciences and Beijing Key Laboratory of Behavior and Mental Health, Peking University, Beijing 100871, China
Key Laboratory of Machine Perception, Peking University, Beijing 100871, China

<baoming@mail.ioa.ac.cn, clh20000@gmail.com>

Abstract

The ability to encode the temporal sensory events is fundamental for adaptive behavior. The present study examined the temporal ensemble coding towards a sequence of sound beeps containing multiple sub-second inter-intervals, with psychophysics and Magnetoencephalography (MEG) recording. Immediately after hearing a sound sequence (6 sounds, with mean inter-interval 600 ms), participants produced time interval which was half, equal, or double of the mean auditory inter-interval (600 ms). Participants showed a general over-estimation of the mean interval, and they produced time interval more accurately for the "double" condition. Moreover, analysis of the auditory evoked component revealed that the M100 amplitude, evoked by the final tone of the preceding sequence, increased in the "half" condition, suggesting that it is task-demanding to segment short time intervals.

Human beings have fascinating abilities to perceive averaging sensory properties of objects and construct statistical representations over various dimensions (Ward et al., 2016). Studies have shown that observers were able to report statistical summaries of properties ranging from motion direction (Dakin and Watt, 1997), size (Chong and Treisman, 2003), to facial identity (de Fockert and Wolfenstein, 2009) and emotion (Haberman and Whitney, 2007). However, these studies were limited to statistical properties of visual stimuli. Later, Albrecht, Scholl, and Chun (2012) explored statistical summarizing in audition with an averaging pitch from a sequence of tones, and the results illustrated that the perceptual averaging could span different sensory modalities and occur efficiently over temporal sequences.

The ability to encode the temporal sensory events and estimate motor-sensory time intervals in sub-second range is fundamental for adaptive behavior (Acerbi et al., 2012; Hellström and Rammsayer, 2004). To our best knowledge, however, few studies have focused on the ensemble coding (i.e., "perceptual averaging") of time interval. To explore how this process operates on a sequence of sound beeps, the present article used psychophysics and Magnetoencephalograph (MEG) recordings to investigate the statistical summarizing in auditory interval duration. By forming the ensemble representation of the temporal information within multiple beeps, human observers could overcome the information overload in otherwise complex acoustic scenes, and use the "averaged" temporal information to predict the target events (Albrecht et al., 2012).

Specifically, we utilized an interval production task, in which participants were required to produce half, equal or double of the mean inter-interval among multiple beeps

in a sound sequence, with either a regular or irregular rhythm (different temporal contexts). This experimental design allowed us to test whether individuals could perceive and estimate the average duration of the inter-intervals in the auditory sequence, and how the processing magnitude in temporal domain for the "half", "equal", and "double" estimation were implemented. The results indicated a general over-estimation of the mean interval. M100 amplitude evoked by the final tone of the sequence increased in the "half" condition, showing a demanding task to segment time interval in short range.

Method

Participants

Eight undergraduate and graduate students (4 males; M_{age} = 22.38 years; SD = 2.83 years; age range: 18–25 years) completed the experiments after providing written informed consent and received monetary compensation for their participation. All participants were right-handed, with normal or corrected-to-normal vision and normal hearing. None of participants had a history of psychological or neurological disorders.

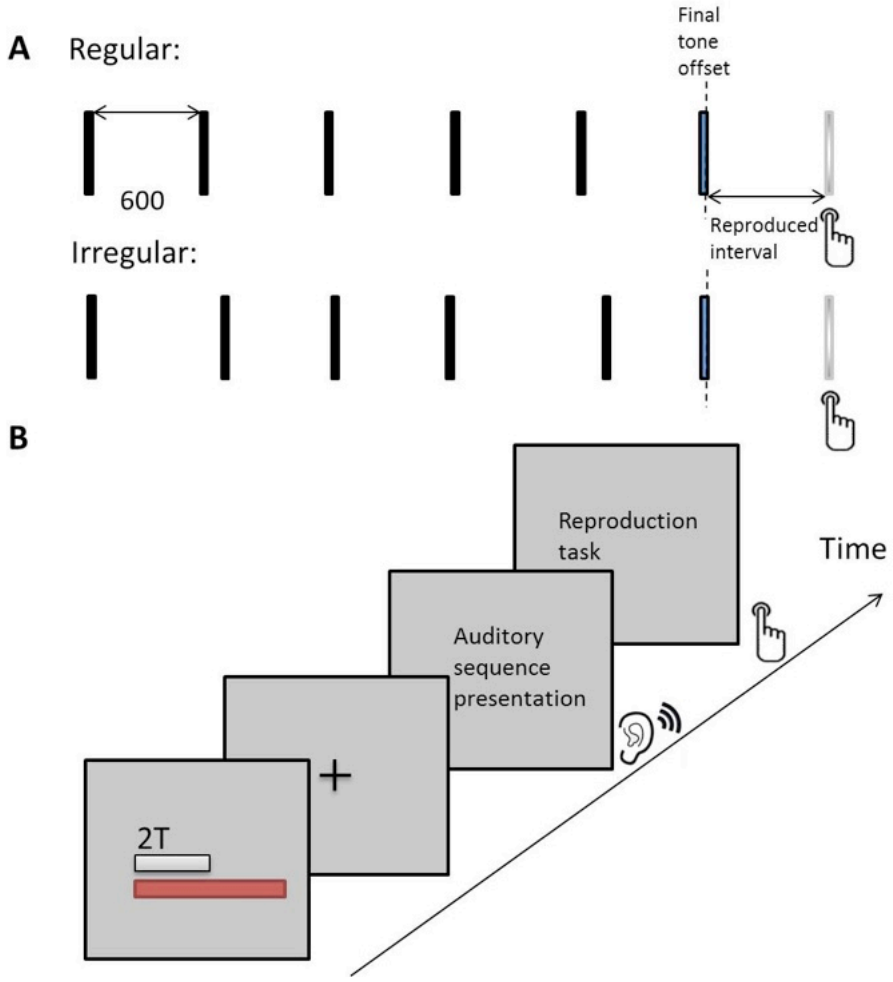

Fig. 1. (A) Schematic representation of the stimuli. The experiment contained two types of stimuli: Regular and irregular sequences. The mean duration of the inter-intervals in both sequence types was set to 600 ms. (B) Time course of a sample trial.

Stimuli and Apparatus

The auditory stimuli were sequences consisting of six 30-ms tones, which were separated by five intervals of either a fixed duration (600 ms) ("regular" sequence) or random intervals between 480 and 720 ms ("irregular" sequence), but the mean interval was 600 ms (Fig. 1A). The frequency of the first five tones was maintained at 1000 Hz, while the last tone changed to 500 Hz, so that it distinguished from the previous five beeps. Moreover, to avoid a repetitive motor response pattern from the participants when reproducing intervals, jitter stimuli consisting of five or seven pure tones were randomly presented in catch trials.

In the experiment, before the sound sequence occurring in each trial, participants were informed of the task conditions with a visual cue. It was composed of two bars, and the ratio of the two in length was set to 2:1, 1:1, or 1:2, to indicate the task of producing the "half", "equal", or "double" of the mean interval of the multiple inter-intervals. Correspondingly, labels of "1/2 T", "1 T", or "2T" were given on the top of the two bars, with "T" referring to the mean interval duration of the subsequent sound sequence.

The computer programs for controlling the experiment were developed with MATLAB (MathWorks Inc.) and the Psychophysics Toolbox (Brainard, 1997; Pelli, 1997). The auditory stimuli were generated by a sound card (RME Fireface UFX), delivered binaurally with a tube phone attached to ear plugs inserted into the ear canal, and presented at a comfortable listening level adjusted individually for each participant. Visual stimuli were presented to the participants with a viewing distance of approximately 60 cm, on the center of a LCD screen (100 Hz refresh rate; 1024 × 768 pixel resolution) with a gray background (10.6 cd/m^2 in luminance)

MEG Recording

Neuromagnetic signals were recorded through the Vectorview TM whole-head MEG system (Elekta-Neuromag, Helsinki, Finland) with 306 MEG channels in a magnetically shielded room. MEG data were acquired continuously at a sampling rate of 1000 Hz with participants in seating position.

Design and Procedures

A 2 (auditory sequence: regular, irregular) × 3 (tasks: half, equal, or double) factorial design was implemented in the experiment. There were 5 acquisition runs per participant in the MEG scans. During each run, each experimental condition had 12 trials in succession: 10 trials with the auditory sequence consisting of 6 sound beeps, and the remaining 2 catch trials with jitter stimuli. The presentation order of the experimental conditions within each run was randomized for each participant. Totally, there were 360 trials, 60 repetitions of each of the 6 conditions. Short breaks of 2–3 min were provided after every run.

As shown in Figure 1B, a typical trial in the main experiment started with a visual cue on the monitor lasting for 2800 ms to inform participants of the task conditions. Then a fixation cross appeared at the center of the monitor, with a random duration of 300 - 500 ms. After a blank interval of 100 ms, the auditory stimulus appeared. The sequence began with a standard 30-ms tone (1000 Hz) and ended with a 30-ms target

tone (500 Hz). For the regular sequence, the duration of the silent interval was set to 600 ms. For the irregular sequence, it was randomized between 480 and 720 ms. Upon offset of the target tone, participants produced half, equal or double times of the mean auditory inter-intervals in the preceding sequence, by pressing the button "8" with their right index fingers to terminate the estimated duration. Therefore, the duration between offset of the target and the onset of the keypress was the produced subjective interval.

Behavioral Data Analysis

We only focused on the interval reproduction for the auditory sequence consisting of six beeps in the experiment, and trials in which the reproduced interval deviated more than 3 standard deviations from the mean were removed. Then we calculated the mean values of the duration and the Weber fraction (the percentage of duration difference between the reproduced interval and accurate average interval) of the reproduced intervals for each participant and for each experimental condition. For these obtained data, we conducted a repeated measures of ANOVA with temporal rhythms of the sequence (regular, irregular) and tasks (half, equal, and double) as within-participants factors, which were followed by (Bonferroni corrected) post hoc analyses to assess any significant main effects.

Analysis of Event-Related Fields (Sensor Level)

The evoked response analysis was time locked to the onset of the final tone of the sequence. The analysis epochs were 650 ms in total duration, including a 100 ms pre-onset period. The data were baseline corrected to the -100 to -1 ms pre-onset time-window and low-pass filtered at 40Hz. Electrooculographic (EOG) and electrocardiographic (ECG) trace were chosen to be removed from the data.

As we were primarily interested in auditory cortical responses to target sounds (final tones in the sequences), we selected the 78 channels positioned over the estimated location of the auditory cortices in both hemispheres, to examine the 100 msec post-stimulus (M100) responses and further reveal the underlying brain activity in the auditory system. The root mean square (RMS) of the field strength across 78 channels was calculated at each sample point for each condition and participant, and the M100 peak was determined as the peak RMS value in the interval 85–115 ms. For illustration purposes, the group-RMS (RMS of the individual participants' RMSs) time series was plotted (Fig. 3A). However, statistical analysis was always performed on the peak RMS values extracted from each participant's data.

Results and Discussion

Extraction of Statistical Summary in Time Dimension

For the mean durations (Fig. 2A), the main effect of tasks was significant, $F(2, 14) = 164.861, p < 0.001, \eta_p^2 = 0.959$. Bonferroni corrected comparison revealed significant differences of the mean durations between "half" (522.2 ms), "equal" (804.3 ms), "double" (1363.3 ms) conditions, all $ps < 0.001$. The main effect of rhythms of the sequence was marginally significant, $F(1, 7) = 4.423, p = 0.074, \eta_p^2 = 0.387$, with the mean duration for regular sequences (875.3 ms) shorter than that for irregular sequences (917.9 ms). The interaction effect between rhythms and tasks was not significant, $F(2, 14) = 0.261, p =$

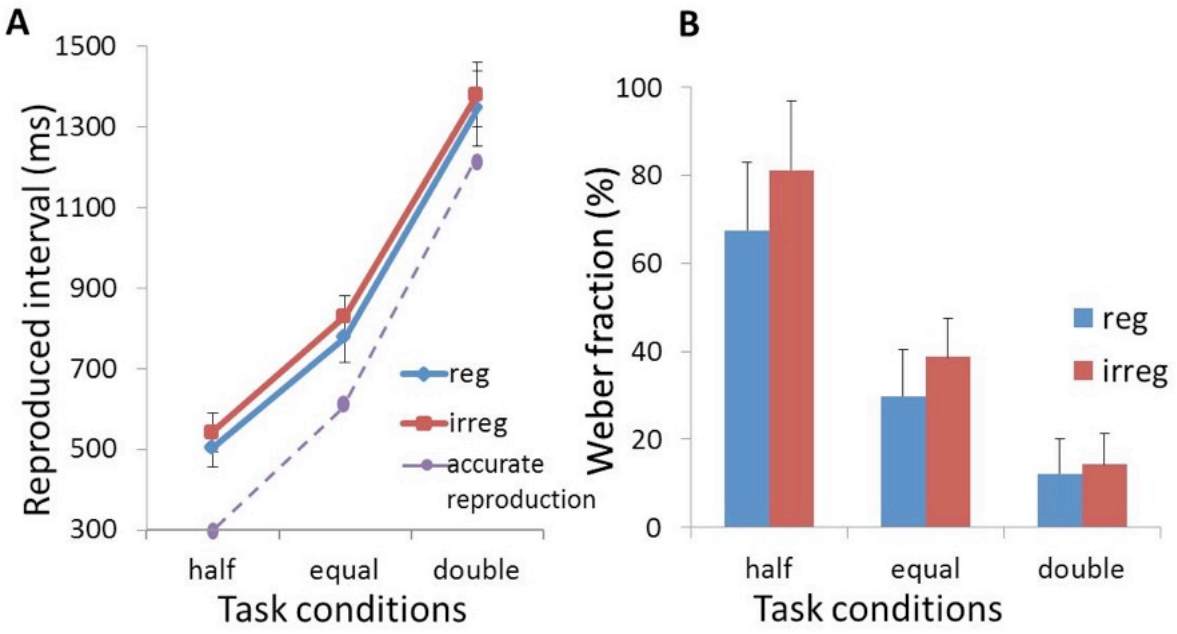

Fig. 2. Group means of the duration and the Weber fraction of the reproduced intervals in different conditions. All the error bars show the associated standard errors of the means.

$0.774, \eta_p^2 = 0.036$. In general, participants performed well in different averaging tasks, resulting in the clearly distinguishable estimated durations from "half", "equal", and "double" conditions. Importantly, this result showed a general over-estimation of the mean interval of the sequence.

For the Weber fractions (Fig. 2B), ANOVA results revealed a significant main effect of rhythms of sequences, $F(1,7) = 6.149, p < 0.05, \eta_p^2 = 0.468$, and also a significant main effect of tasks, $F(2,14) = 22.135, p < 0.001, \eta_p^2 = 0.760$. No significant interaction effect between rhythms and tasks was found, $F(2,14) = 2.976, p = 0.085, \eta_p^2 = 0.298$. Bonferroni corrected comparison showed that the Weber fraction for irregular sequences (44.7%) was significant larger than that for regular sequences (36.5%), $ps < 0.05$. Pairwise comparison also revealed significant differences in the Weber fractions between "half" (74.3%), "equal" (34.3%), "double" (13.3%) conditions, all $ps < 0.05$. The results indicated that participants performed poorly on the inter-interval averaging task for the irregular sequence, which could be attributed to the non-isochronous auditory rhythm. Compared with the "equal" and "double" conditions, the significantly larger Weber fraction in "half" condition may suggest a demanding task to segment time interval in finer scale.

Temporal Encoding: Featured in the M100 amplitudes

ANOVA of M100 peaks evoked by the final tone of the sequence showed that the main effect of tasks was significant, $F(2,14) = 3.92, p < 0.05, \eta_p^2 = 0.359$. However, no significant main effect of the rhythm was found, $F(1,7) = 0.038, p = 0.851, \eta_p^2 = 0.005$, neither the interaction between the two factors, $F(2,14) = 1.058, p = 0.373, \eta_p^2 = 0.131$. Bonferroni corrected comparison revealed that the M100 peak amplitude in "half" condition (225.8 fT) was statistically higher than that in "double" condition (212.2 fT), $ps < 0.05$. The amplitude in "equal" condition (221.1 fT) was statistically equated with those in "half"

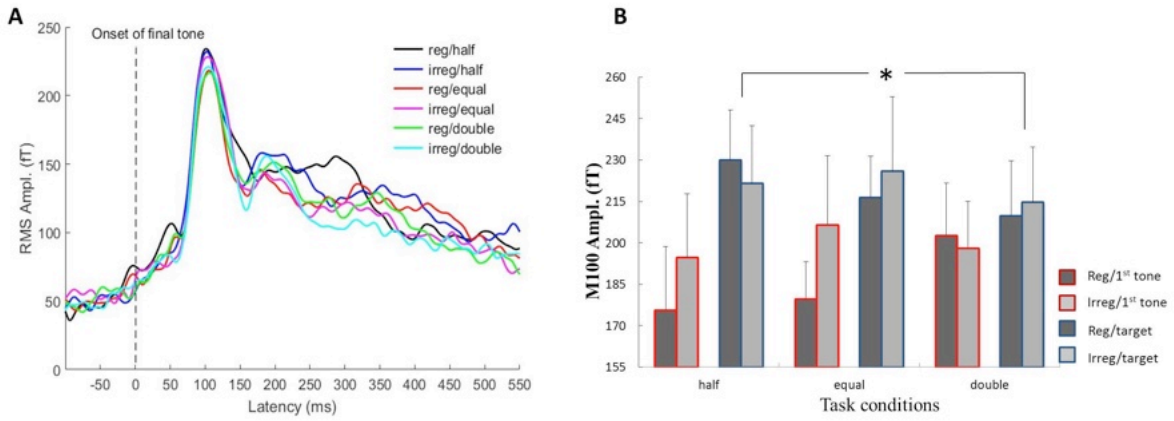

Fig. 3. Results for M100 analysis. (A) Measured M100 responses (group RMS), time locked to the onset of the final tone. (B) The mean peak values of the M100 responses to the first tone and the final tone in the sequence for each experimental condition. The error bars represent standard errors ($^*p < 0.05$).

and "double" conditions, all $ps > 0.05$. This result suggested that M100 amplitude was modulated as a function of different task conditions. The M100 measures for the "half" task yielded an enhanced ERF in auditory cortex than for the "double" task.

In addition, to compare the brain responses evoked by auditory beeps in different serial position, we also calculated the peak RMS values of M100 elicited by the first tone of the sequence. These values as well as the evoked responses to the final tone were entered into an analysis of variance (ANOVA), with temporal rhythms ("regular" and "irregular"), tasks ("half", "equal", and "double"), and stimuli ("the first tone" and "target") as within-participants factors. As illustrated in Figure 3B, the results revealed a significant interaction effect between the stimuli and task conditions, $F(2, 14) = 5.198, p < 0.05, \eta_p^2 = 0.426$. No other positive results were found. Further, simple main effects showed that different task conditions only affected the amplitudes of M100 evoked by the target, with a larger peak value in "half" condition (225.8 fT) and a relatively smaller peak value in "double" condition (212.2 fT), $F(2, 14) = 3.92, p < 0.05$. There was no statistical difference in the M100 amplitudes elicited by the first tone between "half" (185.2 fT), "equal" (193.1 fT), and "double" (200.4 fT) conditions.

Based on observations of the amplitude variation of the M100 component evoked by the first and last tone of the sequence, it seemed that M100 components elicited by the first tones varied little in amplitudes across different task conditions, in spite of the fact that the task cue was showed to participants before the sequence presentation. With the following tones unfolding over time, the M100 neural generator was modulated by the task divergence and the modulation contributed to the statistical difference in magnetic response around the temporal points of targets.

In conclusion, we used the auditory sequences to investigate the statistical summary of inter-intervals in the present study. Behavioral results indicated that perceptual averaging task could be implemented in time dimension and occur over temporal sequences, even a general over-estimation was reported when extracting the mean inter-interval duration of the auditory sequence in different tasks. Moreover, analysis of the auditory evoked component revealed a relatively larger M100 amplitude evoked by the final tone of the sequence in "half" condition, showing a demanding task to segment time interval

in short range.

References

Ward, E. J., Bear, A., & Scholl. B. J. (2016). Can you perceive ensembles without perceiving individuals?: The role of statistical perception in determining whether awareness overflows access. *Cognition,* 152, 78–86.

Dakin, S. C., & Watt, R. J. (1997). The computation of orientation statistics from visual texture. *Vision Research,* 37, 3181–3192.

Chong, S. C., & Treisman, A. (2003). Representation of statistical properties. *Vision Research,* 43, 393–404.

de Fockert, J., & Wolfenstein, C. (2009). Rapid extraction of mean identity from sets of faces. *The Quarterly Journal of Experimental Psychology,* 62, 1716–1722.

Haberman, J., & Whitney, D. (2007). Rapid extraction of mean emotion and gender from sets of faces. *Current Biology,* 17, 751–753.

Albrecht, A. R., Scholl, B. J., & Chun, M. M. (2012). Perceptual averaging by eye and ear: Computing summary statistics from multimodal stimuli. *Attention, Perception, & Psychophysics,* 74, 810–815.

Acerbi, L., Wolpert, D. M., & Vijayakumar, S. (2012). Internal representations of temporal statistics and feedback calibrate motor-sensory interval timing. *PLOS Computational Biology* 8, e1002771.

Hellström, A., & Rammsayer, T. H. (2004). Effects of time-order, interstimulus interval, and feedback in duration discrimination of noise bursts in the 50- and 1000-ms ranges. *Acta Psychologica,* 116, 1-20.

Brainard, D. H. (1997).The psychophysics toolbox. *Spatial Vision,* 10, 433–436.

Pelli, D. G. (1997). The Video Toolbox software for visual psychophysics: transforming numbers into movies. *Spatial Vision,* 10, 437–442.

PHONOLOGY AND PSYCHOPHYSICS: IS SONORITY REAL?

Yoshitaka Nakajima, Kazuo Ueda, and Gerard B. Remijn
Department of Human Science/Research Center for Applied Perceptual Science, Kyushu University, Fukuoka, Japan

Yuko Yamashita
Department of English Communication, College of Engineering, Shibaura Institute of Technology, Tokyo, Japan

Takuya Kishida
Graduate School of Design, Kyushu University, Fukuoka, Japan

Phonology is a field in linguistics, in which speech sounds are classified and related to temporal structures of specific languages. Sound units studied in phonology must be based on subjective properties of acoustic signals. If a way to connect physical and linguistic natures of speech sounds is established, it will form a new basis of a psychophysical investigation. It is known that spectral changes are important for speech communication, but it is not easy to find a paradigm to clarify common mechanisms among different languages.

Ueda and Nakajima (2017, Sci. Rep.) performed factor analyses summing up spectral changes of speech signals between 50 and 6400 (or 7000) Hz. The frequency range was divided into 20 critical-band filters simulating the function of the auditory periphery. The sound intensity fluctuations in these bands were summarized into a fewer number of factors. They discovered that 3-factor analyses led to similar results in 8 languages/dialects in 3 different language families. One of the factors was related to two separate frequency ranges around 300 Hz and around 1500 Hz, and the other two factors to a different frequency range each: around 1100 Hz and above 3300 Hz. It was often possible to separate the first factor into two factors related to one frequency range each, leading to 4-factor analyses.

Nakajima et al. (2017, Sci. Rep.) argued that the factor around 1100 Hz corresponds to what is called 'sonority' in phonology; higher sonority indicates higher suitability for syllable nuclei. They reached this idea examining correspondence between obtained factor scores and phonemes of British English, which were labeled in a speech database. The English phonemes located in the factor space clearly reflected sonority, as it appeared in linguistics literature.

Kishida et al. (2016, Front. Psychol.) improved the above-mentioned factor analysis by shifting the origin to calculate variances, in the variate space, to the acoustically silent point. This enabled them to resynthesize speech directly from factor scores as noise-vocoded speech. If only 1 or 2 factors were extracted, the intelligibility was close to zero, but if 3 factors were extracted, it leaped to $\sim 70\%$. To use more than 4 factors made the intelligibility $> 80\%$.

Yamashita et al. (2013, Front. Psychol.) examined whether the factor corresponding to sonority, hypothetically at that time, would appear in the developmental process of infants. The factor was observed in babbling infants of 15 months of age, and the rhythmic nature of this factor, manifesting a periodicity in a range 0.1–0.4 s, was clearer at higher ages up to 24 months.

The concept of sonority thus seems to combine many different aspects of speech production and perception. (This study was supported by the Japan Society for the Promotion of Science.)

MEASUREMENTS OF THE VELVET HAND ILLUSION

Tetsu Miyaoka
Faculty of Informatics, Shizuoka Institute of Science and Technology
<miyaoka.tetsu@sist.ac.jp>

Abstract

The purpose of the study was to measure the amounts of the Velvet Hand Illusion (VHI)and to propose mechanisms and a mathematical model for the VHI. The experimental stimuli were instruments with two straight rods positioned parallel to each other. The participant held the two rigid rods between his/her hands and moved the both hands simultaneously in an orthogonal direction toward the rods. The participant judged the amounts of the VHI by the magnitude estimation. The results showed the largest amount of VHI when the distance between the rods was 100 mm and showed smaller amounts of VHI when the distances were longer or shorter than 100 mm. We inferred mechanisms which produced the VHI and proposed a mathematical model to explain the VHI amounts.

You can easily feel the Velvet Hand Illusion (VHI) if you hold a coarse-wire net between your hands and move the both hands simultaneously on the net. You feel the surface of each contralateral hand very soft and smooth as if you touch the surface of the velvet. And you do not need even to use the wire for experiencing the VHI. You only need two rods stretched parallel to each other (shown in Fig. 1). If you hold the two rods between your hands and move the hands simultaneously in the orthogonal direction towards the rods, you have the same perception which you had experienced by the coarse-wire net.

The VHI is one of the clearest illusions in the haptics. But few studies were conducted about the VHI (Ohka et al., 2010; Miyaoka, 2012; Miyaoka, 2014; Rajaei et al., 2012; Rajaei et al., 2013; Rajaei et al., 2016). The purpose of the study was to measure amounts of the VHI by the magnitude estimation. We inferred the brain mechanisms which produced the VHI and proposed a mathematical model to explain the amounts of VHI.

Experiment

The purpose of the experiment was to determine amounts of the VHI by the magnitude estimation.

Method

Participants. Eight males and one female in their twenties participated in the experiment. All participants had no experience of psychophysical experiments.

Stimuli. Two straight iron rods covered with plastics were used as stimuli. As shown in Fig. 1, the rods were set in a U-shaped frame. The two rods were stretched parallel to each other. The diameter of the rods was 3 mm. Distances between the two rods (the d in Fig. 1) were seven. They were 20, 40, 60, 80, 100, 120, and 140 mm.

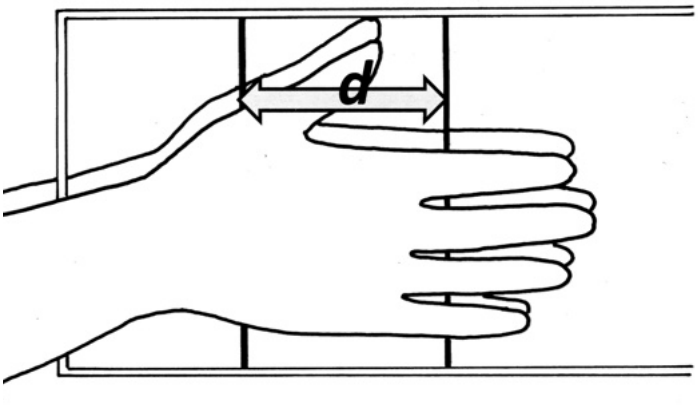

Fig. 1. An example of the stimuli used in the experiment. The participant held two rods between his/her hands and moved the hands simultaneously in the orthogonal direction toward the rods and responded amounts of the VHI. The d shows the distance between the rods.

Procedure. The participant sat on a chair and wore an eye-mask to prevent visual inspection of the stimuli. Two stimuli, one was a standard stimulus and the other was a comparison stimulus, were set right and left on the experimental desk in front of the participant. The two stimuli were apart 25 cm to each other. In the magnitude-estimation procedure, a modulus was used. The standard stimulus, the distance between the two rods was 80 mm, was given a modulus "100" for the VHI amount. The participant was asked to give a suitable number to a VHI amount for a comparison stimulus when it was compared with the standard stimulus VHI amount. The experimenter informed the participant which was the standard stimulus before each trial.

The maximum-presenting time for each trial was 15 seconds and the inter-stimulus interval was 20 seconds. Each participant responded 20 times for each stimulus set, therefore the total number of the experimental trials for each participant was 140. Presenting order of each stimulus set was random. Temperature in the laboratory was maintained higher than 25°C in the experiment to avoid the decline of tactile sensitivity.

Results and Discussion

The geometric mean values of the magnitude estimation were calculated based on the experimental data of the nine participants. The results were shown in Fig. 2. The gray diamonds in the figure show the geometric means.

The figure shows that the mean values of magnitude estimation increased when the distances between two rods increased from 20 mm to 80 mm, reached maximum at the 80 mm (the mean-estimation value: 102) and at the 100 mm (the mean-estimation value: 103). The magnitude-estimation values decreased when the distances increased over 100 mm. The magnitude-estimation value was 24.3 when the distance was the 20mm and 66.1 when the distance was the 140 mm.

The participants reported that the tactile impression of the two rods was strong at the 20-mm distance condition. The tactile impression of the 20-mm distance masked the illusion and made the VHI weaker. On the other hand, the participants reported that

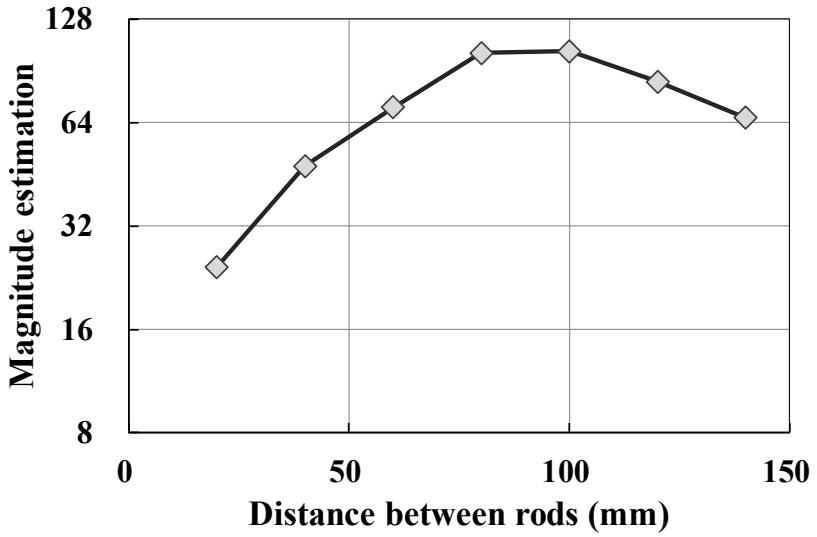

Fig. 2. The amounts of the VHI measured by the magnitude estimation. The vertical axis shows the magnitude-estimation values and the horizontal axis shows the distances between the two rods. Each diamond in the figure shows the geometric mean of the magnitude-estimation values.

the 140-mm distance was too large to hold the two rods simultaneously and to move the hands enough. It made the VHI weaker.

The results of the magnitude-estimation experiment showed that the amounts of VHI were determined by the distances between the rods (the "d" in Fig. 1). The illusion-amount curve was convex upward and the VHI amounts were in the largest level when the distances were between the 80 $\sim$ 100 mm. The VHI amounts decreased when the distances were below 80 mm and over 100 mm. But the reasons that caused the VHI decrease might be different between the short and long d.

We inferred emergence mechanisms of the VHI in the experiment as follows: The participant holds two rods between his/her hands and moves the both hands simultaneously. He/she touches the rods and the surface of the contralateral hand. The rods move on the hands, but the hands do not move to each other because the participant moves the both hands simultaneously. The contralateral-side surface of the hand gives no friction. The participant brain infers that the hands are moving on a surface of something. However, the surface gives no friction. Therefore, the brain concludes that the contralateral-side surface of the hands is very smooth and soft.

General Discussion

Proposal of a Simulation Model

From the experimental data, we induced a simulation model. The model had two hypotheses.

The first hypothesis is as follows: As a distance between the two rods becomes larger and the moving length of hands shortens, the illusion amounts decrease. If a distance between the rods is too large to touch the both rods simultaneously, the participant feels no illusion. The first hypothesis is shown squares and dotted line in Fig. 3 and the

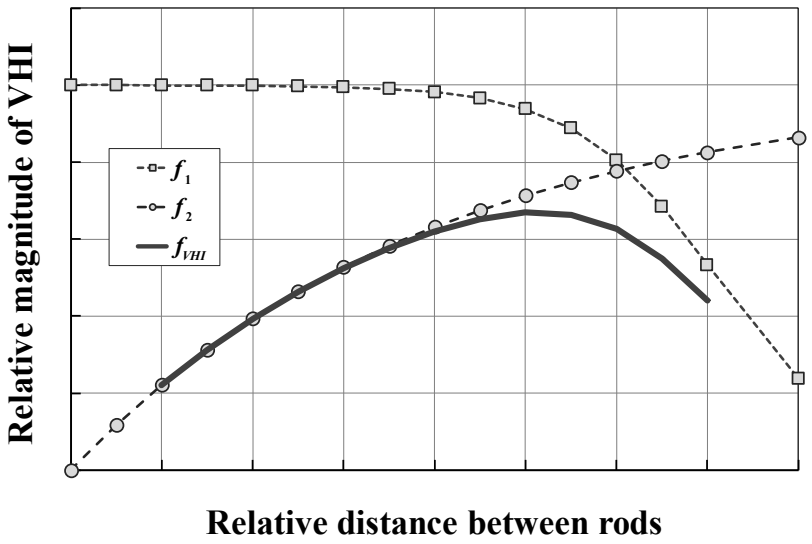

Fig. 3. A simulation model of the VHI. The f_1 in the legend is shown by grey squares and a dotted line. The f_2 is shown by the grey circles and a dashed line. The f_{VHI} is a multiplication of the f_1 and the f_2 and shown by the thick dark-grey line.

equation $f_1(x)$ in the legend is shown as

$$f_1(x) = \frac{\exp\{-a(x-b)\}}{1+\exp\{-a(x-b)\}} \qquad (a > 0,\ b > 0). \tag{1}$$

The second hypothesis is as follows: When a distance between the two rods is shortened, the impression of the rods is stronger and it masks the VHI. This hypothesis

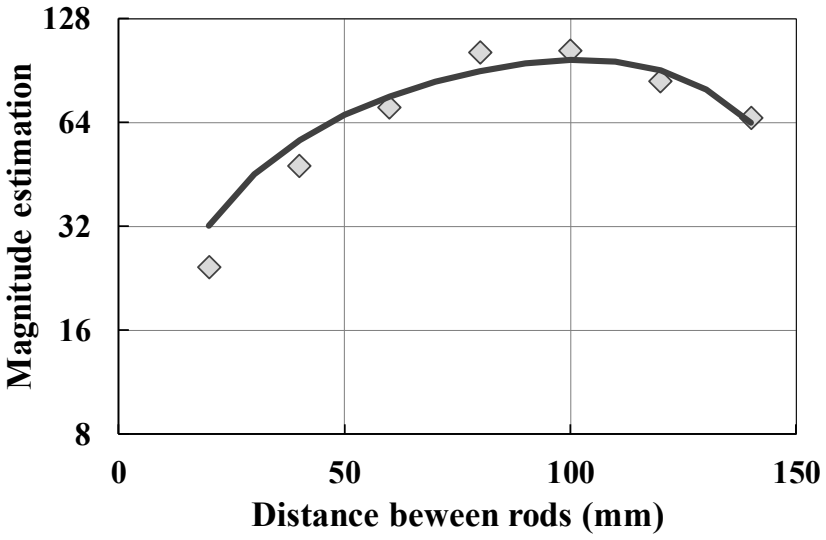

Fig. 4. A curve fitting to the magnitude-estimation data. Each diamond shows the amounts of the VHI measured by the magnitude-estimation experiment. A thick dark-grey line is the fitted curve to the experiment data.

is shown circles and dashed line in Fig. 3 and the f_2 in the legend is

$$f_2(x) = 1 - \exp(-cx) \qquad (c > 0). \tag{2}$$

The total amount of the VHI, the $f_{VHI}(x)$, is shown as a multiplication of the $f_1(x)$ and the $f_2(x)$ and the thick dark-grey line in the figure. The $f_{VHI}(x)$ is

$$f_{VHI}(x) = mf_1(x)f_2(x) = m\frac{\exp\{-a(x-b)\}\{1 - exp(-cx)\}}{1 + \exp\{-a(x-b)\}}, \tag{3}$$

where the m is a parameter determined depending on the unit of measurement. The fitted results of the equation to the magnitude-estimation data are shown in Fig. 4 and the calculated parameters are

$$f_{VHI}(x) = 145\frac{\exp\{-0.0645(x-142)\}\{1 - \exp(-0.0125x)\}}{1 + \exp\{-0.0645(x-142)\}}. \tag{4}$$

The magnitude estimation data are shown as the grey diamonds and the equation $f_{VHI}(x)$ is shown as the thick dark-grey line in Fig. 4.

Conclusion

In this study, we performed the magnitude-estimation experiment and showed the amounts of the VHI were the largest at the distances between two rods were around 100 mm. We inferred mechanisms which produced the VHI. And we proposed a mathematical model to explain amounts of the VHI and fitted the model to the experimental data. We need further studies to reveal neural mechanisms which produce the VHI.

Acknowledgements

This work was supported by JSPS KAKENHI Grant Numbers 25540061.

References

Ohka, M., Kawabe, Y., Abdullah, C., Rajaei, N., Yussof, H. B., and Miyaoka, T. (2010). Investigation on Velvet Hand Illusion using psychophysics and FEM Analysis. *International Journal of Smart Sensing and Intelligent Systems,* 3, 488–503.

Miyaoka, T. (2012). Measurements of Velvet Hand Illusion by the magnitude estimation and paired comparison. *Proceedings of the 28th Annual Meetings of the International Society for Psychophysics,* 268–273.

Miyaoka, T. (2014). A mathematical model to explain the quantity of Velvet Hand Illusion. *Proceedings of the 30th Annual Meetings of the International Society for Psychophysics,* 48.

Rajaei, N., Kawabe, Y., Ohka, M., Miyaoka, T., Chami, A., and Yussof, H. B. (2012). Psychophysical experiments on Velvet Hand Illusion toward presenting virtual feeling of material. *International Journal of Social Robotics,* 4(1), 77–84.

Rajaei, N., Ohka, M., and Miyaoka, T., et al. (2013). Investigation of VHI affected by the density of mechanoreceptive units for virtual sensation. *International Journal of Smart Sensing and Intelligent Systems,* 6(4), 1516–1532.

Rajaei, N., Ohka, M., Nomura, H., Komura, H., Matsushita, S., and Miyaoka, T. (2016). Tactile mouse generating velvet hand illusion on human palm. *International Journal of Advanced Robotic Systems,* September-October, 1–10.

Part XII
Free Talk Session 7

USING THE EFFECTS OF FOREPERIOD-VARIATION ON READINESS TO BREAK IN DRIVING SIMULATION

Friedrich Müller and Wiebke Melcher
Leuphana Universität, Lüneburg
<f.mueller@uni-lueneburg.de>

Abstract

Range and frequency of varying foreperiods in reaction time experiments affect the expectancy of the reaction signals and the readiness to react in a systematic manner. In a study investigating braking safety as a function of the driver's footwear we made use of this regularity. In order to provoke unforeseeable situations which require speedy brake applications at first the time intervals between consecutive braking signals (interstimulus interval; ISI) were varied so as to establish a time-reference-system. At later stages of the experiment, a few ISI at considerably lower durations were presented. These ISI perceived as too short significantly increased breaking times if the subjects wore flip-flops compared to foot-covering shoes.

Reaction times are influenced by the foreperiod (FP) which is the interval between a warning signal applied to direct attention to an upcoming reaction signal and the stimulus. If the FP is kept constant within a range of 1 to 7 s in single reaction experiments, we find reaction times (RTs) nearly linearly decreasing with increasing length of FP (Fig. 1). When we present variable FP, however, reaction time follows a typical pattern as shown in Fig. 2 with relatively slow reactions at the shortest FP and decreasing RT up to the median FP. For longer than medium FPs the RT remains constant (Müller, 1980). These data are in line with results shown by Baumeister et al. (1967) and Niemi (1979).

For Fig. 2 the RTs are averaged over the relative length of FPs out of 4 series each consisting of equally spaced FPs ranging from either 1 to 4 s; 2.5 to 5.5 s, 4 to7 s or 1 to 7 s. The effect of FP on RT is less pronounced if FPs are presented in random order compared to a condition where the same sequence of FPs is repeatedly presented.

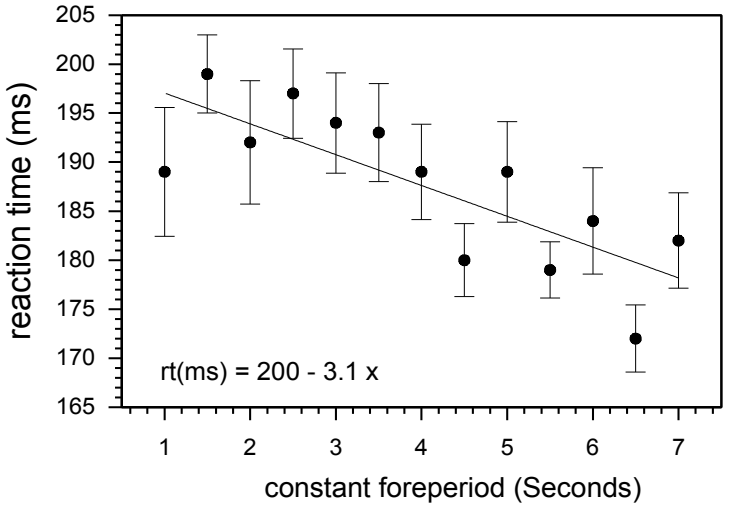

Fig. 1. RT to signals of white light at constant foreperiods between 1 and 7 s.

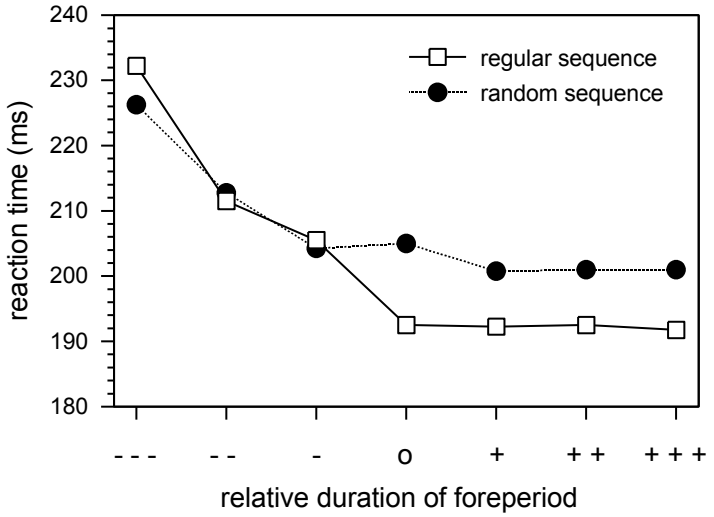

Fig. 2. RT to signals of white light at relative positions of the foreperiods in time-reference-systems.

In a paper given at Fechner Day 92 (Müller, 1992) it was shown that the RT is linearly related to category-scaled psychological tension. It was argued that in each case the set of FPs forms an orienting time reference system (*Zeitbezugssystem*) according to Witte (1966) and Heller (1990) wherein subjects try to maximize readiness for the midpoint between shortest and longest FP of the system. If the reaction signal appears at this point readiness will be optimized, resulting in short RT. If the signal appears later, a reactive increase of psychological tension is mobilized (Düker, 1963) which prevents a slowing of RT for longer than medium FP (Müller, 1981).

Prompting critical reactions using a foreperiod-reference system

If the above outlined thoughts hold, we expect participants being astonished and unprepaired if unexpectedly a FP appears which is clearly shorter than the shortest in an established time reference system. In experiments designed to evaluate the effect of different footwear on the brake application time (Backhaus & Müller, 2016) in a driving simulator (following an cross-modal ABBA-design), 40 participants each executed 84 braking actions when using enclosing footwear and when wearing flip-flops. In order to provoke critical braking manoeuvres at first 5 different ISI of either 10, 12.5, 15, 17.5 and 20 s between upcoming braking signals (yellow light, red light or a person suddenly appearing on the street) were presented three times in succession in irregular order. Then the 16th signal appeared unexpected already after 4 s. During the time course of the entire experiment this pattern (15 time system conforming ISI followed by an unusual short period) was repeated 8 times; interrupted by two breaks which were used to change footwear. The driving task required to follow an imagined, hence not visible pathway directed by two laterally displayed arrows which indicated the direction of deviations from the track. This task alone absorbs a high degree of attention, which overall causes relatively long reaction times.

Despite the fact that attention of the participants was focussed on the tracking task and various aspects of the experimental setup, as the change of stimuli and footwear interrupted and altered the flow of the experiments, the overall recorded RTs (960 tri-

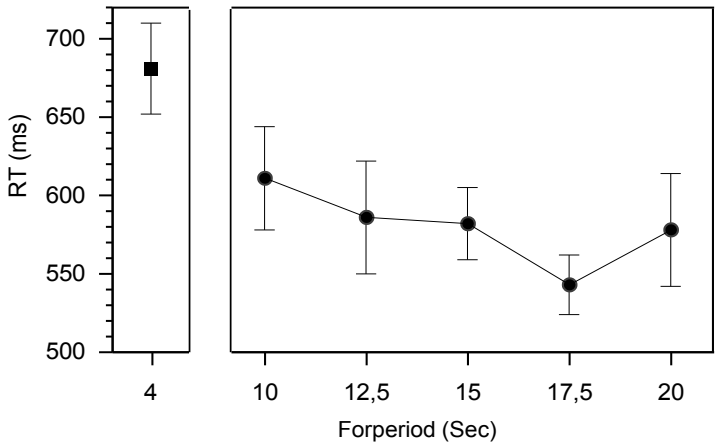

Fig. 3. On the right: Breaking response to traffic lights and persons on the road at variable ISI. Left: Reaction to rare ISI outside the time reference system.

als/foreperiod) given with Fig. 3 show a foreperiod-dependency near to the one described in Fig. 2. The intention to provoke a critical break-condition by introducing a FP outside the time reference system was achieved as shown in the very left mark in Fig. 3. For this critical ISI it was clearly demonstrated that breaking time, defined as the interval between signal-onset and full application of the brake pedal, is longer if subjects wear flip-flops (mean = 1110 ms; SD = 287) compared to foot-covering shoes (mean = 1017, SD = 177); ($t = 2.665, p < 0.01$).

References

Backhaus, C., Müller, F. (2016) Bediensicherheit von Pedalen in Abhängigkeit des getragenen Schuhwerks. *Z. Arb. Wiss.* 70(4), 231–241.

Baumeister, A., Dugas, J. & Erdberg, P. (1967) Effects of warning signal intensity, reaction signal intensity, preparatory interval, and temporal uncertainty on reaction times of mental defectives. *Psychological Record,* 17, 503–507.

Düker, H. (1963) Über reaktive Anspannungssteigerung. *Z. exp. angew. Psychol.* 10, 46–72.

Heller, O. (1990) Scaling and Orientation. In: F. Müller (Ed.) *Proceedings of the 6th Annual Meeting of the International Society for Psychophysics.* Würzburg: International Society for Psychophysics; pp. 52–57.

Müller. F. (1981) Zeit-Bezugssysteme bei Vorperioden im Reaktionszeitexperiment. In O. Heller (Ed.) *Forschungsbericht 1980.* Würzburg: Julius-Maximilians-Universität, Psychologisches Institut III, 78–108.

Müller, F. (1981) Validierung der Skalierung psychischer Anspannung im Reaktionszeitexperiment. In L. Tent (Ed.) *Erkennen, Wollen, Handeln—Festschrift für Heinrich Düker zum 80. Geburtstag.* Göttingen: Hogrefe; pp. 226–232.

Müller, F. (1992) Scaling of psychological tension in reaction time experiments for the measurement of the efficiency of psychological performance with and without background noise. In G. Borg (Ed.) *Proceedings of the 8th Annual Meeting of the International Society for Psychophysics.* Stockholm: International Society for Psychophysics; pp. 147–152.

Niemi, P. (1979) Stimulus Intensity effects on auditory and visual reaction processes. *Acta Psychologica* 43, 299-312.

Witte, W. (1966) Das Problem der Bezugssysteme. In W. Metzger (Ed.): *Handbuch der Psychologie,* Band 1, 1. Halbband. Göttingen: Hogrefe; pp. 1003–1027.

ACCURACY AND LATENCY OF KICKING FOOT IDENTIFICATION FOR FOOTBALL OPPONENTS IN RELATION TO TEAM FAMILIARITY AND GAME EXPERIENCE

Benjamin B. Moore[1], Roger D. Adams[1], Nicholas J. O'Dwyer[1], Kylie A. Steel[2] and Stephen Cobley[1]

[1] *University of Sydney, 75 East Street, Lidcombe, NSW, 2141, Australia*

[2] *Western Sydney University, Penrith, NSW, 2751, Australia*

<bmoo4834@uni.sydney.edu.au; roger.adams@sydney.edu.au; nicholas.odwyer@sydney.edu.au; K.Steel@uws.edu.au; stephen.cobley@sydney.edu.au>

Abstract

Although only 18% of Australian Football players are left-footed, defending against them requires different strategies to defending against right-footers. This research collected both discrimination and response latency data to examine the ability of football players to identify left- versus right-footed kickers. Players identified the kicking foot of teammates and opponents from static facial images presented in a randomised sequence. Accuracy, reaction time (RT), and discrimination capability (AUC) were examined. Participants were less accurate and had slower RTs when identifying the kicking foot of opposing team players compared to that of their teammates. Left-footed opponents who had played for longer were identified with greater accuracy and reduced RT, and participant game experience correlated with faster RT. Opposing team familiarity and game experience were both found to affect kicking foot identification in Australian Football and this finding has potential for training and performance benefits.

Research in perceptual-cognitive sport expertise has consistently demonstrated superior acquired characteristics in highly experienced or expert performers relative to intermediates or novices (Abernethy et al., 2012). In both team and individual sport contexts, it is visual and perceptual domain exposure along with the development of sport-specific knowledge and memory (Roca et al., 2013) accumulated via extensive training and competition that appear critical to perceptual-cognitive skill.

The ability to identify and respond to laterally associated movement is evident in many sporting contexts (Raymond et al., 1996). In AF, perceptual-cognitive skills are particularly important (Farrow et al., 2008) as players continuously interact with opponents and teammates at different distances when executing a kick, evading a tackle (Bradshaw et al., 2011) or when receiving or defending a pass (Steel et al., 2011). Although both sides can be used for kicking and handballing in AF (Parrington et al., 2015), most elite players exhibit a strong 'footedness' preference (Ball, 2011) and coaches expect the dominant foot to be used in most instances (Farrow & Ball, 2011). The frequency of left-footed players in AF is estimated to be approximately 20% (Champion Data, 2015).

In the absence of knowledge regarding kicking-foot preference, the reliance on using 'present time' player biological motion to make decisions may lead to missed opportunities (Ward & Williams, 2003). These concerns are likely more pertinent in less experienced players, who are less able to extract meaning from kinematics for forthcoming movements (Steel et al., 2006). Therefore, a player's default option—based on lower frequencies and experience—may be to assume that an opposing player has a right-foot kicking preference; even though this may be costly (Loffing et al., 2015). To illustrate, Figure 1 highlights

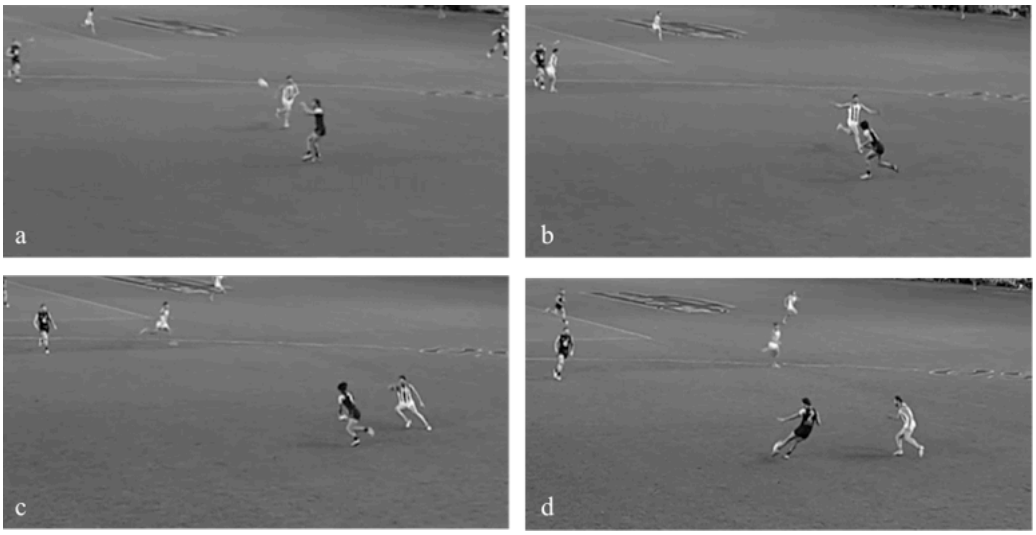

Fig. 1. Illustration of Kicking-Foot identification error in professional AF (a) The defender preparing to 'man-the-mark' goes towards the right shoulder of the opposing player. He is expecting the opponent to swivel right and use his right foot for kicking (b) The attacking player receives the ball and steps to his left. The defender is still moving towards the right shoulder of the attacker (c) The attacking player now prepares to kick using his left foot. The defender is out of position and cannot react quickly enough to tackle and prevent a 'left-foot' kick (d) The attacking player makes a successful forward kick using his left foot.

the occurrence and consequence of such an error in a professional AF game. The offensive player has time and space to kick with the preferred left-foot after the defender incorrectly assumes or inaccurately identifies a right-footed kick. Such perceptual-cognitive error can lead to points conceded, hence determining whether players are less accurate or slower in recognising the less frequent left-footed players is significant (Abernethy et al., 2001).

The aim of this study was to determine whether professional AF players' accuracy, reaction time, and discrimination of 'Kicking Foot' identification (Kicking Foot-ID) were affected by left- v right-footer frequencies, team-mates v opposing team members, and game experience. Hypothesis 1 stated participants would be less accurate, and slower in identifying left-footers. Hypothesis 2 predicted participants would be more accurate, faster, and more capable in identifying the preferred kicking-foot of teammates than opposing players. Hypothesis 3 predicted that game experience would moderate these capabilities, leading to better accuracy, lower RT's, and an enhanced capability to discriminate the preferred kicking foot used by opposing players. Likewise, opposing players with more game experience would be more accurately and quickly identified.

Method

The study was undertaken on two separate occasions during the final third of an AFL season. Different participant groups were used on each occasion, and participation in either Part 1 or 2 of the study was aligned to those players selected to play against the upcoming opposing team in that week of the season (i.e. Opponent 1 or Opponent 2)

Fig. 2. Diagrammatic illustration of randomised sequence presentation for the first 7 photographs for Opponent 1 test with Own Team players inter-dispersed (note: each player's head and shoulders were included in the actual presentation).

Participants

13 and 10 male AF players respectively, from a professional football club, participated in parts 1 and/or 2 of the study (3 participated in both parts). Participants had varying levels of 'first-grade' AF competition experience (Opponent 1 participant group—M games played = 122.6, $SD \pm 80.4$; Opponent 2 participant group—$M = 117.4, SD \pm 82.6$).

Procedure

Participants completed a standardised 15-minute Kicking Foot-ID video task using a 38cm notebook monitor (ACER Aspire 9420). Participants were shown a randomised sequence of 60 player photos that included 30 teammates and 30 upcoming opposing team players. Opponent players were chosen for the sequence based on those players most frequently selected in the team's playing squad up to that point in the season. Figure 2 provides an illustration of the player video presentation. Participants had to identify as accurately and quickly as possible, the kicking-foot preference (i.e. left or right-footed) of each player. Kicking-foot preference was determined using the player profiles held by Champion Data Statistics (Champion Data, 2015). Seven of thirty "Own Team" players (i.e. 23%), nine of thirty in Opposition Team 1 (30%) and six of thirty in Opposition Team 2 (20%) were left-footed.

A latency-timing box (Steel et al., 2006) captured participant responses. The box panel consisted of a central home key (starting position) and six equidistant (i.e. 5.18 cm) response certainty keys, arranged adjacent and in a semi-circular pattern. Participants applied dominant hand index finger pressure on the home key and responded by moving to a choice key as quickly as possible. The three key choices to the right represented levels of certainty for a right-foot identification decision (i.e., RF-LC = Right Foot–Low Certainty; RF-MC = Right Foot–Medium Certainty; RF-HC = Right Foot–High Certainty), while the three keys to the left represented certainty levels for a left-foot decision (LF-LC = Left Foot–Low Certainty; LF-MC = Left Foot–Medium Certainty; LF-HC—Left Hoot–High Certainty). The latency-timing device enabled valid measurement of Response Accuracy, Reaction Time (i.e., initial release of pressure from home key), and Response Certainty. Participants completed the Kicking Foot-ID task in an afternoon two days prior to an upcoming game.

Data Analysis

Accuracy & Latency (Reaction Time). Kicking Foot-ID accuracy (% correct) and latency (RT ms) were analysed separately using a two-factor Repeated Measures (RM) ANOVA, with the factors of Foot (Left-Right) and Team (Own-Opposition) entered as independent variables.

Foot Preference Discrimination: Receiver Operating Curve (ROC) analysis. To assess participant capability in Kicking Foot-ID, a non-parametric signal detection Receiver Operating Curve (ROC) analysis was used (Swets et al., 2000). Left-footers were considered as signals and right-footers as noise, and decision certainty levels represented different response cut-offs. Data were entered into the ROC sub-routine within SPSS (Version 22.0 SPSS, Inc., Chicago, IL). Preferred foot (i.e., 'left or right-footer') was entered as a state variable and certainty rating entered as the continuous variable. The ROC routine generated an area under the curve (AUC) value for each participant reflecting accuracy and certainty, with 0.5 representing chance and 1.0 representing perfect Kicking Foot-ID discrimination. A paired t-test examined the difference between Own-Team and Opposition-Team members.

Game Experience. To determine whether player game experiences affected preferred Kicking Foot-ID, Pearson's correlations examined whether participants' own professional game experience (i.e., AF games played), and the number of games played by an opponent were correlated with Kicking Foot-ID accuracy, RT, and discrimination capability.

Results

Accuracy of Kicking Foot Identification (KF-ID)

Opponent 1. RM-ANOVA revealed significant main effects for Foot, $F_{(1,12)} = 101.53$, $p < 0.001, \eta_p^2 = 0.89$ and Team, $F_{(1,12)} = 115.48, p < 0.001, \eta_p^2 = 0.91$. Identification accuracy was lower when participants attempted to identify left-footed players, and when they attempted to identify the kicking foot of opposition players. Likewise, there was a Foot x Team interaction, $F_{(1,12)} = 103.33, p < 0.001, \eta_p^2 = 0.90$. The reduction in identification accuracy when viewing left-footers relative to right-footers was greater for participants when they viewed opposing team members compared to when viewing teammates.

Opponent 2. RM-ANOVA revealed that while mean patterns were close to significance, no main effect for Foot was evident, $F_{(1,9)} = 3.94, p = 0.08, \eta_p^2 = 0.30$, or the interaction, $F_{(1,9)} = 4.432, p = 0.07, \eta_p^2 = 0.33$. However, a main effect for Team was evident, $F_{(1,9)} = 7.97, p < 0.05, \eta_p^2 = 0.47$. Identification accuracy was lower when participants attempted to identify the kicking foot of opposition players.

Latency of KF-ID (Reaction Time)

Opponent 1. RM-ANOVA identified no main effect for Foot, $F_{(1,12)} = 1.56, p = 0.24, \eta_p^2 = 0.12$, though a significant main effect for Team was apparent, $F_{(1,12)} = 25.51, p < 0.001, \eta_p^2 = 0.68$, with slower reaction times occurring when participants were responding to images of opposing players. There was no interaction, $F_{(1,12)} = 0.01, p = 0.91, \eta_p^2 =$

0.001.

Opponent 2. There was again no main effect for Foot, $F_{(1,9)} = 0.09, p = 0.77, \eta_p^2 = 0.01$, though there was a main effect for Team, $F_{(1,9)} = 65.39, p < 0.001, \eta_p^2 = 0.88$, with slower reaction times when recognising opposing players. The interaction was significant, $F_{(1,9)} = 5.62, p < 0.05, \eta_p^2 = 0.39$, as participants were faster in reacting to left-footers in Opposition 2 team members. This suggested something unique about Opposition 2, and a follow-up t-test revealed that career games played by Opposition 2 members ($M = 116.55, SD = 83.15$) was significantly greater than Opposition 1 ($M = 75.07, SD = 66.35; t(60) = -1.98, p < 0.05$). The game differences specifically in left-footers was not significant, though the small sample size and descriptive statistics should be noted (i.e., Opponent 2—$M = 135.5$ games; $SD = 63.49$; Opponent 1—$M = 77.44$ games; $SD = 78.52$).

Foot Preference Discrimination: ROC Analysis

Opponent 1. ROC analysis produced AUC scores indicating the capability to identify left-footers from right-footers in the sample of players. A paired t-test between Own-Team (AUC $M = 1.0$) and Opponent 1 (AUC $M = 0.81$) showed a significant superiority in the capability to identify left-footers amongst teammates relative to opposing team members ($p < 0.001$, M difference in AUC = 0.19, 95% CI = 0.12–0.25).

Opponent 2. Similarly, the t-test for Own-Team (AUC $M = 0.99$) and Opponent 2 (AUC $M = 0.88$) also showed a superior capability in identifying left-footers amongst teammates relative to Opposing team members ($p < 0.05$, M difference in AUC = 0.11, 95% CI = 0.03–0.19).

Game Experience

Opponent 1 The number of games played by participants was not correlated with Kicking Foot-ID accuracy or associated with discrimination capability (i.e., AUC scores, $r = 0.29, p = 0.33$). However, games played was correlated with the average RT (i.e., left footers $r = -0.59, p < 0.05$; right-footers, $r = -0.62, p < 0.05$); that is, participant game experience was associated with faster RT's. When opposition members had more game experience, accuracy increased when participants attempted to identify left-footers ($r = 0.71, p < 0.05$) but not right-footers ($r = 0.27, p = 0.12$), and average RT's reduced (i.e., left-footers, $r = -0.72, p < 0.05$; right-footers, $r = -0.63, p < 0.005$).

Opponent 2. The number of career games played by participants was not correlated with Kicking Foot-ID accuracy, average RT or discrimination capability. Professional game experience in Opponent 2 members was not correlated with Kicking-Foot ID accuracy. However, it was associated with reductions in average RT for Kicking Foot-ID for right-footers ($r = -0.84, p < 0.005$), but not left-footers.

Discussion

For Opponent 1, professional AF participants were significantly less accurate in identifying left-footed than right-footed players, and the accuracy of identifying the preferred foot was

greater when viewing team-mates compared to when viewing opposing team members. By contrast, laterality did not affect RT's. These findings provide partial support for Hypothesis 1, the frequency-dependent hypothesis (Raymond et al., 1996), suggesting that lower frequency encounters with left-handers/footers could confirm identification accuracy performance advantages in selective sporting situations (Hagemann, 2009).

For Opponent 2, laterality did not affect accuracy and did not affect RT's. However, the RT interaction was significant. When participants attempted to discern the preferred foot of opponent left-footers, RT's were quicker than when viewing opposition right-footers; a finding which might be explained by Opposition 2 containing players with a significantly greater number of AF games played (i.e., reflecting higher familiarity). Correlations support this notion, as opponent team member game experience was associated with improved recognition accuracy and quicker identification.

With reference to Hypothesis 2, findings across both upcoming opponents showed participants were more accurate and had faster RT's when viewing teammates. Participants were able to identify left-footers amongst teammates with more accuracy and certainty than left-footers for Opponent 1 and Opponent 2. So, whilst findings highlighted expected discrepancies in comparing Kicking Foot-ID capability when viewing own and opposing team members, they also highlight the potential benefit that could be achieved by using a similar protocol to train less experienced players to improve their perceptual capability (in terms of quickly and accurately identifying footedness) when competing against less familiar opponents (Schorer et al., 2012).

Results also provided partial support for Hypothesis 3. For Opponent 1 (i.e., the team with less-experienced and less-familiar players), participant game experience did not influence Kicking Foot-ID error, though experience was associated with faster RT's. However, more AF games played by opposing team members was associated with greater accuracy for identifying left-footed players and faster RT's in identifying both left- and right-footers. This is consistent with the view that accuracy and RT improvement can be accrued from opponent player familiarity and knowledge (Loffing et al., 2012a).

Conclusion

In two samples of professional AF players tasked with identifying the Kicking Foot of teammates and players from two opposing teams, participants made more errors and were slower when identifying the preferred kicking foot of opposing players who were (a) left-footed, (b) members of an opposing team, or (c) less familiar in general. These tendencies were moderated when opponent players were more familiar (e.g., Opposition 2) and had played a greater number of AF professional games. Perceptual training aimed at reducing Kicking Foot identification error and RT may be beneficial in improving the decision-making capability of AF players.

References

Abernethy, B., Gill, D. P., Parks, S. L., & Packer, S. T. (2001). Expertise and the perception of kinematic and situational probability information. *Perception,* 30(2), 233-252.

Abernethy, B., Schorer, J., Jackson, R. C., & Hagemann, N. (2012). Perceptual training methods compared: The relative efficacy of different approaches to enhancing sport-specific anticipation. Journal of Experimental Psychology: Applied, 18(2), 143-153.

Ball, K. A. (2011). Kinematic comparison of the preferred and non-preferred foot punt

kick. *Journal of Sports Sciences,* 29(14), 1545-1552.

Bradshaw, R. J., Young, W. B., Russell, A., & Burge, P. (2011). Comparison of offensive agility techniques in Australian Rules football. *Journal of Science and Medicine in Sport,* 14(1), 65-69.

Champion Data. (2015). *Official 2015 Australian Football League Statistics,* Melbourne: Champion Data.

Farrow, D., & Ball, K. A. (2011). *Providing an evidence-based model for non-preferred kicking skill development.* Report for the AFL Research Board. Melbourne.

Farrow, D., Pyne, D., & Gabbett, T. (2008). Skill and physiological demands of open and closed training drills in Australian football. *International Journal of Sports Science & Coaching,* 3(4), 485-495.

Hagemann, N. (2009). The advantage of being left-handed in interactive sports. *Attention, Perception & Psychophysics,* 71(7), 1641-1648.

Loffing, F., Hagemann, N., Schorer, J., & Baker, J. (2015). Skilled players' and novices' difficulty anticipating left-vs. right-handed opponents' action intentions varies across different points in time. *Human Movement Science,* 40, 410-421.

Loffing, F., Hagemann, N., & Strauss, B. (2012a). Left-handedness in professional and amateur tennis. *PloS One,* 7(11), e49325.

Loffing, F., Schorer, J., Hagemann, N., & Baker, J. (2012b). On the advantage of being left-handed in volleyball: further evidence of the specificity of skilled visual perception. Attention, Perception & Psychophysics, 74(2), 446-453.

Parrington, L., Ball, K., & MacMahon, C. (2015). Kinematics of preferred and non-preferred handballing in Australian football. *Journal of Sports Sciences,* 33(1), 20-28.

Raymond, M., Pontier, D., Dufour, A.-B., & Moller, A. P. (1996). Frequency-dependent maintenance of left handedness in humans. *Proceedings of the Royal Society of London. Series B: Biological Sciences,* 263(1377), 1627-1633.

Roca, A., Ford, P. R., McRobert, A. P., & Williams, A. M. (2013). Perceptual-cognitive skills and their interaction as a function of task constraints in soccer. *Journal of Sport & Exercise Psychology,* 35(2), 144-155.

Schorer, J., Loffing, F., Hagemann, N., & Baker, J. (2012). Human handedness in interactive situations: Negative perceptual frequency effects can be reversed! *Journal of Sports Sciences,* 30(5), 507-513.

Steel, K. A., Adams, R. D., & Canning, C. G. (2006). Identifying runners as football teammmates from 400 msec video clips. *Perceptual and Motor Skills,* 103(3), 901-911.

Steel, K. A., Adams, R. D., Coulson, S., Clothier, P., & Walker, D. (2011). *Video self-modeling and kicking accuracy on the non-preferred side.* Paper presented at the Science and Football VII: The Proceedings of the Seventh World Congress on Science and Football, Nagoya, Japan.

Swets, J. A., Dawes, R. M., & Monahan, J. (2000). Better decisions through science. *Scientific American,* 82-87.

Ward, P., & Williams, A. M. (2003). Perceptual and cognitive skill development in soccer: The multidimensional nature of expert performance. *Journal of Sport & Exercise Psychology,* 25(1), 93-111.

CHARACTERISTICS OF SIMULTANEOUS TAPPING BY DIFFERENT HANDS/FEET

Yoshiyuki Sato[1,2], Kaori Sakai[2], Eriko Aiba[2], and Yutaka Sakaguchi[2]
[1]*Graduate School of Arts and Sciences, The University of Tokyo*
[2]*Graduate School of Information Systems, The University of Electro-communications*

Abstract

People require temporally precise coordination of multiple body parts to perform various motor tasks, e.g., playing a musical instrument. However, little is known about the mechanism by which the human brain produces and maintains precisely synchronized voluntary movement in multiple body parts. In the present study, we aimed to answer these questions by analyzing the temporal characteristics of bimanual simultaneous tapping. We also investigated how sensory feedback contributes to the maintenance of simultaneity by examining the inter-participant correlation of auditory or tactile temporal-order sensitivity and tapping simultaneity. We further explored how subjective simultaneity was determined using a hand-foot simultaneous tapping task. Our results suggest that humans can achieve temporally precise movement of two body parts more easily than we can discriminate these movements based on auditory or tactile information, though the movements may nevertheless be produced so that the two sensory feedback signals become simultaneous.

We often need to make simultaneous movements of multiple body parts to perform various motor tasks in daily life, including playing the piano and the drums. There have been studies on the mechanism by which we synchronize our action to an external rhythmic events (Repp, 2005; Repp & Su, 2013; Roy, Dalla Bella, & Lagarde, 2017) and on the mechanism by which we detect inter-sensory synchronization (Chen & Vroomen, 2013; Stein, 2012). However, little is known about the mechanisms involved in simultaneous voluntary movement of different body parts.

There are several possible events in the neural processing pathway that the brain tries to synchronize when moving different body parts. When we produce an action (e.g., tapping of a finger), a motor command is produced in our brain and transmitted to a motor organ to bring out a tapping action. Then, the action causes physical consequences, which are detected by sensory organs and transmitted to the brain as sensory feedbacks (e.g., tactile sensation from tapping, impulsive sound, and visual feedback). It is not clear which of these sensori-motor events is/are used to perform and maintain simultaneous tapping.

An important example of simultaneous movement in different body parts is bimanual tapping, which is necessary for activities such as playing musical instruments. However, in bimanual tapping, the sensory and motor pathways have almost the same transduction delay for both hands, and the relevant timing for performing simultaneous tapping cannot be dissociated completely. Therefore, we also used the hand-foot tapping task to overcome this limitation. If the brain produces simultaneous motor commands, movements in the hand should precede those in the foot due to the transduction delay in motor commands. In contrast, if the brain attempts to simultaneously receive tactile feedback signals, sensory signals from the foot should precede those from the hand because tactile sensory signals need more time to reach the brain. Another possibility is that the brain compensates for the delay in motor and sensory signals (Harrar & Harris, 2005) to achieve actual simultaneous tapping. By investigating hand-foot tapping, we can identify

these possibilities and gain an insight into the mechanism involved in simultaneous body movement.

In this paper, we investigated the mechanism of simultaneous movement in different body parts by examining bimanual and hand-foot simultaneous tapping in detail. First, we measured the temporal interval of bimanual tapping, and investigated how it could be related to the temporal discriminability of sensory perception, assessed as the temporal threshold of tactile and auditory temporal-order judgment. Next, using the hand-foot tapping task, we aimed to dissociate the timing used to achieve simultaneous tapping of the hand and foot.

Method

Seventeen (15 male and 2 female) people participated in the bimanual tapping task and the perceptual temporal-order judgment (TOJ) task. One male participant was excluded from the following analyses because the participant was unable to perform the tactile TOJ task. Six out of the remaining 16 participants also participated in the hand-foot tapping task. These experiments were approved by the ethics committee at the University of Electro-communications.

Bimanual and Hand-Foot Tapping Tasks

In the bimanual tapping task, participants sat on a chair and naturally placed their hands on tables located on both sides of the chair. Tapping was monitored using contact microphones (AKG, C411PP), which were placed on the surface of the tables near the participants' fingers, and the signals from the microphones were recorded using an audio-interface device (Roland, OCTA-CAPTURE) at a 96-kHz sampling rate. Participants were instructed to close their eyes and tap the tables using their right and left index fingers as simultaneously as possible. They were instructed to continue the tapping task at their own pace, without making a periodic rhythm. The experiment was divided into 3 sessions with a short break between the sessions. Each session was approximately 3 min long.

In the hand-foot tapping task, participants placed one foot (e.g., left foot) on a board located on the floor and tapped the thumb finger of the foot simultaneously with the index finger of the hand on the other side (e.g., right hand). The side of the hand/foot to be used was counterbalanced across participants. Other experimental details were the same as in the bimanual tapping task.

Perceptual Temporal-Order Judgement Tasks

In the perceptual TOJ tasks, participants sat on a chair and a pair of either tactile or auditory stimuli were presented to them. The participants judged which of the two stimuli, right or left, was presented first. In the tactile TOJ task, the participants placed both hands at nearly the same position as those in the bimanual tapping task, and short ($\sim$ 1 ms) tactile stimuli were delivered to their index fingers using vibrating devices. Stimulus onset asynchrony (SOA) between right and left stimuli was randomly chosen for each trial from -100 ms to 100 ms (plus sign indicates right stimulus first) with 10-ms intervals. Each SOA was repeated 10 times, for a total of 210 trials. In the tactile condition, white noise was always presented via headphones to block sounds from the vibrator. In the auditory

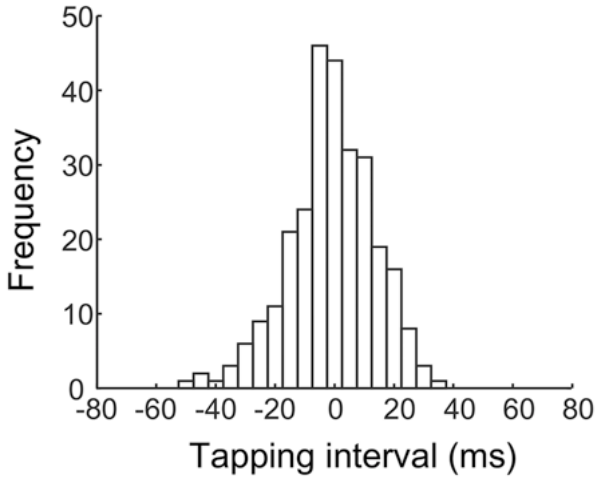

Fig. 1. Histogram of tapping interval for a representative participant. Plus sign indicates that the right hand was tapped before the left hand.

TOJ task, a pair of short "click" sounds were presented via two loud speakers (Bose, MM-1) placed near the participants' hand in the bimanual task. The SOA between the right and left stimuli were also randomly chosen from -100 ms to 100 ms with 10-ms intervals, but without 0 ms SOA in the auditory condition. Each SOA was repeated 10 times, for a total of 200 trials.

In both tasks, participants were instructed to close their eyes and their task was to identify the stimulus that was presented first by pressing either the left or right foot switch placed on the floor.

The results of the TOJ tasks were fitted to a cumulative Gaussian psychometric function, and the point of subjective simultaneity (PSS) and the just noticeable difference (JND), defined as the temporal difference between PSS and either 75% or 25% judgment rate point, were calculated for each participant and task condition.

Results

Most participants performed temporally precise bimanual tapping, distributed around an almost 0 ms temporal interval (Fig. 1 for a representative participant.) The precision, i.e., the standard deviation, of tapping was about 10 ms and surprisingly uniform across participants (Fig. 2.) The JNDs for the tactile and auditory TOJ tasks were roughly in the 30–40 ms range (Fig. 2) and much worse than the tapping precision (paired t-test, $p < 10^{-4}$), suggesting that both tactile and auditory sensory feedbacks are not temporally sensitive enough to reliably compensate for the temporal delay between tapping. As additional evidence that the sensory feedback is not directly relevant to tapping precision, we checked the across-participant correlation between tapping precision and sensory JNDs (Fig. 3). The results clearly show that there was no correlation between tapping precision and temporal sensitivity in sensory perception ($p = 0.86$ for tactile and $p = 0.49$ for auditory result as an output of MATLAB's corrcoef function).

Next, we analyzed hand-foot tapping to investigate whether sensory feedback contributes to the adjustment of the accuracy of simultaneous multiple tapping in different body parts. The results show that the foot was tapped first (Fig. 4, t-test, $p = 0.048$) in

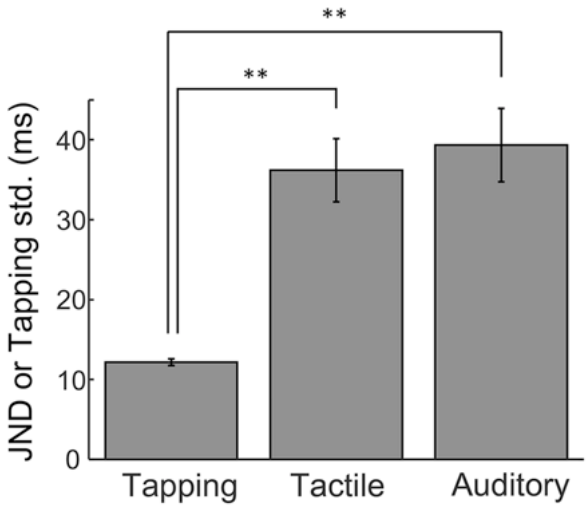

Fig. 2. Comparison between the standard deviation of bimanual tapping and the just noticeable difference (JND) of the tactile or auditory TOJ task. The error bars show their standard error across participants ($^{**}p < 10^{-4}$).

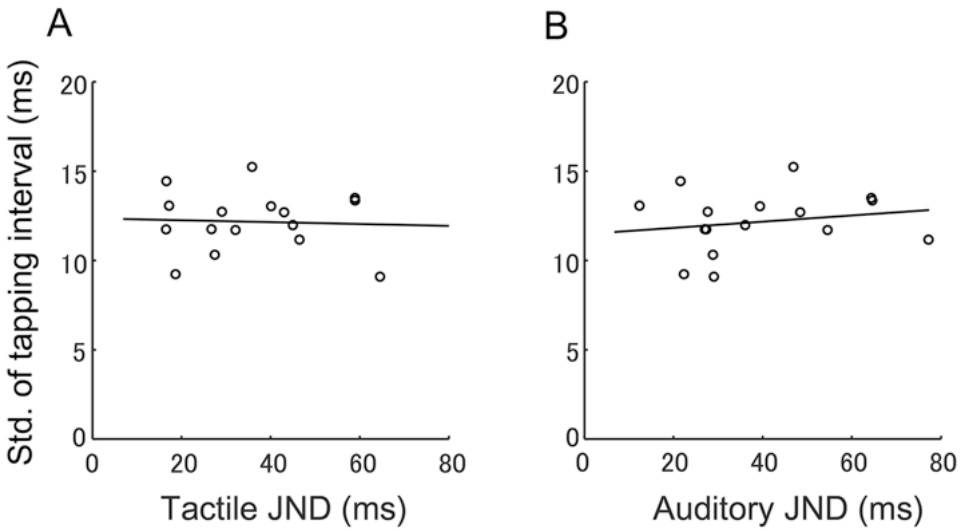

Fig. 3. Scatter plots for just noticeable difference (JND) in A) tactile and B) auditory tasks vs. standard deviation of the tapping interval in the bimanual task. The solid lines indicate linear regression.

the hand-foot tapping task, even though tapping was simultaneous on average in the bimanual tapping task (t-test, $p = 0.58$), and the mean temporal interval for the hand-foot task was significantly different ($p = 0.019$). This result is consistent with the idea that the simultaneity of hand-foot tapping is based on the timing of sensory feedback from tapping rather than other factors like motor commands.

Discussion

In this study, we aimed to elucidate the mechanism of simultaneous tapping in different body parts. First, we showed that bimanual tapping had high temporal precision and

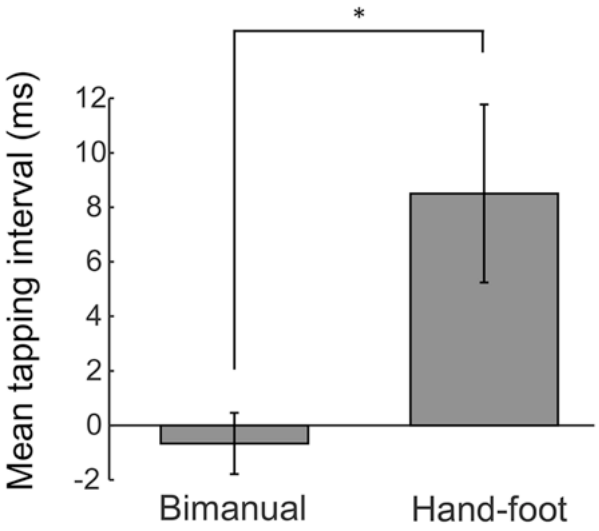

Fig. 4. Mean tapping interval in bimanual and hand-foot tapping tasks. In the bimanual condition, plus sign indicates right hand tapped earlier. Note that the result is normalized for the hand-foot condition so that the plus sign indicates that a foot tapped first. The error bars represent the standard error across participants ($^*p < 0.05$).

both tactile and auditory sensory feedbacks could not provide enough sensory feedback to achieve such high temporal precision.

On the other hand, using a hand-foot simultaneous tapping task, we also showed that the simultaneity of hand-foot tapping was based on the timing of sensory feedback rather than other factors such as the timing of motor command production. We showed that tapping of the foot must precede that of the hand by about 8 ms on average for them to be perceived as simultaneous. This is comparable to the previously reported temporal difference (11.5 ms) between tactile stimuli to a hand and a foot required to be judged as perceptually simultaneous (Bergenheim, M., Johansson, H., Granlund, B., & Pederson, 1996). This suggests that simultaneous hand-foot tapping is almost completely based on the perceived temporal difference in sensory feedback.

Overall, our results suggest that the mean temporal interval of simultaneous tapping is dependent on sensory feedback, but the feedback is not precise enough to improve the temporal precision of tapping, thus simultaneity precision in trial-by-trial tapping might mostly reflect the precision of another neural process such as synergetic motor commands.

Acknowledgements

This study is partially supported by JSPS KAKENHI Grant Number 16K16071 and 26280101.

References

Bergenheim, M., Johansson, H., Granlund, B., & Pederson, J. (1996). Experimental evidence for a synchronization of sensory information to conscious experience. In *Toward a Science of Consciousness: the First Tucson Discussions and Debates* (pp. 303–310).

MIT Press Cambridge, MA.

Chen, L., & Vroomen, J. (2013). Intersensory binding across space and time: a tutorial review. *Attention, Perception & Psychophysics,* 75(5), 790–811.

Harrar, V., & Harris, L. R. (2005). Simultaneity constancy: detecting events with touch and vision. *Experimental Brain Research,* 166(3–4), 465–73.

Repp, B. H. (2005). Sensorimotor synchronization: a review of the tapping literature. *Psychonomic Bulletin & Review,* 12(6), 969–992.

Repp, B. H., & Su, Y.-H. (2013). Sensorimotor synchronization: A review of recent research (2006–2012). *Psychonomic Bulletin & Review,* 20(3), 403–452.

Roy, C., Dalla Bella, S., & Lagarde, J. (2017). To bridge or not to bridge the multisensory time gap: bimanual coordination to sound and touch with temporal lags. *Experimental Brain Research,* 235(1), 135–151.

Stein, B. E. (Ed.). (2012). *The New Handbook of Multisensory Processing.* MIT Press Cambridge, MA.

THE IMPORTANCE OF VESTIBULAR INPUT AND THE ENVIRONMENT TO EARLY CHILD DEVELOPMENT AS DETERMINED THROUGH PSYCHOPHYSICAL PRINCIPLES

Patricia Hannan[1], Millard F. Reschke[2], and Eugene Galanter[3]
[1]*PlayWisely LLC, Dallas TX, USA*
[2]*NASA Neuroscience, Johnson Space Center, Houston TX, USA*
[3]*Psychophysics Laboratory, Columbia University, New York NY, USA*
<coachpatty@playwisely.com>

Adaptation to the gravitational vector must be considered in the ecology of early child development. Proprioceptive/vestibular interactions occur as early as the first synapse in the brain. This interaction is a critical catalyst to the proper development and functioning, required for efficient learning and movement ability. The recent rise of sensory processing issues coinciding with demands for STEM literacy requires us to consider how recent cultural changes have impacted a child's natural experience within the gravitational vector and how changes driven by this interaction may be impacting the quality of future learning and movement ability. Viewing human development through the lens of psychophysical principles will illustrate the critical impact gravity has upon optimal sensory system function and physical development.

We will present a psychophysical model that demonstrates how gravity profoundly affects the form and function of human development. Sensory systems require gravity to function optimally and have critical periods for development. Core motor, sensory, perception and cognitive systems are in place and develop relatively rapidly after birth. Through a complex choreography of quantity and quality of experiences within the gravity vector a human develops the sensory processing systems necessary for efficiently navigating the psychosensory field and body field. Analyzing human development utilizing our knowledge of neural navigation architecture, planes of space, axis of motion and haptic awareness we can employ a psychophysical model providing a new platform for observing, measuring and analyzing human development.

Technological and medical advancements and an increasingly mobile society is affecting the natural trajectory of human development. Screen time replacing physical play, infants sleeping on backs instead of in prone, and restrictive devices including car seats all limit a child's mobility within the gravity vector. Repetition and intensity of stimuli is required for stabilizing neural pathways and hopefully reducing unnecessary redundant information. A lack of sufficient duration and intensity of biologic system experience within the gravity vector plausibly contributes to the rise in sensory processing and integration disorders, including dyslexias, attention deficit disorders and autism, conditions where information may be overwhelming and the child unable to inhibit the redundant information.

Psychophysical science is based upon the assumption that a quantitative relationship exists between environmental stimuli and sensory perception. Extending traditional Fechnarian principles to include the gravity vector and the development of biologic systems a new psychophysical model can be realized. This model presents the opportunity for new assessments, interventions, technologies and programs to address the rise in sensory processing issues and prepare young minds to thrive in a changing world demanding STEM literacy.

Part XIII
Symposium 2—The 2nd International Five-Sense Symposium

An Introduction to Symposium 2: The 2nd International Five-Sense Symposium

Symposium Organizers: Lihan Chen, Yoshitaka Nakajima, and Kiyoshi Toko

How different sensory modalities work together in various situations will be discussed with persuasive examples, and the dynamic nature of our perception in real life will be clarified. This symposium is a second attempt to put researchers studying different sensory modalities together for intensive discussion.

TACTILE IMAGES FOR THE VISUALLY IMPAIRED VISITORS OF MUSEUMS

Yang Wenzhen[1], Luo Jiali[1], Wu Xinli[1], Jiang Zhaona[1], Qiu Ke[2]
[1] *Virtual Reality Laboratory Zhejiang Sci-Tech University, Hangzhou, China, 310018*
[2] *Shanghai Shangte Culture Communication Company, Shanghai, China, 201206*

Abstract

At present, there is almost no way for the visually impaired visitors to feel the museum collections, which are not allowed to be touched in many museums. How to get closer to the distance between the visually impaired visitors and the museum, the tactile image is an effective method. Through the image-based 3D printing technology, this paper uses a 3D tactile images method for the blind to recognize the museum collections. This paper also proposes an improved JSEG algorithm based on the image tactile sensing model with region features. The digital images of the museum collections are used to restore the tactile characteristic of the collections, which allow the blind to feel the collections by the tactile feedback devices. Experimental results show that the proposed algorithm can segment image regions more accurately, and improve the accuracy of image tactile perception.

According to WHO statistics, there were 285 million visually impaired persons worldwide (the best corrected visual acuity of less than 0.3). Text recognition technology converts text information into sound, which enables the blind to obtain text information through their hearing. However, how can the blind obtain the information conveyed by an image? Touch is almost the only way for the blind.

Although many museums are open for free, an invisible divide has prevented the visually impaired visitors because the vast majority of the museum collections are prohibited to be touched (Cock et al., 2015). For the visually impaired visitors, there are few specially designed museums to display some replica models of cultural relics, valuables or art objects. Visually impaired visitors can use their fingers to feel the contours of these replica collections, and draw the outline of these collections in their minds (Raša et al., 2016). In addition, some of the museums customize some replica collections for the visually impaired visitors. But these replicas have a long production cycle, limited categories, limited numbers and high cost. It is difficult to satisfy the needs of the visually impaired visitors.

We envisage using blind touchpads to display the museum collections. So the blind can touch the contour of the museum collections conveyed from the images of museum collections (Ping-Sing et al., 1994, Seales et al., 1995). The core of this idea is fast, and also inexpressive to create a variety of blind touchpads.

In this paper, two approaches are adopted to realize this idea. The first approach is to produce physical blind touchpads directly through the image-based 3D printing technology. The second approach is to display the digital images of the collections in the computer and generate digital blind touchpads, and then the blind recognizes the collections with the haptic feedback device.

Blind Touchpads of Museum Collections

We propose an image-based 3D printing technology that uses 3D printers to make digital images of collections into blind touchpads. Haptic texture information restoration and object surface contour representation are the core contents of this technique. The surface roughness of the collections is expressed by each pixel height value, which is obtained on the digital images of collections using the pixel height value solving algorithm. And then the triangle meshes are used to construct the 3D profile of the collections. Finally, the blind touchpad is printed through a 3D printer.

Figure 1 shows the relics of Chinese ancient Fazan. The blind can touch the Fazan touchpads recovered from the Fazan 2D image to understand the ancient women's hair accessories. Figure 2 is Mr. Sun Zhongshan's calligraphy. The traditional view believes we can understand cultural works only through vision, like calligraphy and ink paintings. Therefore, these have almost no relationships with the blind. With this technique, we can

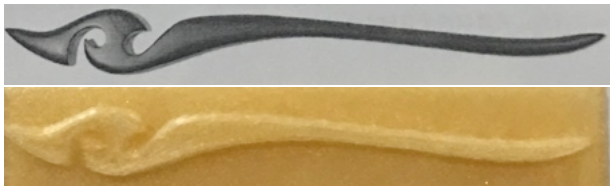

Fig. 1. Chinese ancient Fazan.

Fig. 2. Calligraphy .

Fig. 3. Costume patterns and oracle bones.

easily manufacture the blind touchpads of cultural works, so as to benefit the blind. For examples, such as the Chinese costume pattern, oracle bones (Figure.3) etc., we use this technique let the blind recognize them that can be visually understood by touch.

Because the channel to acquire the digital images of the collections is remarkably convenient, the technique is simple, fast and cheap to print a variety of touchpads for the blind recognizing museum collections.

Tactile Images for Digital Blind Touchpads

The tactile information, such as, uneven surfaces (roughness), compliance (friction and stickiness), and softness (stiffness and flexibility), help visually impaired visitors to understand the museum collections. Usually, the tactile information lies on the different regions of tactile images. So, reasonable regional division of images is the key to produce digital blind touchpads (tactile images).

The regional division is to extract the regional characteristics of images. Many algorithms of image regional division have been proposed (Deng et al., 2001; Deng et al., 1999; Wesolkowski et al., 2001; Hanmandlu et al., 2004), such as area division based on edge detection, regional division based on region growth, regional partitioning based on wavelet transform, regional division based on statistical theory, and region division based on texture etc. Not all of these algorithms are suitable for the generation of tactile images, because it is necessary to not only obtain reasonable regions of images, but also to minimize the time complexity but ensuring the authenticity of tactile perception. Here, we propose an improved JSEG (Joint Systems Engineering Group) algorithm, which can obtain reasonable image regions and achieve more realistic tactile information of images in real-time.

The JSEG algorithm has the phenomenon of over-partitioning (Hertzmann et al., 2005), and it needs to be improved in multi-scale template matching, the iterative calculation based on the color histogram, the region division process and the algorithm time complexity. After quantifying the color, we use the incremental seed region growth method to form the initial division area on the basis of the class diagram, and eliminate the process of selecting the seeds with the local value iteration. The merging process based on the color histogram is replaced by the region merging of the fusion edge contour information.

The improved JSEG algorithm takes into account the color and spatial edge information, which can be divided into two parts. First, the initialization of the image region is completed by using an incremental region growing method for color-quantized images. Then, considering the regional color, edge and adjacency, the regional distance is calculated, and the similarity regions are merged into different stages to form a rule to stop the region merging until the condition is completed.

The Initial Division of the Image

Based on the JSEG algorithm, we use the incremental region growth method to complete the initial segmentation of an image. The seed region of the pixel is defined to meet the following conditions:

1) The color is the same after quantization;

2) The area of seed region shall reach a certain proportion of whole image area (according

to the difference in the accuracy of the division, the proportion shall be 0.001%, 0.01%, 0.1%).

Pixels that are not in the seed region are assigned to the nearest neighbor region, if it satisfies the independent conditions:

1) Constituting four neighborhoods in the pixel space with other new grown seed regions;

2) The average distance of these pixels is less than the average distance of seed regions;

3) Satisfying the proportion conditions of the seed regions.

By this way, it is possible to form a new seed region, which is more favorable for the discovery of some detail regions, and the algorithm time complexity is relatively lower compared with JSEG algorithm, which selects the seed region under different multi-scale template matching.

Region Merging

Calculations of region distance for region merging. The region distance is an important parameter for the region merging, and affects the quality of the region division. Suppose that there are $|r_i|$ and $|r_j|$ pixels in the region i and region j, respectively, $\overrightarrow{u_i}$ and $\overrightarrow{u_j}$ denote the color mean of the region i and j respectively, and the color distance D_{ij}^c can be expressed as:

$$D_{ij}^c = \frac{|r_i| \cdot |r_j|}{|r_i| + |r_j|} \| \overrightarrow{u_i} - \overrightarrow{u_j} \|. \tag{1}$$

Based on Canny operator, the edge distance formula is defined as:

$$D_{ij}^e = \frac{1}{|E_{ij}|} \sum_{(k,1 \in E_{ij})} \| \overrightarrow{X_k} - \overrightarrow{X_1} \|. \tag{2}$$

Where $|E_{ij}|$ is the number of pixels on the edge of region i and j, $\overrightarrow{X_k}$ and $\overrightarrow{X_1}$ are the color values of pixel k and pixel l on both sides of the edge. In addition, if region i is adjacent to region j, then we set $\Delta_{ij} = 1$, otherwise $\Delta_{ij} = +\infty$. So, the region distance is calculated:

$$D_{ij}^r = (D_{ij}^c)^p \cdot (D_{ij}^e)^q \cdot \Delta_{ij}. \tag{3}$$

In the process of regional merging, this paper adopts the hierarchical merging strategy, which starts from the smallest area, merges in an incremental way, and adjusts the new regional distances after regional merging.

Termination rules for region merging. Termination rules for region merging directly determine the quality of regional division. Usually, the JSEG algorithm adopts the threshold method to stop the region merging. The region distance is continually calculated based on color histogram, and the threshold should be adjusted according to different images. Here, we propose a new criterion for terminating the region merging, which is based on the relationship between the loss of color information and the ratio of the number of remaining regions in the process of zone merging to the total number of initial regions. The areas where the colors in the merged area are not uniform and the areas reserved at the time of termination are merged, both of which achieves the best compromise. That is,

when the minimum value is obtained, it can be understood that when the emerged area is as low as possible, the degree of un-uniform of the color to be the lowest, the region merging is stopped.

Here, we use within-class scatter for the region merging, J_w^r denotes the color dispersion of a region in the image, and J_t is the color dispersion of the whole image. So, we define the color uniformity J_1 as follows:

$$J_1 = \frac{\sum_{r=0}^{k_1} J_w^r}{J_t}. \tag{4}$$

After regional division, we use the within-class scatter to calculate the color dispersion, and number the regions according to the increasing order of color dispersion.

Post-processing phase. When region merging is completed, the post-processing phase is to remove the noise, smooth boundary of the image, and improve the image quality. This paper uses a circular area, whose radius is 3 pixel distance, to expand and corrode the image after region division.

Experiments

Region division experiments

In order to validate the improved JSEG algorithm, we develop an image tactile perception system based on the VS2010 platform. Three images (see Figure 4) were tested for the comparisons between the JSEG algorithm and our improved JSEG algorithm.

From the comparisons of three images, we observe that our improved JSEG algorithm is better to distinguish the main region of three images, improve the quality of region division relative to the JSEG algorithm. For the calligraphy image in Figure 4, the division result of JSEG algorithm is over-partitioned, and the watermark is obvious. For the teapot image in Figure 4, because of the unevenness of the surface brightness of the teapot, the JSEG algorithm divides the teapot into too many regions, such as the shadow of teapot. For the woman portrait image in Figure 4, there are also too many regions segmented by JSEG algorithm, such as the forehead regions. However, the results of our improved JSEG algorithm shall be more consistent with the subjective visual. The improved JSEG algorithm can obtain reasonable regions, which are benefit for the recovery of tactile information.

Table 1 lists the time complexity comparisons. This improved JSEG algorithm is more effective than the JSEG algorithm.

Table 1. Time complexity comparisons (unit: s).

Images	JSEG algorithm	Improved JSEG algorithm	Relative time is reduced
1	16.37	14.56	11%
2	9.88	9.32	5%
3	18.05	16.22	10%
average	14.76	13.37	9%

(a)Original images (b) JSEG division results (c) Our algorithm division results

Fig. 4. Regional division comparisons.

Image tactile perception experiments

In the image tactile perception system, we use triangle meshes to display tactile textures, and use PHANTOM Omni device to feedback the tactile information.

We use six images (See Figure 5) to test the effectiveness of the image tactile perception system. We selected 10 subjects, including 6 men and 4 women, from 22 to 51 years old. During the process of experiments, the subjects can't see these images and the test order of images are randomly arranged. We required the subjects to recognize these images through tactile perceptions delivered by the PHANTOM Omni device. Subjects used PHANTOM Omni device to touch the texture, contour and softness of tactile images, gave their judgements about these six images.

Experimental results are shown in Table 2. The correct rates of image recognition are higher. For (b), (e) and (f), all of subjects can recognize them, and they said the contours of these images are very obvious to be touched. For (a) and (d), two subjects make error judgement because of too complex textures. The subjects indicated that there are obvious tactile differences among image regions, and the tactile perception of these

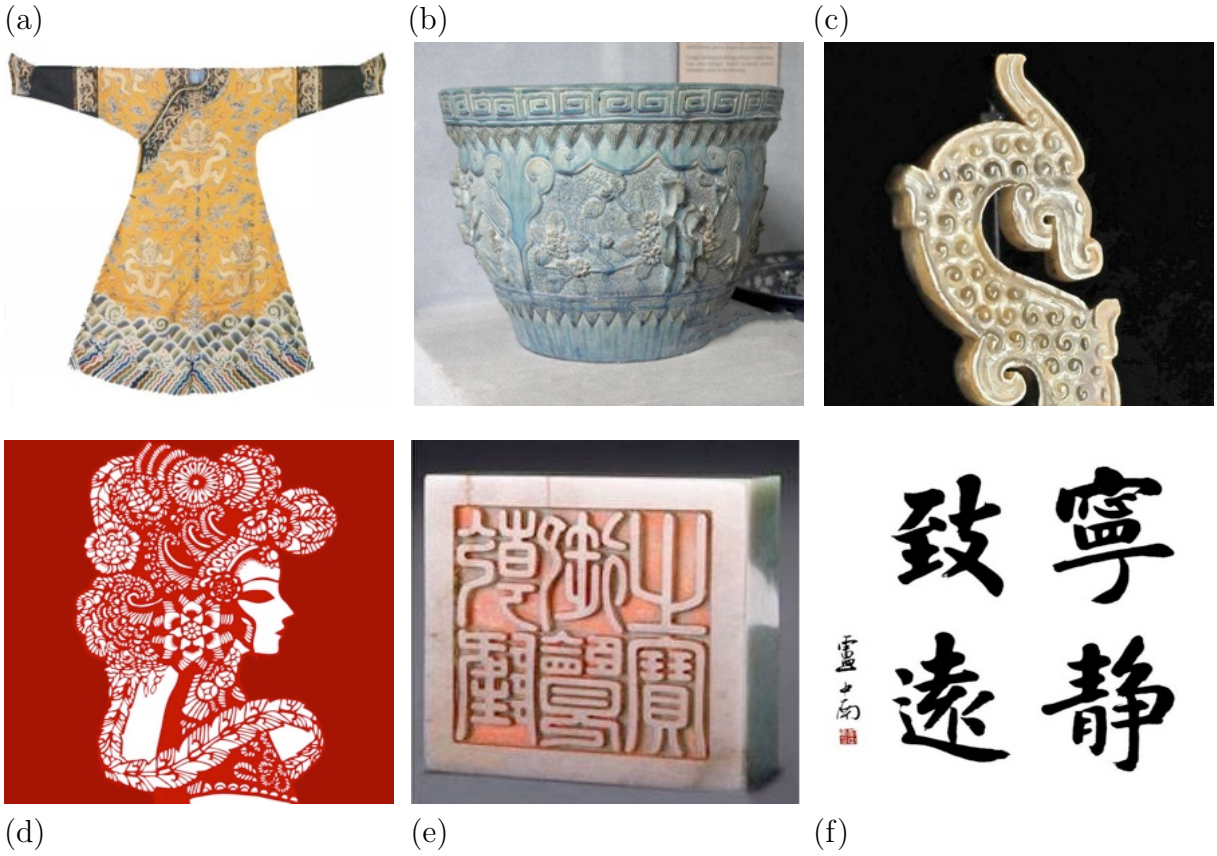

Fig. 5. Tactile images with reasonable regions.

Table 2. Correct rates of image recognition among 10 subjects.

Subjects	(a)	(b)	(c)	(d)	(e)	(f)	Correct rates (%)
1	√	√	√	√	√	√	100
2	×	√	×	√	√	√	66.7
3	√	√	√	√	√	√	100
4	√	√	√	√	√	√	100
5	√	√	√	√	√	√	100
6	√	√	√	√	√	√	100
7	√	√	√	×	√	√	83.3
8	×	√	√	×	√	√	66.7
9	√	√	√	√	√	√	100
10	√	√	√	√	√	√	100
Correct rates (%)	66.7	100	90	66.7	100	100	

images is satisfactory.

Conclusions

Tactile image is an effective method to narrow the distance between visually impaired visitors and museums. Through the image-based 3D printing technology, this paper uses a 3D tactile images method for the blind to recognize the museum collections. We also develop

an image tactile perception system, which is based on an improved JSEG algorithm.

This system is able to spread the digital museum collections across the limitations of time and space, so that the visually impaired visitors through the virtual tactile perception interact with precious collections. The system lets the blind perceive the collections of soft or hard, roughness or flexibility, and other non-visual information, with unique and irreplaceable experiences. Furthermore, this virtual touch for the visually impaired visitors conveys the cultural connotation of collections, historical civilization, and the connotation of cultural relics.

This study will help the blind to obtain digital image information through touch. In the interactive experience of museums, the revolutionary of this technique is to turn the command human-computer interaction into the tactile human-computer interaction, so that visitors can "truly" touch museum collections. Under the combined functions of vision, touch and human brain imagination, visitors can touch and manipulate the "collections", and this will provide people unprecedented interactive experiences.

Acknowledgements

This study was supported by Zhejiang Province Public Welfare Project of China (No. 2016C33174), Key Project of the National Natural Science Foundation of China (No. 61332017), Zhejiang Provincial Natural Science Fund Project of China (No. LY13E050025).

References

Cock M, Saeed K. (2015). Help the Blind Access your Collections. *Museums Journal,* 5(11), 5-15.

Raša U, Matej P. & Urška E. (2016). Development of Tactile Floor Plan for the Blind and the Visually Impaired by 3D Printing Technique. *Journal of Graphic Engineering and Design,* 7 (1), 19-26.

Ping-Sing T. & Shah M. (1994). Shape from shading using linear approximation. *Image & Vision Computing,* 12(8), 487-498.

Seales B. & Faugeras D. (1995). Building Three-Dimensional Object Models from Image Sequences. *Computer Vision and Image Understanding,* 61(3), 308-324.

Deng Y. & Manjunath S. (2001). Unsupervised segmentation of color-texture regions in images and video. *IEEE Transactions on Pattern Analysis & Machine Intelligence,* 23(8), 800-810.

Deng Y. (1999). Peer Group Filtering and Perceptual Color Image Quantization. *IEEE International Symposium, Circuits and System,* 4, 21-24.

Wesolkowski S. & Fieguth P. (2001). Color image segmentation using a region growing method, In *the 9th Congress of the International Color Association,* Canada: Edmonton.

Hanmandlu M. Madasu K. & Vasikarla S. (2004). A Fuzzy Approach to Texture Segmentation. *International Conference on Information Technology: Coding and Computing Proceedings,* 636-642.

Hertzmann A. & Seitz M. (2005). Example-based photometric stereo: shape reconstruction with general, varying BRDFs. *IEEE Transactions on Pattern Analysis & Machine Intelligence,* 27(8), 1254-1261.

ODOR-INDUCED AROUSAL DISSOCIATES FROM PERCEIVED OLFACTORY INTENSITY AND VALENCE

Wei Chen, Fangshu Yao, Bin Zhou, and Wen Zhou
Institute of Psychology, CAS Key Laboratory of Behavioral Science
CAS Center for Excellence in Brain Science and Intelligence Technology
Chinese Academy of Sciences
University of Chinese Academy of Sciences
<chenwei@psych.ac.cn, yaofs@psych.ac.cn,
zhoub@psych.ac.cn, zhouw@psych.ac.cn>

Emotional experience is commonly considered to build upon two fundamental dimensions, valence and arousal. With olfactory stimuli, perceived odor intensity has been treated as a surrogate for subjective arousal despite abounding anecdotes that certain odors are generally energizing whereas others are calming. We assessed the possibility that odor-induced arousal is dissociable from perceived odor intensity and valence with the attentional blink paradigm and resting-state magnetoencephalograms. The results indicated that continuous exposure to citral as opposed to vanillin profoundly altered T2 detection accuracy in the attentional blink task and decreased resting-state alpha oscillation, both pointing to increased subjective arousal, despite that the two odorants were matched in both perceived intensity and valence.

THE MULTISENSORY NATURE OF THE BODY: INSIGHTS FROM THE MOVING RUBBER HAND ILLUSION

Andreas Kalckert
School of Psychology, University of Reading Malaysia, Educity
72900 Iskandar, Johor, Malaysia

In recent years there is an increasing interest in the experience of the body. Perceptual illusions like the rubber hand illusion created new avenues in the experimental investigation of the bodily self. It gave researchers a tool to manipulate the experience of the body in a controlled experimental setting, in which participants perceive a model hand as part of their own body. This so-called sensation of ownership is a consequence of the integration of visual and tactile stimuli applied to the hand. Studies have shown that the integration of these stimuli adheres to principles found in multisensory integration.

In this talk I will introduce the basic principles of this illusion, and compare these to a different variant of this paradigm, which is based on movements instead of tactile stimulation. This moving rubber hand illusion involves a different set of sensory cues (kinaesthestic information), but results in an identical or similar experience of ownership. These studies, and also others, have shown that the experience of body ownership relies on multiple sensory cues, and that different combinations of these can give rise to the experience of the body, as long these follow basic principles of multisensory integration.

This line of research represents an interesting example of how perceptual processes with specific perceptual features give rise to higher order experiences like self-awareness.

DETECTING A TOUCH THAT WASN'T THERE: INTRODUCING THE SOMATIC SIGNAL DETECTION TASK (SSDT) IN EXAMINING SENSORY INTEGRATION

Treshi-marie Perera
School of Psychology and Clinical Language Sciences, University of Reading Malaysia

Research suggests that vision modulates perception of sensory events. In relation to this, a task irrelevant visual stimulus presented in conjunction with a tactile stimulus not only increases detection of the tactile event, but also leads to false or *illusory* tactile perceptions when none is present (Johnson et al., 2006). The Somatic Signal Detection Task (SSDT; Lloyd et al., 2008) is a simple tactile detection task requiring the detection of tactile stimuli (present in 50% of trials) regardless of whether or not they were accompanied by visual stimuli. In line with previous studies, the task has revealed an increase in both correct and illusory tactile reports in the presence of the task irrelevant visual stimulus. Using signal detection theory (MacMillan and Creelman, 1991) analyses, the SSDT allows determining whether changes in tactile detection are driven by tactile sensitivity (*d'*—an individual's ability to discern between signal and noise) or response criterions (*c*—tendency to positively report feeling touch, regardless of whether or not it was present). As such, the task serves as an excellent means of examining the mechanisms driving altered sensory integration in a variety of research and clinical settings. In this talk, I will discuss past and potential future applications of the SSDT in investigating the mechanisms driving sensory integration in clinical and research settings—particularly, in relation to research relating to somatic perception.

MULTISENSORY INTEGRATION AND TELEOPERATION IN VIRTUAL REALITY

Lihan Chen[1–3]*, Qiongyu Wang[1], Nicholas Katzakis[4], Frank Steinicke[4], Fang Fang[1–3,5,6]
[1]*Psychological and Cognitive Sciences, Peking University, Beijing, 100871, China*
[2]*Beijing Key Laboratory of Behavior and Mental Health*
Peking University, Beijing, China
[3]*Key Laboratory of Machine Perception (Ministry of Education)*
Peking University, Beijing, China
[4]*Department of Informatics, Universität Hamburg*
[5]*Peking-Tsinghua Center for life sciences*
[6]*PKU-IDG/McGovern Institute for Brain Research*
*Correspondence: <CLH@pku.edu.cn>

Abstract

Effective dexterous human-robot interaction requires the understanding of how the enormous amount of sensory information (e.g., visual, tactile, proprioceptive and kinaesthetic) is integrated and how the coupling between perception, action planning (execution) and learning is resolved. The reliance on spatial and temporal constraints as principle of functional appropriateness for multisensory integration was examined in virtual reality, rendered through head-mounted display (HMD). Here we reported three examples: audiovisual integration under perceived far/near psychological distances, coupling of perception and action for distance estimation in peripersonal fovea/periphery space, sensory reshaping effect in which visual stimuli can change the qualitative properties of haptic stimuli. The results indicated that in virtual reality, we are more tolerant for the spatio-temporal disparities between sensory events. Moreover, psychologically 'weak' sensory signals gain the benefits from multisensory integration, although the crossmodal correspondence is subject to recalibration and hence leads to a certain degree of perceptual bias.

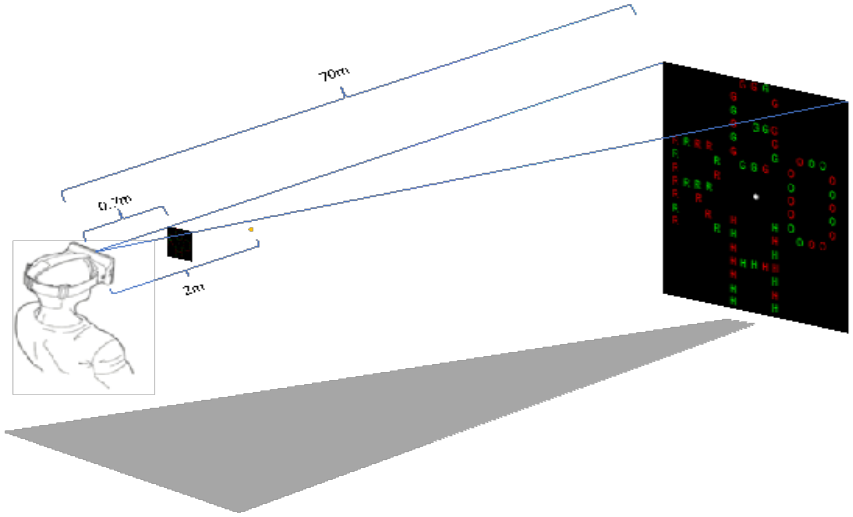

Fig. 1. Audiovisual (temporal) integration with Navon letters in virtual reality.

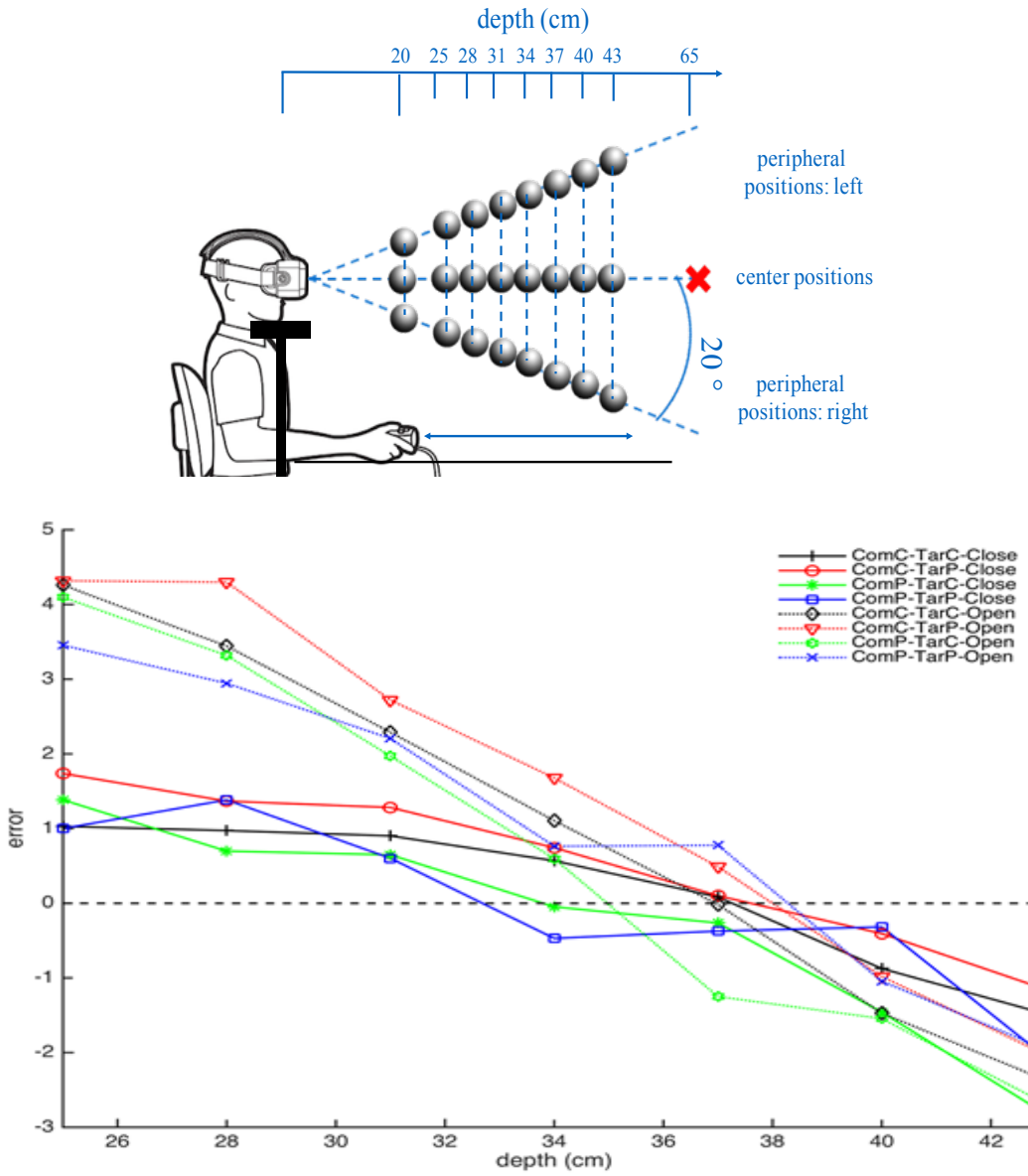

Fig. 2. Visual-tactile integration for depth perception in virtual reality. Left: experimental setup. Right: biased depth perception as a function of visual depth, open/close loop for tactile feedback and central fovea/periphery visual field correspondence.

Firstly, to explore how visual information is represented in visual working memory under multisensory context, we presented Navon letters either at near or far distances in a virtual reality environment, with or without concurrent sounds. We hypothesized that auditory influence upon the representation of VWM would differ with respective to the perceived distance in depth between audiovisual stimuli, where the short distance make the observers focus on the fine details of the individual elements while the far distance guide them to pay attention on the global outline (Liberman & Förster, 2009). The results showed an overall global precedence effect, while precision of visual working memory encoding was hampered when the visual object was presented at far distance with asynchronous sounds (Figure 1). This study has ecological implications for studying memory representation in real multisensory scenario.

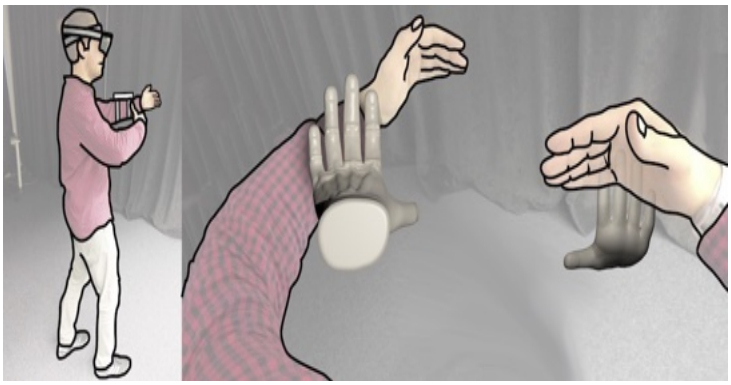

Fig. 3. Illustration of Stylo/Handifact in an interactive t'ai Chi training system. The visualization in the right image shows two virtual hands displayed on an augmented reality head-mounted display that indicate motion corrections to the practitioner: the left Handifact is pushing the practitioner's arm away from the torso, whereas the right Handifact is pushing the arm (from the opposite side) closer to the torso.

A genuine perception of the space and understanding of the action in the given peripersonal space is essential for effectively controlling a remote robot system. Therefore, in a second study, we examined spatial perception in a virtual reality setup by analysing how users perceive distances in the peripersonal space (Van der Stoep et al., 2015), with open-loop control in which the operators received tactile feedback information about the current state of their controlling body part. We believe that the benefits of closed-loop scenarios lie in the increased precision and efficiency for dexterous operation. We implemented a 2 (tactile feedback: closed-loop vs. open-loop) $\times$ 2 (comparison's position: center vs. periphery) $\times$ 2 (target's position: center vs. periphery) within-subject design, with blocked comparison's position and target's position. Participants wore Oculus-Rift CV1 head-mounted-display and PZT tactile components to right fore-finger for tactile feedback. The virtual environment was rendered in Unity 3D. We used two Optitrack cameras to capture the hand/arm's motion. The results showed an overestimation bias at near distance, and an underestimation at far distance. Tactile feedback improved the accuracy for visual depth discrimination under cross-modal context (Figure 2).

In a third study, with the framework of Sino-German 'crossmodal learning' project (TRR 169), we developed Stylo-Handifact, which is a novel spatial user interface consisting of a haptic device (i.e., Stylo) attached to the forearm and a visualization of a virtual hand (i.e., Handifact) (Piateski & Jones, 2005), which in combination provide visuo-haptic feedback for posture training applications, such as in yoga, t'ai Chi, dance, training, or martial arts. We evaluated the mutual effects of Handifact and Stylo on visuo-haptic sensations in a series of psychophysical experiments. Results indicated the functional domiance of visual spatial processing (Welch & Warren, 1980). A visual stimulus can modulate the perceived strength of a haptic stimulus by more than 5%. With a wrist docking task, we showed that Stylo-Handifact results in improved task performance (with reduced completion time) compared with the on-going state-of-art technique (Figure 3).

Acknowledgements

The above studies were supported by grants from the Natural Science Foundation of China (NSFC)(31200760, 61527804) and partially funded by the NSFC and the German Research Foundation (DFG) in project Crossmodal Learning, NSFC 61621136008/DFG TRR-169.

References

Liberman, N., & Förster, J. (2009). The effect of psychological distance on perceptual level of construal. *Cognitive Science,* 33(7), 1330–1341.

Piateski E, Jones L, 2005 Vibrotactile pattern recognition on the arm and torso. *Proceedings of the First Joint Eurohaptics Conference and Symposium on Haptic Interfaces for Virtual Environment and Teleoperator Systems, Pisa, Italy* (Los Alamitos, CA: IEEE Computer Society) pp 90–95.

Van der Stoep, N., Nijboer, T. C. W., Van der Stigchel, S., & Spence, C. (2015). Multisensory interactions in the depth plane in front and rear space: A review. *Neuropsychologia,* 70, 335–349.

Welch, R.B., & Warren, D.H. (1980). Immediate Perceptual Response to Intersensory Discrepancy. *Psychological Bulletin,* 88, 638–667.

EVALUATION OF FOOD CRISPNESS BY USING SOUND EMISSION DURING BITING OR CHEWING

Takahisa Nishizu
Department of Applied Life Science, Gifu University, 501-1193 Gifu, Japan
<nishizu@gifu-u.ac.jp>

The Zen monks are warned against making chewing sounds when they eat. It is usually rude to make noises loudly while eating. However, it is difficult to eat without making any sound. Indeed, when gnawing and chewing pickles, apples, and rice crackers, the chewing sounds that can be heard will be inevitably produced. Eating food and sound cannot be separated from each other.

In Japanese it is often expressed in onomatopoeia such as *paripari, pari,* and *garigari.* Those words remind us the feeling when we are chewing. There are the similar expressions in other languages as well. The sound heard by the ear when eating food is one of the factors to make it delicious.

Szscesniak et al. reported the results of a word association test that had been conducted on one hundred employees from General Foods Corporation (Szczesniak and Kleyn, 1963). According to their report, the results of texture, flavor, color, form or temperature, appearance, aroma, and others were listed in the order of most responses. Spence had conducted the similar questionnaire with an evaluation item related to "hearing" added. He reported that the role of auditory information in palatability evaluation was almost naught (Spence, 2015). However, on the other hand, people know that crispness is synonymous with freshness in many fruits and vegetables. Therefore, people prefer the crispy lettuce of BLT sandwiches, even though people are not conscious of the auditory information (Spence, 2015). In that sense, sound is the forgotten flavor sense (Spence, 2015). The perception of hearing while eating is strongly influenced by the textural characteristics of food material. Because a chewing sound is a vibration caused by oral destruction or breakdown of food material, it could reflect the textural characteristics as destructive characteristics. In ISO 11036: 1994, "texture" is defined by the following: All the mechanical, geometrical and surface attributes of a product perceptible by means of mechanical, tactile and, where appropriate, visual and auditory receptors (ISO 11036, 1994).

In the presentation, we focus on the sound generated while eating the crispy or crunchy foods.

References

Szczesniak, A.S., & Kleyn, D.H. (1963). Consumer awareness of texture and other food attributes, *Food Technol.,* 17, 74–77.

Spence, C. (2015). Eating with our ears: assessing the importance of the sounds of consumption on our perception and enjoyment of multisensory flavor experiences, *Flavour,* 4:3.

ISO 11036 (1994). *Sensory analysis—Methodology—Texture profile.*

VISUAL ANALYSIS, MODULATION, AND CROOSMODAL EFFECT OF FOOD APPEARANCE

Katsunori Okajima
Faculty of Environment and Information Sciences, Yokohama National University
79-7 Tokiwadai, Hodogaya, Yokohama, Kanagawa 240-8501 Japan
<okajima@ynu.ac.jp>

Deliciousness cannot be determined by only taste or flavor of the food itself. Food appearance and the visual environment are also critical factors that affect the feeling of deliciousness of the dishes and beverages. For example, color and visual texture of food affect people's taste perception. However, the effects of food appearance have been unclear because it is difficult to prepare the same foods with different appearance.

We developed Augmented Reality (AR) systems that were capable of changing the color, shape and texture etc. of real foods or beverages in real time. By using the HMD-system with a camera, we conducted a series of experiments designed to investigate how the visual texture and appearance of food and beverage influences taste and flavor perception. Participants viewed a video of food (baked cake etc.) or beverage (coffee etc.) presented on a dish placed in front of them. We changed the color, the luminance histogram, and/or the visual texture of the food. The results demonstrated that people's perception of food and beverage can be modulated by changing the visual image. Especially, we found that we can modulate the softness/dryness of foods by controlling the luminance histogram without changing the color. The experimental results also showed that the taste/flavor of food and beverage can be modulated by changing the visual texture of the visual image cross-modally. For example, the visual texture of milk enhanced the flavor of milk in a coffee, and saturated color of orange juice increases the perceived density of the juice. In addition, we found that dynamic visual information; a virtual steam and a liquid motion with a modified viscosity, modifies beverage perception.

By using a Projector-Camera (Projection Mapping) system we developed, we also conducted a series of experiments. The food image on a dish was captured with a single camera, and the food region was extracted from the image using color cues. A digital projector projected a texture image created to fit the shape of the food area on the actual food. Participants estimated the sweetness of a cake with different colors using the present system. The results showed that the sweetness is significantly modified by controlling just only saturation of the food color without changing the food itself, suggesting that this system must be useful for controlling diet and for designing food appearance.

Acknowledgement

This work was supported by JSPS KAKENHI Grant Number 15H05926.

References

Spence, C. Okajima, K. Cheok, A.D. Petit, O. & Michel, C. (2016). Eating with our eyes: From visual hunger to digital satiation, *Brain and Cognition*, 110, 53-63.

Nishizawa, M. Wanting, J. & Okajima, K. (2016). Projective-AR System for Customizing the Appearance and Taste of Food, *Proceedings of 18th International Conference on Multimodal Interaction*, MVAR2016-Article#6.

TASTE SENSOR : ELECTRONIC TONGUE TO QUANTIFY TASTE

Kiyoshi Toko
Graduate School of Information Science and Electrical Engineering
Research and Development Center for Taste and Odor Sensing, Kyushu University
Fukuoka 819-0395, Japan

Gustatory sense is a kind of chemical Kansei (Fig. 1). A taste sensor, which was first developed in Japan, is a kind of electronic tongue with a property of global selectivity that implies ability to decompose the taste into basic taste qualities (sweetness, bitterness, sourness, saltiness, umami and sometimes astringency) and quantify them. Umami is the fifth basic taste independent of other taste qualities, elicited by seaweeds, mushrooms and meat, which was found by a Japanese researcher about 100 years ago. The taste sensor comprises several kinds of electrodes with a lipid/polymer membrane, and is sold by Intelligent Sensor Technology (INSENT), Inc. (Fig. 2). Over 400 taste sensor machines have been applied to many kinds of foods such as coffee, tea, meat, rice, bread, beer, milk, and wine, and have also been used to measure the taste of amino acids and medicines. It can provide a scale of taste, and can be utilized to produce new foods and medicines or control/monitor their qualities, and also demonstrate the taste property in the case of marketing. Since there are "musical scores" in our sense of hearing, we can reproduce the music of, for example, Bach or Beethoven today. If we can invent "food scores" in the sense of taste, we would be able to preserve and transmit food scores, and then reproduce the taste and quality of the desired foods anytime, anywhere. Each sensor electrode of the taste sensor is specific to each taste quality in principle, with the low selectivity and high cross-selectivity instead of high selectivity to each chemical substance, as in the case of gustatory system. The taste sensor can measure the aftertaste felt by humans using the CPA (Change in membrane Potential due to Adsorption of chemical substances) measurement, which reflects the amount of chemical substances adsorbed onto the membrane and the surface charge density of the membrane. Therefore, koku or kokumi, which is a kind of enhanced aftertaste of basic taste qualities, can be estimated using the taste sensor. Research and Development Center for Taste and Odor Sensing, Kyushu University was established about four years ago based on the success of the taste sensor.

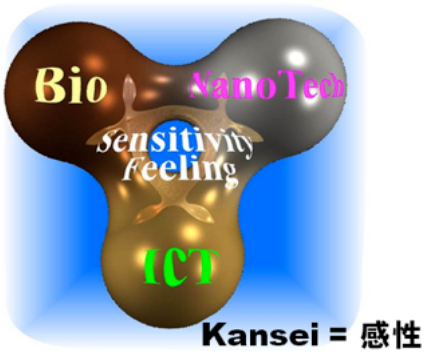

Fig. 1 To express chemical Kansei.

Fig. 2 Taste sensor (Taste-sensing system, TS-5000Z, Intelligent Sensor Technology, Inc.).

ODOR SENSING, VISUALIZATION, AND APPLICATION

Kenshi Hayashi
Department of Electronics, Information Science and Electrical Engineering
Kyushu University, 819-0395 Fukuoka, Japan
<hayashi@ed.kyushu-u.ac.jp>

Abstract

Techniques for objective evaluation of quality and quantity of odor substances are required to resolve issues related to volatile chemical compounds. In this study, two odor visualization methods are presented; odor quality visualization and odor space visualization. Odor quality is difficult to be expressed by quantitative data or linguistic words. Odor sensation is brought about by various kinds of volatile compounds; therefore, quantitative measurements of odor must detect such numerous chemicals. In this study, the odor quality visualization is realized by the odor cluster map observed in biological olfactory system, which can be synthesized with molecularly odor code information via sensors having molecular recognition abilities. On the other hand, the odor space visualization has been achieved by an odor image sensor development; the sensor can spatially visualize the shape, spread and concentration distribution of odor substances, which never be detected with sense of sight. Optical methods are adopted based on fluorescent probes and high-speed localized surface plasmon resonance (LSPR) film, where odor molecules alter the optical properties of the probes through molecular associations to the probes. These odor visualizations produce completely novel chemical space information that can be applied for explosive or harmful chemical leakage detection, human lifesaving, agricultural ICT, forensic science, or medical diagnosis.

In recent years, techniques for objective evaluation of quality and quantity of odor substances are required to resolve various issues such as odor nuisance, medical diagnoses, gas explosions and poisoning gas detections. In this paper, two odor visualization methods are presented; odor quality visualization and odor space visualization (Imahashi 2013, Liu 2013, Yoshioka 2015).

Odor quality is difficult to be expressed by quantitative data or linguistic expression because human brain has not been developed to evaluate olfactory sensation like sense of sight. Odor sensation is brought about by various kinds of volatile compounds; therefore, quantitative measurements of odor must detect such numerous chemicals. In biological olfactory system, an odor cluster map, which is produced on the surface of the olfactory bulb through olfactory receptors, is essential information to evaluate odor quality of the odorant. The odor quality visualization is realized using similar images based on the odor cluster map, which can be synthesized with molecularly odor code information via sensor signal having molecular recognition abilities such as molecular imprinted polymer and peptide aptamers (Imahashi 2013).

On the other hand, odor space visualization has been achieved by an odor image sensor development; the sensor can spatially visualize the shape, spread and concentration distribution of odor substances, which never be detected with sense of sight. This visualization can be realized using optically operated gas sensors.

Visualized odor quality and space can be processed our sense of sight effectively. Therefore, the obtained data is easy to understand, and can be used various application

using conventional pattern recognition analyses, such as human detection, biometrics (Jha 2016), detection of poisonous gases, design of odor space in virtual reality, and agricultural ICT (evaluation of agricultural product and growth control of plants).

Method

Odor quality visualization are examined via activated map on olfactory bulb, where clusters of activated glomeruli are formed based on physicochemical properties of the odorants. Open data on the olfactory map are evaluated using various multivariate analyses (Johnson 2007). And relationship between odor expression words and molecular properties, or odor cluster maps are also examined.

Odor space visualization are realized using various optical methods, such as fluorescent probes and 2 dimensional plasmonic gas sensors. Molecular recognizing materials are also important to detect each odorant selective. For selective gas sensing, MIP (molecularly imprinted polymer) and MIFA (MI filtering adsorbent) are used. Surfaces of plasmonic gas sensor using localized plasmonic resonance of metal nanoparticles are covered with molecular selective materials. These optical sensors can be observed by ordinal video systems, and the 2 dimensional optical probes give the spatio- and temporal-changes of odor space.

Results and Discussion

Odor Quality Visualization

Figure 1 shows the results of the analyses of odor cluster maps, where the important molecular parameters are obtained (Imahashi 2015). Such parameters can be used for the design of odor sensors. The sensor system which can selectively evaluate odor molecules

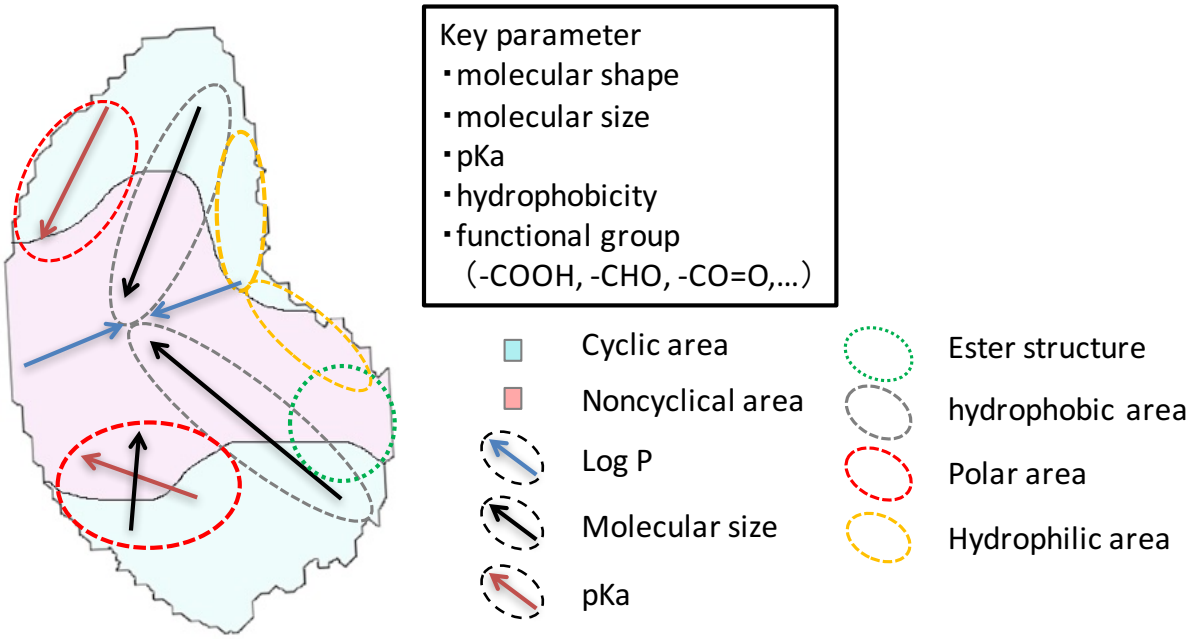

Fig. 1. Molecular parameters and olfactory map.

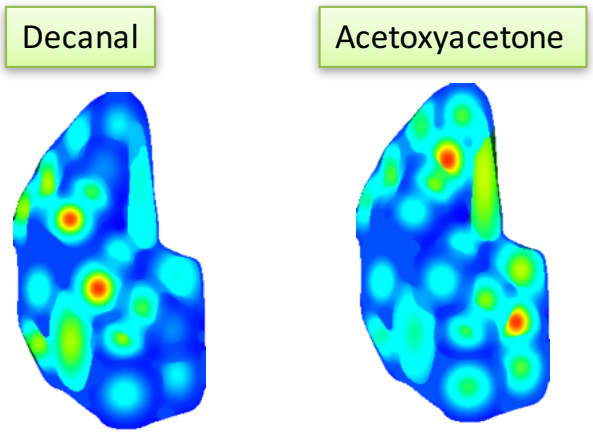

Fig. 2. Examples of artificially generated olfactory maps based on molecular parameters of each odorant.

by appropriate parameters will give sufficient information about corresponding olfactory cluster maps. The visualized map information might be good key to suggest the odor quality and to understand the odor of the molecule.

The odor cluster maps can be generated artificially if the molecular parameters of a certain odor molecule are obtained with experimental (e.g. odor sensor system having parameter sensitivity) or computational (e.g. molecular modelling software) methods. It means that we can visualize odor qualities of the molecules using the generated map. Figure 2 shows two examples of calculated olfactory maps. The estimated maps are activated pattern appeared on the olfactory bulb, therefore, essential information of odor quality might be included in the map.

Odor Space Visualization

Figure 3 shows some examples of odor visualization with odor image sensing setup for fluorescent gel films. Gas flow detections, which are measured with fluorescent probe gel films, can be applied for odor source localization. Palm odor visualization can be used for forensic application or biometrics. Odor from plant leaf can be used to evaluate conditions of plant growth and can be applied for agricultural ICT, where odor visualization techniques give much information for evaluation of agricultural product and growth control

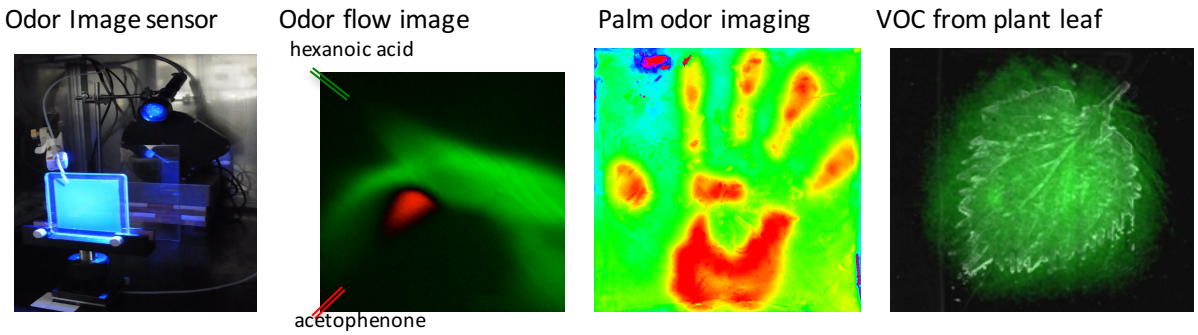

Fig. 3. Examples of visualized odor space.

in agricultural field.

Using the odor imaging technique, we realized various odor visualization, such as, high speed gas flow detection using LSPR MIP sensor (Chen 2016, Liu 2013), region segmentation of visualized odor (Yoshioka 2015), extraction and estimation of elemental odorants and concentration which composed odor images (Yoshioka 2015), and distribution of human body odor adhering on clothes.

The visualized odor images are the information which have not been used by biological system so far. The values of the information are not sure at present because no living system have not used the odor images, however, our surrounding world is composed of various volatile chemicals (VOCs) and almost all things can be distinguished with odor information. Consequently, the odor information will give highly valuable information for various application relating mixture of VOCs.

References

Chen B, Liu C, Ge L, Hayashi K (2016). Localized surface plasmon resonance gas sensor of Au nano-islands coated with molecularly imprinted polymer: Influence of polymer thickness on sensitivity and selectivity, *Sens. Actuators B,* 231, 787–792.

Imahashi M, Hayashi K (2013). Concentrating materials covered by molecular imprinted nanofiltration layer with reconfigurability prepared by a surface sol–gel process for gas-selective detection, *J. Colloid. Interf. Sci.,* 406, 186–195.

Imahashi M, Hayashi K (2014). Odor Clustering Based on Molecular parameter for odor sensing, *Sens. Materials,* 26, 171–180.

Jha SK, Josheski F, Marina N, Hayashi K (2016). GC–MS characterization of body odour for identification using artificial neural network classifiers fusion, *Int. J. Mass Spectrometry,* 406, 35–47.

Johnson BA, Leon M (2007). Chemotopic odorant coding in a mammalian olfactory system, *J. Comp. Neurol.,* 503, 1-34.

Liu C, Furusawa Y, Hayashi K (2013). Development of a fluorescent imaging sensor for the detection of human body sweat odor, *Sens. Actuators B,* 183, 117–123.

Yoshioka H-T, Liu C, Hayashi K (2015). Multispectral fluorescence imaging for odorant discrimination and visualization, *Sens. Actuators B,* 183, 117–123.

Part XIV
Free Talk Session 8

A NEW PROBABILISTIC APPROACH TO DESCRIBING THE STREAM OF DECISION-MAKING EVENTS NEAR PERCEPTION THRESHOLD

Ihor Lubashevsky and Kosuke Hijikata
University of Aizu
Ikki-machi, Aizu-Wakamatsu, Fukushima 965-8580, Japan
IL: <i-lubash@u-aizu.ac.jp>

Abstract

Within the paradigm of human intermittent control over unstable systems human behavior admits the interpretation as a sequence of point-like moments when the operator makes decision on activating or halting the control. These decision-making events are assumed to be governed by the information about the state of system under control which the operator accumulates continuously. In the present work we propose the concept of reinforcement learning with decision inertia (the status quo bias) that opens a gate to applying the formalism of reinforcement learning to describing human intermittent control. The basic feature of such reinforcement learning is that human behavior in a sequence of selecting available options exhibits quasi-continuous dynamics. Numerical simulation based on a fairly simple model demonstrates that the proposed formalism does possess the required properties of quasi-continuous behavior.

Model Background

Nowadays human intermittent control has become a dominant paradigm of describing human behavior in controlling various unstable systems (for a review see, e.g., Loram et al., 2011). It assumes a human operator to activate and, then, halt the control alternately instead of keeping it active continuously though the whole course of actions. The event-driven mechanism of human intermittent control is now accepted to be the main mechanism governing such human actions. According to the event-driving scenario the operator activates the control when the state of controlled system deviates from the desired one substantially and halts the control when this difference becomes rather small and the operator cannot recognize or affect it with a required accuracy. The threshold model of control activation is rather popular in mathematical description of human intermittent control. It assumes an operator to activate the control when the difference between the current and desired states exceeds a certain threshold and to halt it in the opposite case. However, recently (Zgonnikov et al., 2014) based on experiments on balancing overdamped pendulums, we proposed a novel concept of control activation. It is called the noise-induced activation and implies the control activation to be probabilistic in nature. In particular, the noise-induced activation represents a certain interplay between the necessity of starting the control process and the possibility of postponing it until this necessity becomes absolutely clear.

The formalism of reinforcement learning allows for such aspects in adopting to changing environment and finding an optimal choice via the trial-error strategy (see, e.g., Frank and Claus, 2006). Unfortunately, this approach on its own cannot be applied directly to describing human intermittent control. The matter is that on time scales much larger than the elementary step the produced decision-making process is strongly discontinuous. Conversely, the desired decision-making process must demonstrate the choice of the same option on scales comprising many elementary steps of decision-making. This

human behavior can be captured turning to the notion of decision inertia. Decision inertia can arise via some mechanism by which a human operator (agent) prefers not to change a chosen option for a relatively long time interval comprising a large number of elementary steps. In particular, it is the status quo bias well-known in economics (Samuelson and Zeckhauser, 1988). Recently Akaishi et al. (2014) found this type phenomenon in direct experiments with human decision-making in a situation similar to human intermittent control.

The introduction of decision inertia opens a gate to describing human intermittent control as (i) continuous accumulation of information about the state of controlled system and (ii) the sequence of events when the subject makes decision on changing the control state in response to the accumulated information.

The goal of presented work is developing a reinforcement learning model that allows for decision inertia. Actually, the present work proposes a fairly simple model for reinforcement learning with status quo bias and demonstrates that it does meet the desired property of quasi-continuous dynamics. The gist of this model is the concept of multichannel information processing used previously (Zgonnikov and Lubashevsky, 2014) to describe human learning affected by novelty-seeking (intrinsic motivation).

Model

An agent is assumed to make repeated choice between finite number of options $i \in [1, N]$ and accumulate the information about them, which in turn affects their choice probability. The processing of information is considered to be implemented through two independent mental channels. One of them is the deliberate analysis of obtained rewards. The other is irrational and exhibits status quo bias which can be explained turning to a reason like this: "If just now I have chosen a new option it is not reasonable to choose another option immediately, it could be better to wait some time until the quality of the chosen option becomes clear." The two channels interact via their cumulative effect on the option selection (Fig. 1).

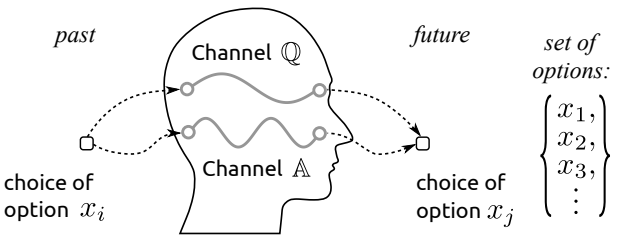

Fig. 1. Two channels of information processing: the channel $\mathbb{Q}$ via which the information about the rewards is processed and the channel $\mathbb{A}$ dealing with the information not directly related to the rewards.

Within the channel $\mathbb{Q}$ each option i is related to the corresponding reward r_i the agent receives each time it has chosen the given option. The preference of choosing option i is quantified by a value q_i; the value q_i results from the experience the agent gains each time it chooses the corresponding option. Namely, at every time step $t_k = k\tau \quad (k \in \mathbb{N})$ the preference values q_i are updated with currently received rewards $r_{q,i}$ and, besides, subjected to the memory loss:

$$q_i(t_{k+1}) = q_i(t_k) + \delta_{ii_k} r_{q,i} - \epsilon_q q_i(t_k)\,, \tag{1}$$

where the index i_k points to the option chosen at the given time step t_k and the value $0 < \epsilon_q < 1$ quantifies the agent memory capacity $\propto 1/\epsilon_q$. The second term on the right-

hand side of Eq. (1) containing the Kronecker delta δ_{ii_k} ($\delta_{ii_k} = 1$ if $i = i_k$ and 0 if $i \neq i_k$) reflects our assumption that only the preference value of chosen options is increased by the obtained rewards. In the present analysis the effects of forgone payoffs as well as different evaluation of rarely or frequently chosen options by humans can be omitted. Below time will be measured in units of the elementary time step τ between the neighboring decision-making events.

The channel $\mathbb{A}$ allows for the effect of status quo bias on choosing the same option at the next time moment. This effect is taken into account through some additional preference value $\Delta_i > 0$ to choose the same option i. This value decreases if the same option i has been chosen again, otherwise, it increases with a certain saturation, namely:

$$\Delta_i(t_k) = \Delta_i(t_{k-1})(1 - \epsilon_a) + (1 - \delta_{ii_k}\delta_{ii_{k-1}})r_{a,i}\,, \tag{2}$$

where the coefficient $r_{a,i}$ specifies the restoration of the status qua bias measure Δ_i for the option i when it has not been chosen. The given model imitates the human preference to wait for a certain time $T_a \sim 1/\epsilon_a$ to recognize the quality of the made choice.

The proposed model assumes the channels $\mathbb{Q}$ and $\mathbb{A}$ to be mutually independent, which implies that the resulting probability of choosing any option i is just the product of their individual contributions. Besides, we consider that only the difference between the preference values has physical sense. Under such conditions the probability of choosing option i is

$$p_i = \frac{1}{Z}\exp\left\{\beta\left[q_i + \Delta_i\delta_{ii_{k-1}}\right]\right\}, \tag{3}$$

where the normalization coefficient Z is determined by the expression

$$Z = \sum_{i=1}^{N}\exp\left\{\beta\left[q_i + \Delta_i\delta_{ii_{k-1}}\right]\right\}. \tag{4}$$

Expression (3) is the mathematical implementation of the concept of fuzzy perception threshold for the given system; for example, the choice between two options becomes practically equiprobable when the difference in their cumulative preference quantities is comparable with the perception threshold $1/\beta$.

It should be noted that the obtained expressions admit the interpretation in terms of transitions to another state j provided currently the state i have been chosen. Namely, the probability of this transition can be written as

$$\mathcal{P}_{i\to j} = \frac{1}{Z_i'}\exp\left\{\beta\left[q_j - q_i\right]\right\}\,,$$

and the probability of choosing the same option i given by the expression

$$\mathcal{P}_{i\to i} = \frac{1}{Z_i'}\exp\left\{\beta\Delta_i\right\}\,.$$

Here the normalization factor Z_i' now depending on the current state i is related to the previous one, Ex. (4), as $Z_i' = Z\cdot\exp\{\beta q_i\}$.

Results and Conclusion

To illustrate the characteristic features of the proposed model the system with two options $i = 1, 2$ symmetric in properties ($r_{q,1} = r_{q_2} = r_q$ and $r_{a,1} = r_{a_2} = r_a$) was studied

numerically. In the numerical simulation time is measured in units of τ and the preference values are measured in units of the perception threshold $1/\beta$. The particular values of system parameter were set equal to $T_q = 1/\epsilon_q = 30$, $T_a = 1/\epsilon_a = 30$, and $Q_{\max} = r_q T_q = 2.5$, $D_{\max} = r_a T_a = 10$. In this case the agent actions should exhibit substantial status quo bias.

Figure 2 demonstrates the obtained results. We see that after selecting an option the agent keeps the made choice for a relatively long time. As a consequence the shown time patterns of difference in the option priorities $(q_1 - q_2)/2$ and, e.g., the status quo bias measure Δ_2 do admit the interpretation as piece-wise continuous dynamics. Finally, the distribution of option life time—the time during which the same option is chosen continuously—mainly comprises values much larger than the elementary time step τ. In particular, its maximum for the analyzed system is about $\tau_{\text{life}} > 40$.

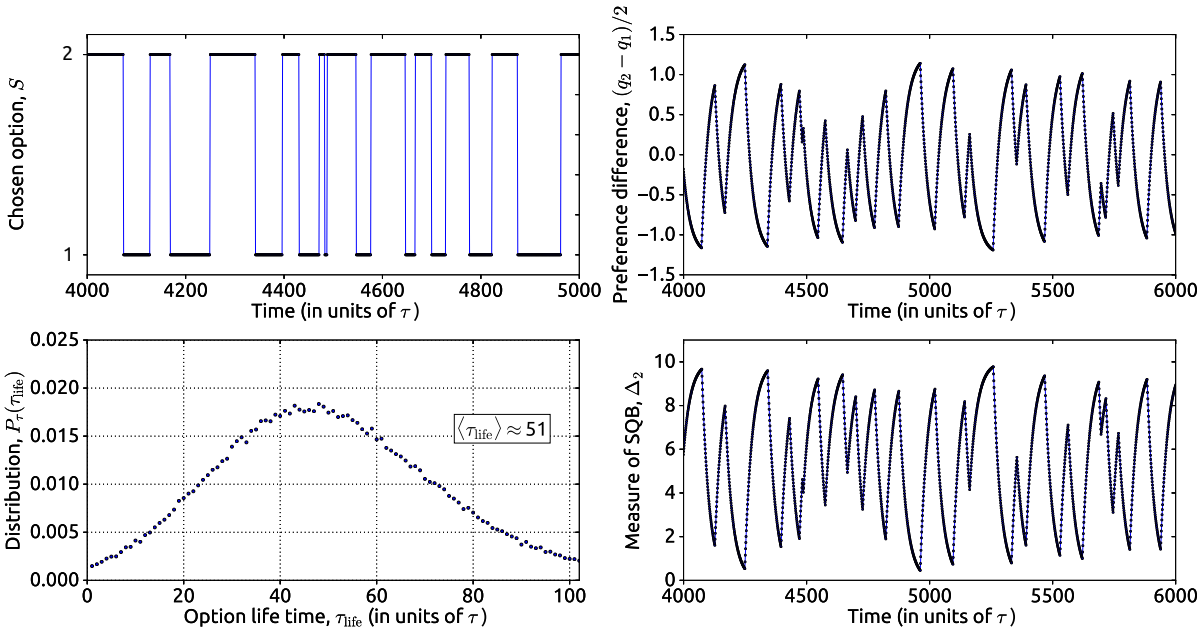

Fig. 2. Time patterns and statistical properties of reinforcement learning dynamics for the system with two equivalent options whose choice is affected by the status quo bias.

In summary, the proposed formalism of reinforcement learning with decision inertia opens a gate toward constructing theories of human intermittent control dealing with (*i*) intentional actions of operators activating or halting the control depending on the system state and (*ii*) allowing for the bounded capacity of human cognition. The main premise of this formalism is the existence of two independent channels of the information processing in the human mind. They are

- a channel responsible for the deliberate analysis of the obtained rewards and ordering them according to their preference; it is the standard component of all the models for reinforcement learning;
- a channel stimulating a subject not to change the current choice and keep it for a certain time interval.

As demonstrated, under such conditions the reinforcement learning with decision inertia can generate time patterns of subject's actions admitting the required smoothness of the

discontinuous stochastic process mimicking, in particular, human actions in controlling unstable mechanical objects.

References

Akaishi, R., Umeda, K., Nagase, A. and Sakai, K.: 2014, Autonomous Mechanism of Internal Choice Estimate Underlies Decision Inertia, *Neuron* **81**(1), 195–206.

Frank, M. J. and Claus, E. D.: 2006, Anatomy of a decision: striato-orbitofrontal interactions in reinforcement learning, decision making, and reversal., *Psychological Review* **113**(2), 300–326.

Loram, I., Gollee, H., Lakie, M. and Gawthrop, P.: 2011, Human control of an inverted pendulum: is continuous control necessary? Is intermittent control effective? Is intermittent control physiological?, *The Journal of Physiology* **589**(2), 307–324.

Samuelson, W. and Zeckhauser, R.: 1988, Status quo bias in decision making, *Journal of Risk and Uncertainty* **1**(1), 7–59.

Zgonnikov, A. and Lubashevsky, I.: 2014, Unstable Dynamics of Adaptation in Unknown Environment due to Novelty Seeking, *Advances in Complex Systems* **17**(3 & 4), 1450013 (17 pages).

Zgonnikov, A., Lubashevsky, I., Kanemoto, S., Miyazawa, T. and Suzuki, T.: 2014, To react or not to react? Intrinsic stochasticity of human control in virtual stick balancing, *Journal of The Royal Society Interface* **11**, 20140636.

AN OBJECT-FREE ALGORITHM FOR GENERATING BIOLOGICAL MOTION STIMULI FROM NATURAL MOVIES

Wataru Suzuki and Noritaka Ichinohe
Department of Ultrastructural Research, National Institute of Neuroscience
National Center of Neurology and Psychiatry
4-1-1 Ogawa-Higashi, Kodaira, Tokyo 187-8502, Japan;
Ichinohe Neural System Group, Laboratory for Molecular Analysis of Higher Brain Functions, RIKEN Brain Science Institute, RIKEN
2-1 Hirosawa, Wako, Saitama 351-0198, Japan

Hiroshige Takeichi
Computational Engineering Applications Unit
Advanced Center for Computing and Communication (ACCC), RIKEN
2-1 Hirosawa, Wako, Saitama 351-0198, Japan;
Department of Developmental Disorders, National Institute of Mental Health
National Center of Neurology and Psychiatry
4-1-1 Ogawa-Higashi, Kodaira, Tokyo 187-8553, Japan

Atsuko Gunji
Department of Developmental Disorders, National Institute of Mental Health
National Center of Neurology and Psychiatry
4-1-1 Ogawa-Higashi, Kodaira, Tokyo 187-8553, Japan;
Department of Advanced Neuroimaging, Integrative Brain Imaging Center
National Center of Neurology and Psychiatry
4-1-1 Ogawa-Higashi, Kodaira, Tokyo 187-8551, Japan;
College of Education, Yokohama National University
79-2 Tokiwadai, Hodogaya, Yokohama 240-8501, Japan

Masumi Inagaki
Department of Developmental Disorders, National Institute of Mental Health
National Center of Neurology and Psychiatry
4-1-1 Ogawa-Higashi, Kodaira, Tokyo 187-8553, Japan

Abstract

We have developed an object-free algorithm for extracting motion information from natural movies by estimating the dynamics of the local normal vectors of the image intensity projected onto the x-y plane. Here, we used the algorithm to generate random dot movies from 60 movies of moving animals. We then tested whether six healthy adult male observers could identify which of two similar random dot movies matched the original movie. The participants made forced-choice judgments on the correspondence between the original movie and the two random dot movies, which were presented normally, temporally reversed, and vertically inverted. The participants showed better-than-chance performance. The results provide a basis for broader application of the algorithm, which could also be used to expand the paradigms used in biological motion studies, most of which use point light walkers.

Motion in the visual environment provides a rich source of information for biological systems (Nakayama, 1985). Biological motion perception (Johansson, 1973) is a good

example. When several lights are attached to a person's body as markers and the person moves in total darkness, the time series of the images of the lighting markers, referred to as a point light walker, provides rich information about the age, gender, and even emotions of the marked person to human observers. This type of stimulus is called a biological motion stimulus. The perception of biological motion stimuli seems to be associated with social functions such as face- or voice-specific responses, which can be impaired in children with developmental disorders (e.g., Annaz, et al., 2012; Gunji et al., 2013; Hirai et al., 2014; Aglieri, et al., 2017).

Most studies of biological motion perception use point light walker stimuli because they enable robust extraction of rich information from complex motion. However, it is not easy to generate a comparable stimulus using a non-human animal or inanimate object as the actor. The use of more general or broader classes of stimuli is favorable for clarification of the neural substrates underlying intact and impaired biological motion perception in humans as well as animal models.

Thus, we have developed a novel algorithm for extracting motion information from natural movies to generate random dot movies (Suzuki et al., in press). In the previous study, we described the algorithm and a neurophysiological experiment on common marmoset (Callithrix jacchus). In this study, we conducted a psychophysical experiment to demonstrate a further application of the algorithm.

Methods

Ethics Statement. This study was approved in advance by the Ethical Committee of the National Institute of Neuroscience and Psychiatry (Kodaira, Japan). All participants gave written informed consent before participating in the experiment.

Participants. Six healthy men (mean age 38) with normal or corrected-to-normal visual acuity volunteered to participate in the experiment.

Stimuli. Details of stimulus generation are described by Suzuki et al. (in press). We made 60 random dot movies from 60 animal movies and divided them into 30 pairs with similar lower-order-motion properties. The pairs were based on six indices that were calculated for each random dot movie: the integrated moving distances in the x- and y-coordinates for all dots, the centroids of the moving distances for all dots during their appearance in x- and y-coordinates, and the distribution of the dots with a large moving distance around the centroid in the x- and y-coordinates. The six indices for all 60 random dot movies were normalized by calculating their z-scores. The Euclidean distances $D_{u,v}$ between two movies, u and v, were used to create pairs. Each pair of random dot movies was selected such that $D_{u,v}$ was minimized. Namely, the first pair comprised the movies with the lowest $D_{u,v}$, the second pair comprised the movies with the next lowest $D_{u,v}$, and so forth until all 30 pairs were formed.

Procedure. The participants sat 57 cm in front of a 19-inch (48 cm) CRT monitor. Head movement was minimized by a chinrest. The spatial resolution of the CRT monitor was 600 pixels in height and 800 pixels in width, and the refresh rate was 60 Hz. The size of the stimulus was 28.5 $\times$ 20.5 cm. The task was controlled using MATLAB (Mathworks, Natick, MA, USA) with the Psychophysics Toolbox. The experiment was carried out in a dark room. The 30 pairs of random dot movies were divided into three sets—stimulus

sets 1, 2, and 3—each consisting of 10 pairs. There were three sessions. The participants received one stimulus set in each session. Participants 1 and 2 received stimulus sets 1, 2, and 3, in Sessions 1, 2, and 3, respectively. Participants 3 and 4 received stimulus sets 2, 3, and 1, in Sessions 1, 2, and 3, respectively. Participants 5 and 6 received stimulus sets 3, 1, and 2, in Sessions 1, 2, and 3, respectively.

Session 1. The participants were asked to match a sample animal movie with a corresponding random dot movie in a temporal two-alternative forced-choice task. A trial started upon pressing the keyboard. A sample animal movie appeared for 1 s. After a 2-s delay in which a random-dot static mask was displayed, the first random dot movie appeared for 1 s. After another 2-s delay with the random dot static mask displayed, the second random dot movie appeared for 1 s. One of the random dot movies corresponded to the animal movie and the other corresponded to the paired movie. The participant pressed button "1" or "2" on the keyboard, depending on whether he judged the dot motion in the first or second random dot movie as corresponding to the animal motion in the sample animal movie. The trial ended when the participant responded. There were 10 trials in each session and each pair appeared only once, with the order of presentation pseudorandomized across participants. The participants were instructed to fixate on a cross presented at the center of the screen throughout the trial.

Session 2. The procedure was the same as that in Session 1, except that the frames of the two random dot movies were shown in reverse order (time-reversal condition). The participants were informed that the random dot movies were reversed.

Session 3. The procedure was the same as that in Session 1, except that the two random dot movies were spatially inverted so that they were upside-down (inverted condition). The participants were informed that the random dot movies were inverted.

Results

Session 1. We examined whether it was possible to match the original animal movie with the random dot movie using the motion information extracted by our algorithm. The participants' performance was 93.3 $\pm$ 8.17% (mean $\pm$ standard deviation, $n = 6$), which was significantly different from chance (50%) ($p < 0.05$, two-tailed binominal test).

Session 2. We examined whether it was possible to match the original animal movie with the random dot movie when it was presented in reverse order. The performance for the time-reversal condition was 93.3 $\pm$ 8.17% (mean $\pm$ standard deviation, $n = 6$), which was significantly different from chance (50%) ($p < 0.05$, two-tailed binominal test)

Session 3. We examined whether it was possible to match the original animal movie with when the random dot movie when it was presented upside-down. The performance for the inverted condition was 88.3 $\pm$ 11.7% (mean $\pm$ standard deviation, $n = 6$), which was significantly different from chance (50%) ($p < 0.05$, two-tailed binominal test).

Discussion

In this article, we describe our new algorithm for extracting motion information from natural movies. Our experimental results confirmed that human observers were able to match the original movie with the extracted motion presented as a random dot movie. Their performance was not impaired under the time-reversal condition, in which the velocity of the random dot motion was reversed, or the inverted condition, in which the spatial distribution of the random dot motion differed from that in the original movies; therefore, the results did not seem to reflect the early visual processing stage of motion detection (DeAngelis et al., 1995). Nor did the results exhibit the deterioration in performance observed under time-reversal and inverted conditions using point light walker stimuli (Sumi, 1984; Pavlova and Sokolov, 2000).

It could be argued that the matching performance in the psychophysical experiment was generally good simply because the motion patterns in the paired movies was sufficiently dissimilar that any motion extraction algorithm could have generated discriminable random dot movies; in other words, the high matching performance might not reflect the high performance of our algorithm in extracting object motion. However, it should be emphasized that the similarity indices for the pairs were calculated from the generated random dot movies, not the original animal movies, and that the pairs with high similarity indices could still be discriminated.

The proposed motion extraction algorithm can be applied to natural movies to generate visual stimuli. The algorithm can provide a variety of complex visual motion stimuli because it does not require parameterized geometric shapes. By applying the algorithm to various natural movies, it is possible to generate random dot motion stimuli for humans, non-human animals, and man-made moving objects. It is also possible to dissociate dynamic and static information because the visual motion stimuli do not contain static shape information and the objects cannot be identified unless they move. This algorithm should be useful for clarifying the critical factors and neural mechanisms underlying biological motion perception and social cognition through the visual modality.

In conclusion, we have described a psychophysical application of a new algorithm. The algorithm can be used to extract motion information from any natural movie and generate a random dot movie. The global motion of an object emerge from the computation of normalized local normal vectors. The participants showed better-than-chance performance, providing a basis for broader applications of the algorithm. Our technique could also expand the paradigms used in biological motion studies, most of which use point light walkers.

Acknowledgements

This work was supported by an Intramural Research Grant (Grant No. 23-7) for Neurological and Psychiatric Disorders from the National Center of Neurology and Psychiatry (NCNP), Grants-in-Aid for Scientific Research (C) (23500409, 26430031, 16K04821), a Grant-in-Aid on Innovative Areas, "Shitsukan" from Ministry of Education, Culture, Sports, Science and Technology (MEXT), and the program for Brain Mapping by Integrated Neurotechnologies for Disease Studies (Brain/MINDS) of Japan Agency for Medical Research and Development (AMED), Japan. The authors would like to thank Ueno Zoo for generously allowing us to film the animal videos, and Rachel Baron, PhD, from Edanz Group (`www.edanzediting.com/ac`) for editing a draft of this manuscript.

References

Aglieri, V., Watson, R., Pernet, C., Latinus, M., Garrido, L., Belin, P. (2017). The Glasgow Voice Memory Test: Assessing the ability to memorize and recognize unfamiliar voices. *Behavior Research Methods* 49, 97-110.

Annaz, D., Campbell, R., Coleman, M., Milne, E., Swettenham, J. (2012). Young children with autism spectrum disorder do not preferentially attend to biological motion. *Journal of Autism and Developmental Disorders,* 42, 401-408.

DeAngelis, G.C., Ohzawa, I., Freeman, R.D. (1995). Receptive-field dynamics in the central visual pathways. *Trends in Neurosciences,* 18, 451-458.

Gunji, A., Goto, T., Kita, Y., Sakuma, R., Kokubo, N., Koike, T., Sakihara, K., Kaga, M., Inagaki, M. (2013). Facial identity recognition in children with autism spectrum disorders revealed by P300 analysis: a preliminary study. *Brain & Development,* 35, 293-298.

Hirai, M., Gunji, A., Inoue, Y., Kita, Y., Hayashi, T., Nishimaki, K., Nakamura, M., Kakigi, R., Inagaki, M. (2014). Differential electrophysiological responses to biological motion in children and adults with and without autism spectrum disorders. *Research in Autism Spectrum Disorders,* 8, 1623-1634.

Johansson, G. (1973). Visual perception of biological motion and a model for its analysis. *Perception & Psychophysics,* 14, 201-211.

Nakayama K. (1985). Biological image motion processing: a review. *Vision Research,* 25, 625-660.

Pavlova, M. and Sokolov, A. (2000). Orientation specificity in biological motion perception. *Perception & Psychophysics,* 62, 889-899.

Sumi, S. (1984). Upside-down presentation of the Johansson moving light-spot pattern. *Perception,* 13, 283-286.

Suzuki, W., Ichinohe, N., Tani, T., Hayami, T., Miyakawa, N., Watanabe, S., Takeichi, H. (in press). Novel method of extracting motion from natural movies. *Journal of Neuroscience Methods.* `http://dx.doi.org/10.1016/j.jneumeth.2017.08.006`

Part XV
Symposium 3—The Future of Vection

An Introduction to Symposium 3: The Future of Vection

Symposium Organizer: Takeharu Seno

In this symposium, we will first introduce "What is Vection." This introduction will be followed by four presentations from leaders in the field of vection research. The symposium will provide an overview of the important controversies and new findings in the field.

SELF-MOTION PERCEPTION FACILITIES AT YORK UNIVERSITY

Robert S. Allison, Laurence R. Harris, and Michael R.M. Jenkin
Centre for Vision Research, York University, 4700 Keele Street
Toronto, ON M3J 1P3, Canada
<allison@eecs.yorku.ca, harris@yorku.ca, jenkin@eecs.yorku.ca>

York University has a long history of research in the perception of self-motion and orientation using purpose-built apparatus. Recently we developed and installed new facilities including new, more capable versions of Ian Howard's tumbling room and sphere devices: (1) The wide field stereoscopic environment (Fig. 1) is a projected, computer-generated, virtual environment that completely fills the participant's visual field with edgeless, high-resolution imagery. (2) The new tumbling room (Fig. 2) allows for full 360 degree rotation of the observer or the visual environment with near perfect visual fidelity. The room walls, floor and ceiling can be removed allowing for locomotion in a cylindrical environment. (3) The sphere environment (Fig. 3) allows for presenting full-field visual motion displays in pitch, roll or yaw while in a wide range of postures with respect to gravity. This presentation will overview the capabilities and illusions elicited in these devices as well as experiments to cross-validate the devices.

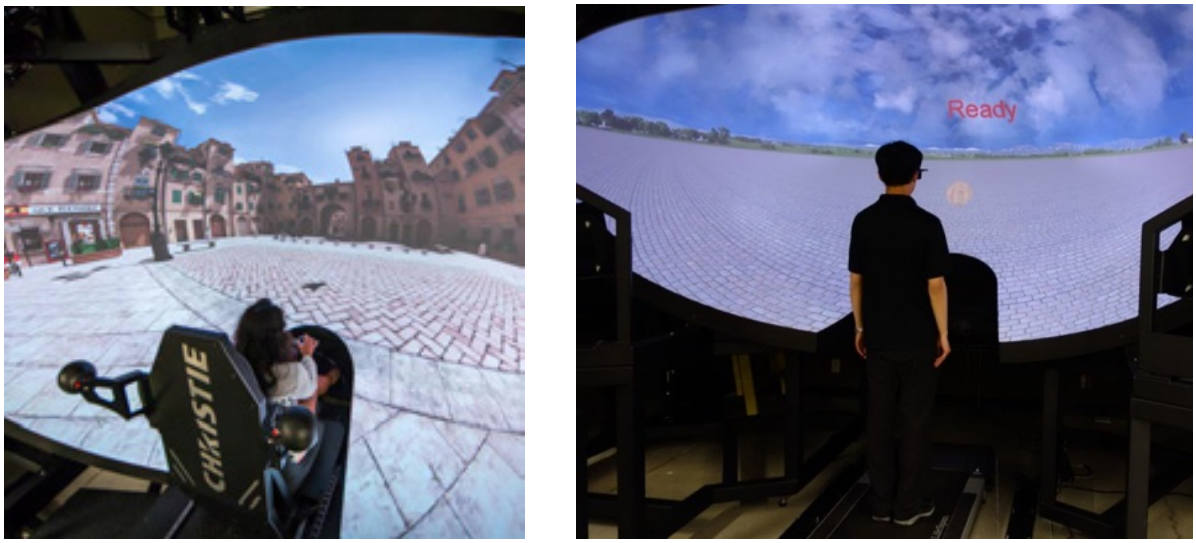

Fig. 1. The Wide-field Immersive Stereoscopic Environment is a projected, computer-generated, virtual environment. It is driven by eight overlapping, blended and calibrated projectors to provide high-contrast, high-resolution virtual imagery over the viewer's entire visual field. It can be used in seated (left) and standing/treadmill (right) configurations. The user's head and limbs can be tracked and the correct perspective projection for the user's vantage point presented in real time.

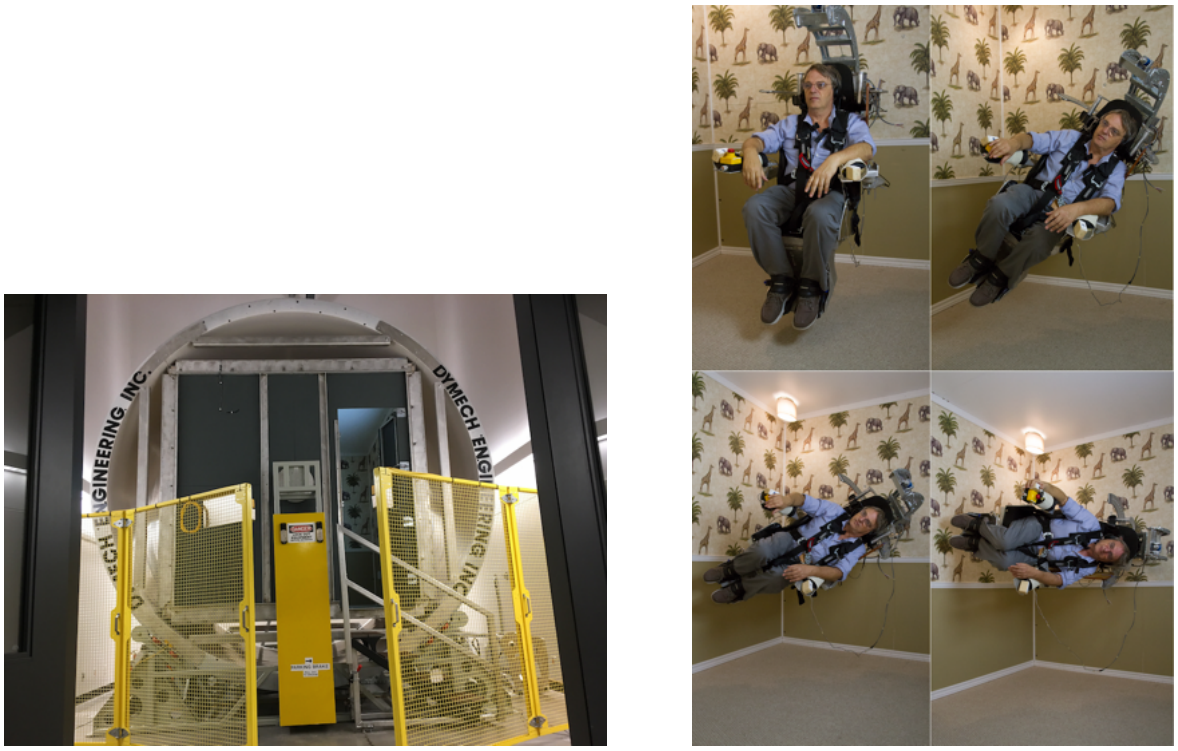

Fig. 2. The Tumbling Room enables motorized rotation of either the room or the observer (or both). In either case, under continuous rotation the observer typically perceives full 360-degree self-rotation (right). The room walls, floor and ceiling can be removed providing a continuous locomotion interface as the room turns. Imagery can be projected on the interior surface of the cylinder in this mode.

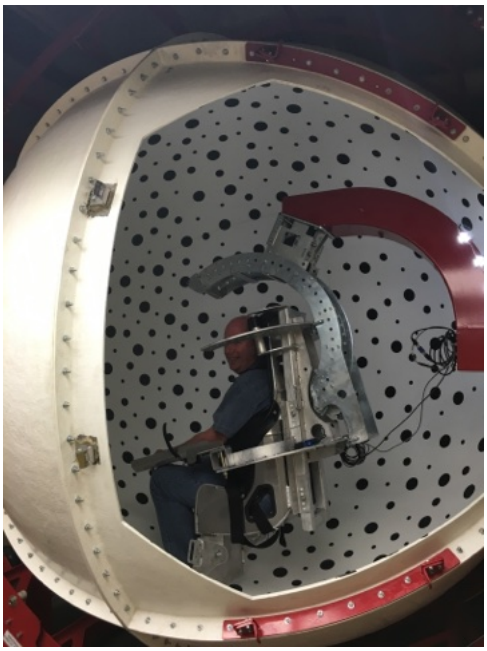

Fig. 3. The Sphere (shown here with access door removed) can provide full-field rotational optic flow to an observer oriented in a variety of postures. In various configurations yaw, pitch and roll vection can be produced.

PHENOMENOLOGICAL APPROACH TO VECTION

Takeharu Seno[1], Kayoko Murata[2], and Hidemi Komatsu[3]
[1]*Faculty of Design, Kyushu University, 4-9-1 Shiobaru Minami-ku Fukuoka, Japan*
[2]*National Graduate School of Humanities, Tokyo Metropolitan University*
1-1 Minami-Osawa, Hachioji-shi, Tokyo, Japan
[3]*Keio University, 2-15-45 Mita Minato-ku Tokyo, Japan*

Visually induced illusory self-motion perception (vection) has been studied in various methods and in various filed of science. For example, experimental Psychological methods have a long history. Also, brain imaging studies have revealed brain areas for vection induction. In this study, we newly introduce Phenomenological approach to vection research. Phenomenological approach is very usefulness and important to know vection more. We recorded the oral reports for 40 seconds when the participants observed vection stimulus and perceived vection. Thirteen volunteers participated in this study. There were two directional conditions, i.e. expansional and contracted optical flows. Two trials were repeated in each condition. We counted the frequencies of uttered words from various viewpoints. Phenomenological analyses suggest what will be the important topics in future vection study. Also, they proved us the validity of the experimental Psychological approach used in some previous vection studies.

INDIVIDUAL DIFFERENCES IN POSTURAL STABILITY PREDICT BOTH VECTION AND SIMULATOR SICKNESS

Stephen Palmisano and Benjamin Arcioni
School of Psychology, University of Wollongong, Australia

Paul J. Stapley
School of Medicine, University of Wollongong, Australia

Abstract

Evidence is mounting that differences in postural responding can be used to predict who will become sick and experience strong self-motion when exposed to global optical flow (e.g., Apthorp et al., 2014; Stoffregen & Smart, 1998). In this study we initially measured fluctuations in centre of foot pressure (CoP) when participants were standing quietly with their eyes open. They were next repeatedly exposed to two different types of self-motion display. As expected oscillating optic flow induced stronger vection and more sickness than the smooth self-motion display. Participants who had displayed lower CoP recurrence rates and had larger sway areas when standing quietly were more likely to later: (1) experience stronger vection; and (2) report motion sickness. We propose that CoP recurrence rates could serve as a useful diagnostic tool for evaluating who will benefit the most/least from exposure to virtual environments.

When people are exposed to visual self-motion simulations, there can be striking individual differences in both the incidence of motion sickness and the symptoms they experience (Keshavarz, Hecht & Lawson, 2015). However, Stoffregen and his colleagues have shown that we can predict who will become sick (even before any exposure to visual motion) based on the individual differences in their spontaneous postural stability (see Smart et al., 2002; Stoffregen & Smart, 1998). Two recent studies also appear to show that these individual differences can be used to predict some future experiences of vection (i.e., visually induced illusions of self-motion—see Apthorp, Nagle & Palmisano, 2014; Palmisano et al., 2014). This study extends this recent vection research. It examines whether postural instability can be used to predict both the strength of the vection and the likelihood of motion sickness when participants are exposed to two different types of radially expanding optic flow display—simulating smooth forwards linear motion either with or without additionally bob and sway head motions. The study also compares the predictive power of both traditional summary CoP measures of postural stability (sway path and sway area) and new dynamic Recurrence Quantification Analysis (RQA) based measures (recurrence rates).

Method

Participants. Fifteen female students (mean age 20.9, SD = 1.6 years) participated in this study at the University of Wollongong. All had normal or corrected-to-normal vision and reported feeling well at the start of the experiment. They had not consumed alcohol in the last 24 hours and were not taking prescription medication. Experimental protocols were in accordance with the ethical standards laid down in the 1964 Declaration of Helsinki.

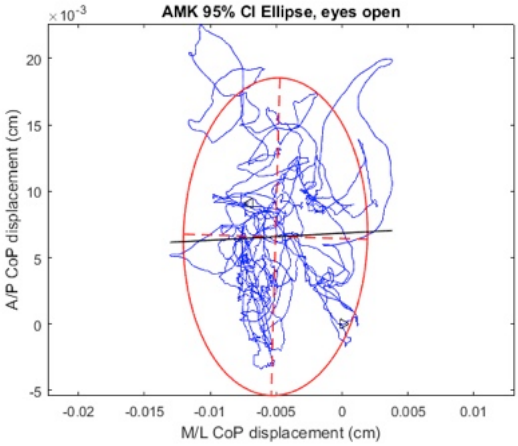

Fig. 1. Sway path (blue) and sway area (red ellipse) for participant AMK.

Displays. We examined two types of vection inducing display: (1) *smooth* radial flow; and (2) *oscillating* radial flow—simulating constant forwards self-motion with/without simulated head oscillation. Each optic flow display was presented for 30s. The dependent variables measured on each of these trials were: (a) the verbally rated vection strength from 0 (no vection) to 10 (strong vection); and (b) a verbal rating of sickness from 0 (no sickness) to 20 (to frank sickness) (using the Fast Motion Sickness Scale—see Keshavarz & Hecht, 2011).

Visual motion stimuli. Each display simulated self-motion through a 3-D cloud consisting of 3000 blue circular objects (cloud dimensions were 12.3 m wide × 5.8 m high and 13.1 m deep). All of the optic flow displays simulated 1.1 m/s forwards self-motion. Half of the displays also simulated combined horizontal (Amp 4.4 cm; freq 1 Hz) and vertical (Amp 2.2 cm; Freq 2 Hz) viewpoint oscillation.

Sway analyses. **Sway path length** was calculated as the total distance travelled by the CoP over each 60 s period of standing quietly (see blue trace in Fig. 1). **Sway area** was calculated as the 95% confidence ellipse around the region covered by the CoP over this same period (see red ellipse in Fig. 1).

Recurrence quantification analysis (RQA) was also conducted on the anterior-posterior and medial-lateral axis CoP data (using the Recurrence quantification toolbox for Matlab; see Li et al., 2004). The specific parameters used for the RQA were an embedding dimension of 8, a delay of 15, a minimum line length of 2, and a threshold of 0.6. Two (time-time) recurrence plots were produced for each 60 s period of eyes-open standing—one for sway along the anterior-posterior axis and the other for sway along the medial-lateral axis (see the left and right plots in Fig. 2. respectively). The **recurrence rate** (0-1) in each case corresponded to the correlation sum of the CoP (with the black regions in these plots indicating recurrent points).

Results

Display type effects on vection and sickness. As expected based on previous research, adding simulated viewpoint oscillation to radial flow displays was found to significantly

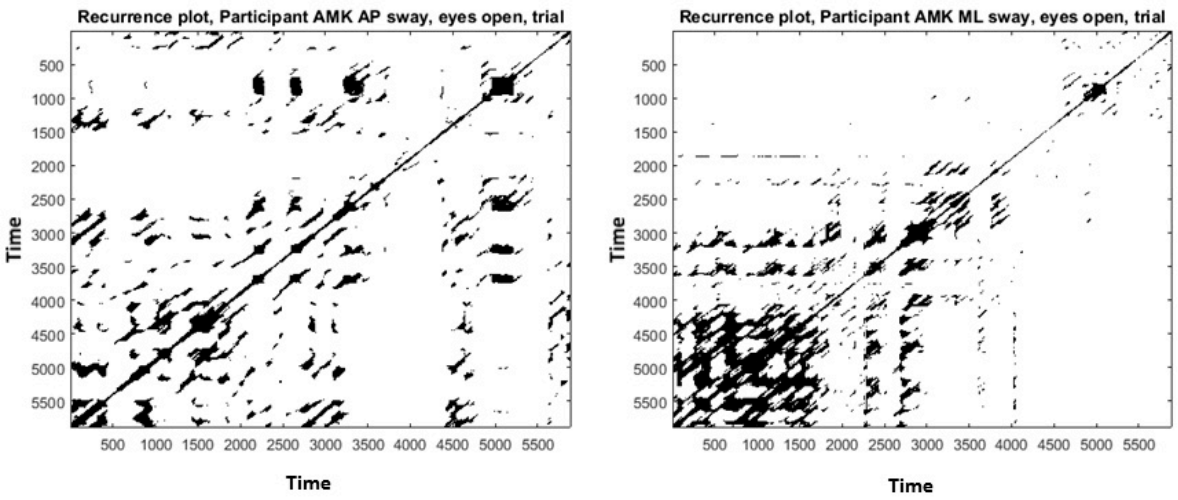

Fig. 2. Anterior-Posterior (left) and Medial-Lateral (Right) axis recurrence plots for participant AMK.

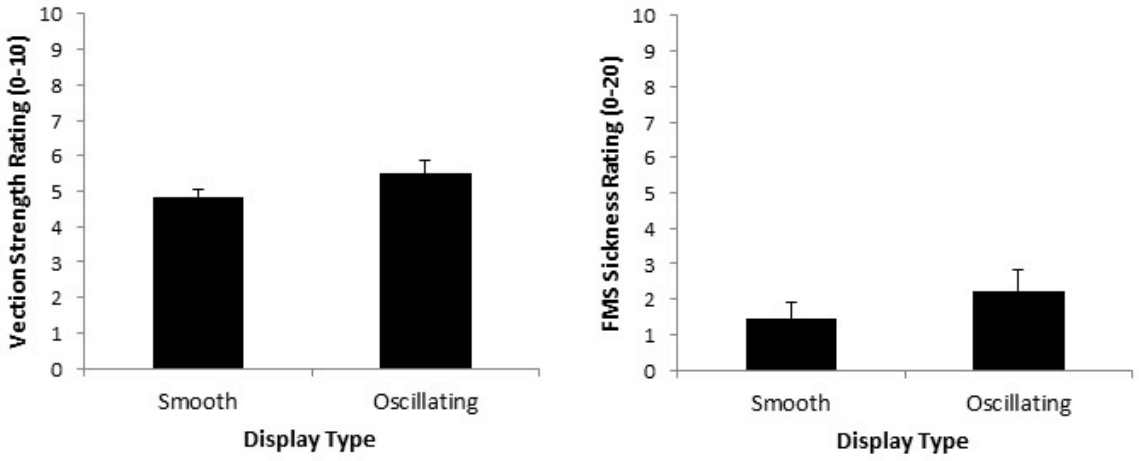

Fig. 3. Anterior-Posterior (left) and Medial-Lateral (Right) axis recurrence plots for participant AMK.

increase vection strength ratings ($t_{15} = 2.62, p = 0.02$) and increase sickness symptoms ($t_{15} = 2.59, p = 0.021$ see Fig.3 left and right) (see Palmisano et al., 2007; 2008; 2011).

Predicting vection from sway measures. Individual differences in sway path did not reliably predict the strength of either smooth or oscillating vection (both linear regressions analyses conducted were $p > 0.05$). As in earlier research by Apthorp et al. (2014), sway area was found to predict the strength of smooth ($R^2 = 0.37, t_{14} = 2.64, p = 0.02$), but not oscillating ($R^2 = 0.07, t_{14} = 0.91, p = 0.38$), vection. By contrast, the RQA based sway measures were able to reliably predict both types of vection (see Fig. 4.). Anterior-posterior recurrence rates were found to significantly predict the strength of the vection induced by smooth radial flow ($R^2 = 0.33, t_{14} = -2.53, p = 0.025$; Fig. 4 Left). Medial-lateral recurrence rates were found to significantly predict the strength of the vection

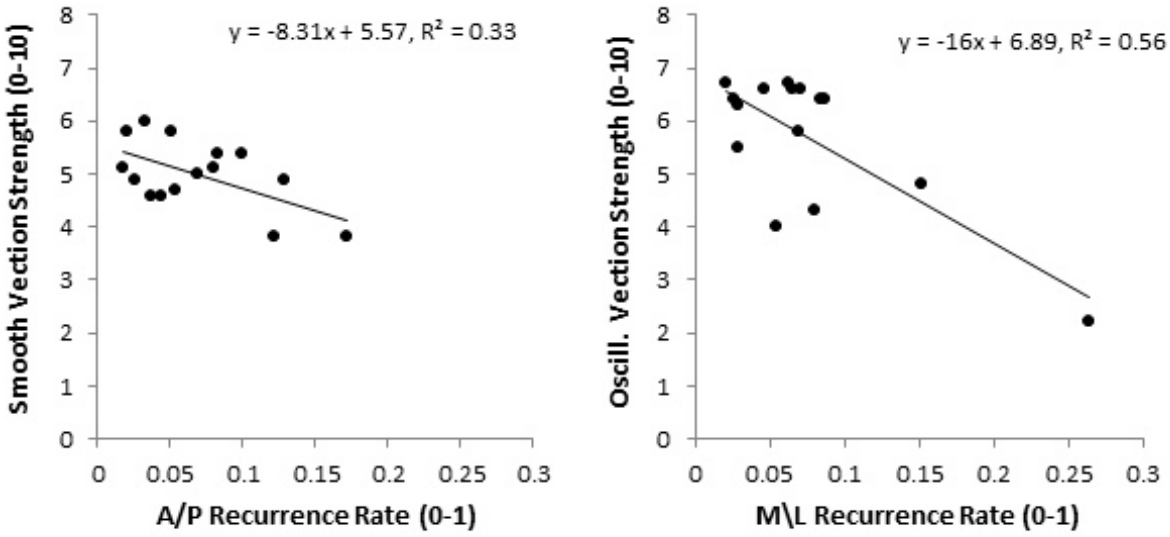

Fig. 4. Relationships between recurrence rates and vection strength ratings for smooth (left plots) and oscillating radial flow displays (right plots). The top plots show recurrence rates along the medial-lateral axis. The bottom plots show the recurrence rates along the anterior-posterior axis.

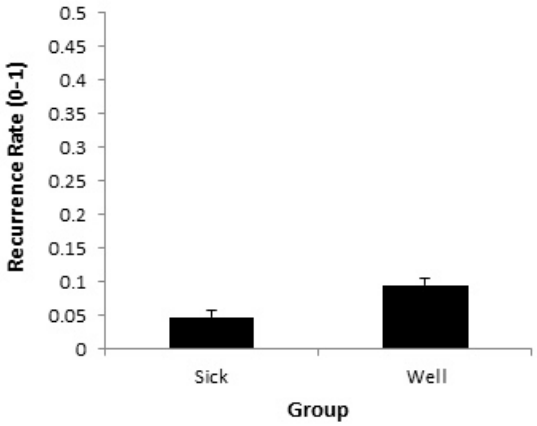

Fig. 5. Mean anterior-posterior recurrence rates during quiet stance for Well and Sick participants. Error bars depict standard errors of the mean (SEMs).

induced by oscillating optic flow ($R^2 = 0.56, t_{14} = -4.056, p = 0.01$; Fig. 4 Right).

Predicting sickness from sway measures. A between-subjects t-test revealed that participants who eventually became sick ($M = 0.05, SD = 0.013$) had significantly lower anterior-posterior recurrence rates than those who remained well ($M = 0.09, SD = 0.016$), $t_{14} = -2.36, p = 0.03$ (see Fig. 5.). While differences in sway path length also appeared to predict these 'sick' and 'well' groups ($t_{14} = -2.17, p = 0.047$), sway area did not ($t_{14} = -1.38, p = 0.19$).

Discussion

Recurrence rates were the most reliable predictor of future vection experiences and motion sickness. In this experiment recurrence rates predicted the strength ratings for both smooth and oscillating types of vection. Recurrence rates were also found to predict the likelihood of sickness when exposed to visual motion stimulation. Specifically, lower recurrence rates tended to be associated with stronger vection experiences and the increased likelihood of experiencing motion sickness. These findings suggest that individuals who display greater spontaneous instability (less recurrence) will be more prone to experiencing both vection and sickness. Consistent with this notion, the sway path lengths and sway areas of these individuals also tended to be larger (even if these effects did not always reach significance). Taken together these findings suggest that vection and visually induced motion sickness might be indirectly related to each other via the person's postural responses to the visually simulated self-motion.

Acknowledgements

This work was supported by a University of Wollongong, Faculty of Social Sciences Seeding grant to SP.

References

Apthorp, D., Nagle, F., Palmisano, S. (2014). Chaos in balance: Non-linear measures of postural control predict individual variations in visual illusions of motion. *PLoS ONE,* 9(12): e113897. doi:10.1371/journal.pone.0113897.

Keshavarz, B., Hecht, H. (2011). Validating an efficient method to quantify motion sickness. *Human Factors,* 53, 415–26.

Keshavarz, B., Hecht, H., & Lawson, B. (2015). Visually induced motion sickness: Causes characteristics, and countermeasures. In K.S. Hale, K.M. Stanney (Eds.), *Handbook of Virtual Environments: Design, Implementation, and Applications.* CRC Press, Boca Raton, FL, 2015, pp. 532–587.

Li, X., Ouyang, G., Yao, X., Guan, X. (2004). Dynamical characteristics of pre-epileptic seizures in rats with recurrence quantification analysis. *Physics Letters A,* 333(1), 164-171.

Palmisano, S., Allison, R.S., Pekin, F. (2008). Accelerating self-motion displays produce more compelling vection in depth. *Perception,* 37:22–33.

Palmisano, S., Apthorp, D., Seno, T., Stapley, P.J. (2014). Spontaneous postural sway predicts the strength of smooth vection. *Experimental Brain Research,* 232, 1185–1191.

Palmisano, S., Bonato, F., Bubka, A., Folder, J. (2007). Vertical display oscillation increases vection in depth and simulator sickness. *Aviation, Space and Environmental Medicine,* 78, 951–956.

Palmisano, S., Allison, R.S., Kim, J., Bonato, F. (2011). Simulated Viewpoint jitter shakes sensory conflict accounts of self-motion perception. *Seeing & Perceiving,* 24,173–200.

Smart, L.J., Stoffregen, T.A., & Bardy, B.G. (2002). Visually induced motion sickness predicted by postural instability. *Human Factors,* 44, 451–465.

Stoffregen, T.A., Smart, L.J. (1998). Postural instability precedes motion sickness. *Brain Research Bulletin,* 47, 437–448.

EFFECTS OF FOOT-STIMULATION (VIBRATIONS AND A WATER-FLOW) ON VECTION

Yasuaki Tamada[1], Kiyoshiro Hara[1], Yoshitaka Fujii[2], Takeharu Seno[2], and Masayuki Sato[1]

[1]*Department of Information Media Engineering, The University of Kitakyushu*
1-1 Hibikino, Wakamtasu-ku, Kitakyushu, Japan
[2]*Institute for Advanced Study, Faculty of Design, Kyushu University*
4-9-1 Shiobaru, Minami-ku, Fukuoka, Japan
<y-tamada@kitakyu-u.ac.jp>

Abstract

The effects of foot-stimulation (vibrations and a water-flow) on the visually induced self-motion perception (vection) were examined in two experiments. The strengths of vection (latency, duration and magnitude) were measured when foot stimulation and/or visual oscillation were added to the visual optic flow simulating a forward self-motion. In Experiment 1, the vibrations were presented to observer's sole. It was very large individual differences in the effects of foot-vibration on vection. In some observers, vection could be facilitated by the foot-vibrations, in others it was inhibited. In Experiment 2, a water-flow from the front was presented to observer's feet. Although the foot-water-flow made the vection duration longer in all observers, the foot-water-flow facilitated or inhibited vection dependently on each observer's characteristics. These results suggest that the integration process between visual inputs and foot-stimulations might vary among individuals.

While vision contributes to the recognition of external world, vision play a major role in the self-motion perception and the body control. Mere exposure to a retinal optical flow induces an illusory self-motion perception, called vection (Palmisano, Allison, Schira, & Barry, 2015). Many sensory organs contribute to the self-motion perception. Vection can be facilitated by the combination of visual input and other sensory input (Shulte-Pelkun, Riecke, & Bülthoff, 2004; Riecke, Väljamäe, & Schulte-Pelkun, 2009; Seno, Ogawa, Ito, & Sunaga, 2011). Shulte-Pelkun et al. (2004) showed that the vection was facilitated by adding the vibration of seat and floor to visual stimulus. To examine effects of foot-stimulation (vibrations and a water-flow) on vection, we measured the strengths of vection when foot stimulation and/or visual oscillation were added to visual optic flow simulating a forward self-motion.

Method

Apparatus

Experiments were conducted in a dark room. The visual stimuli projected by a CRT projector (Christie Digital Systems, Marquee 8500/3D) were presented on a 100-inch rear-screen. The spatial resolution of the display were 1024 × 784 pixels and the refresh rate was 60 Hz. Observers sat at viewing distance of 0.7 m and fixed his/her head using a chin rest. The chromaticity of the visual stimuli was designed to provide dichoptic stimulation with red-blue anaglyph glasses. The foot stimuli (vibration and water-flow) were presented using an electric massager (Twinbird Inc., EM-B705BR) and an electric

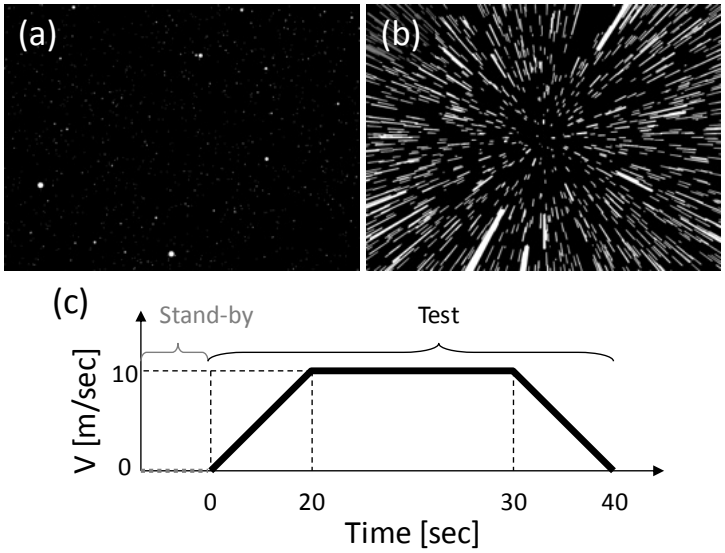

Fig. 1. Test stimulus. (a) Random-dot, (b) Expanding optic flow, (c) Translation profile.

foot bath machine (Alinco Inc., MCR7914), respectively.

Stimuli

Figure 1 (a) and (b) shows the visual stimuli. The discs were randomly placed in a virtual three-dimensional space spread from a screen to 28 meters away with the diameter of 9.9 cm and the density of 0.022 discs/m^3. The size and binocular disparity of discs were changed as a function of the distance from observers. The visual angle of the stimuli was 111 deg $\times$ 95 deg. The expanding optic flow simulating observer's forward translation were added to discs. This optic flow was started with an observer's key press, and the velocity of translation was modulated with the profile shown as Figure 1 (c).

In "with visual oscillation" condition, sinusoidal vertical oscillation was added to visual stimuli with the temporal frequency of 12.5 Hz and the amplitude of 5 cm (in a virtual space). Therefore, the closer dots moved larger.

In "with foot vibration" condition, the vibration was presented to observer's soles with the temporal frequency of 12.5 Hz. In the case of presenting both foot vibration and visual oscillation simultaneously, authors got the impression that the vibration and oscillation were synchronized even though they were not actually.

In "with foot water-flow" condition, the water-flow was presented to observer's feet in a toe-to-heel direction. In addition to the water-flow, micro-bubbles were emitted by a foot bath machine. The micro-bubbles were made for massaging one's soles. Although the detailed parameters of water-flow and micro-bubbles were unspecified, authors convinced that the water flowed from their toe to heel, and got the impression that the bubbles had an effect similar to but weaker than the foot vibration.

Procedure

We measured the vection strength using three vection indices, 1) subjective magnitude, 2) duration, and 3) latency. In one trial, firstly visual oscillation and/or foot stimulation were

presented under the "with visual oscillation" and/or "with foot stimulation (vibration or water-flow)" conditions ("Stand-by phase" in the experimental profile shown as Figure 1 (c)). Secondly, observer pressed a key and started the optic flow display if they could ready for a trial.

We defined forty seconds from the beginning of a trial as the test duration. Observer responded the presence or absence of the self-motion perception using a key-press during the test duration. We also defined the time from the beginning of a trial to the first response as vection latency, and the sum of the time observer responded as vection duration. Finally, observer responded the subjective vection magnitude, ranging 0 (only discs moving) to 100 (only subject moving).

Experiments were divided into two parts, 1) foot vibration and 2) foot water-flow. Each part was designed on the two-by-two conditions composed of foot stimulation (without, with) and visual oscillation (without, with). We repeated each condition four times. The order of conducting four conditions was counterbalanced over the observers.

Subjects

Totally, 27 volunteers participated in the experiments. In preliminary experiment, two volunteers responded the very strong vection (magnitude = 100) regardless of experimental conditions, and two did not respond the vection at all (magnitude = 0). These four volunteers did not go on to the main experiment. Since another two volunteers always kept pressing the response key (latency = 0 sec or duration = 40 sec) in every trial, we decided that these two volunteers did not well know the procedure of the experiments, and omitted these two observers' data into analysis.

There were 18 volunteers who participated in the foot vibration experiment [mean age: 23.4 $\pm$ 4.2 (SD); range: 21–37 yr]. There were 16 volunteers (13 of 16 individuals who took part in the foot vibration experiment, and 3 individuals were new) who participated in the foot water-flow experiment [mean age: 22.6 $\pm$ 2.6 (SD); range: 21–33 yr]. No one except for the three (foot vibration experiment) or two (foot water-flow experiment) authors was aware of the purpose of the experiment.

Data Analysis

Vection data were analyzed with a three-way analysis of variance (ANOVA). The factors were 'Individuals', 'Foot stimulation (without, with)', and 'Visual oscillation (without, with)'. For all multiple comparison tests, Ryan's method was used.

Results and Discussion

Foot Vibration

The results for the three vection indices in the foot vibration experiment are shown in Figure 2 and Table 1. Figure 2(A) shows the vection magnitude. Under the control (without foot vibration and visual oscillation, NoVib-NoOsc for short) condition, middle-magnitude vection occurred. When either of foot vibration or visual oscillation was presented (Vib-NoOsc or NoVib-Osc), vection was inhibited. When both foot vibration and visual oscillation were simultaneously presented (Vib-Osc), vection magnitude was as much as that for NoVib-NoOsc condition. Three-way ANOVAs for vection magnitude

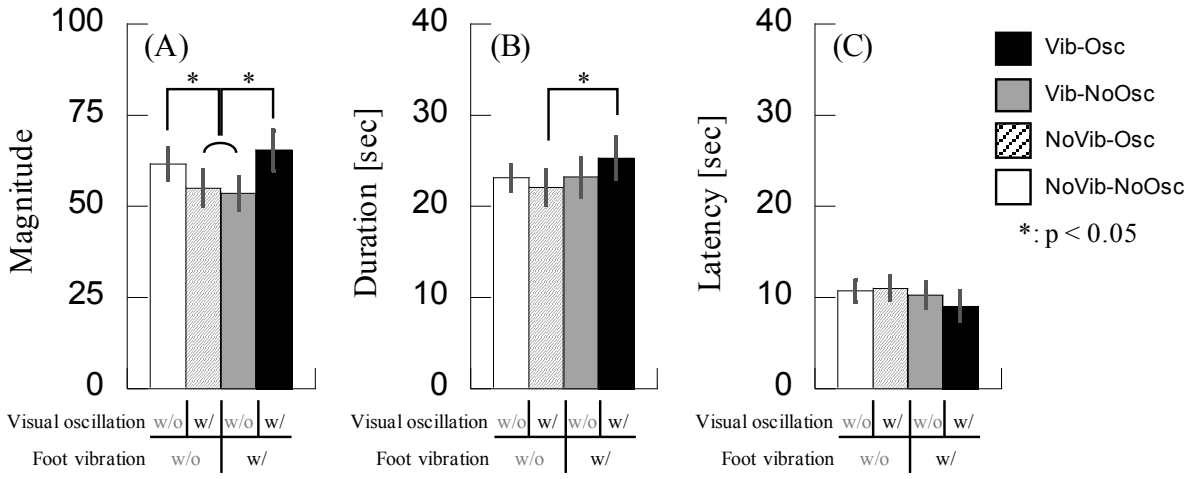

Fig. 2. Three vection indices in foot vibration experiment. (A) Magnitude, (B) Duration, (C) Latency.

Table 1. 3-way ANOVA results in foot vibration experiment.

		Magnitude		Duration		Latency	
	df	F	p	F	p	F	p
A: Individuals	17	16.700	****	14.405	****	7.015	****
B: Foot vibration	1	0.337		3.288	+	1.514	
C: Visual oscillation	1	1.660		0.005		0.085	
A*B	17	1.706	*	1.292		1.337	
A*C	17	4.096	****	2.550	****	1.592	+
B*C	1	22.557	****	3.978	*	1.804	
A*B*C	17	2.263	***	2.169	**	1.031	

+: p<0.1, *: p<0.05, **: p<0.01, ***: p<0.005, ****: p<0.001

confirmed a significant main effect of 'Individuals' ($P < 0.0001$) but not 'Foot vibration' and 'Visual oscillation' (respectively, $P > 0.1$). The interactions among 'Individuals', 'Foot vibration', and 'Visual oscillation' were significant ($P < 0.05$).

Figure 2 (B) shows the vection duration. The longest was Vib-Osc condition, followed in order by Vib-NoOsc, NoVib-NoOsc, and Vib-NoOsc condition. The results of three-way ANOVAs were similar to that for vection magnitude.

Figure 2 (C) shows the vection latency. The shortest was Vib-Osc condition, followed in order by Vib-NoOsc, NoVib-NoOsc, and Vib-NoOsc condition. Three-way ANOVAs for vection latency confirmed a significant main effect of 'Individuals' ($P < 0.0001$) only. As described above, the vection strength differed greatly in individuals. Especially, the effect of foot vibration and visual oscillation depended on individuals. To focus the individual differences, Figure 4 (A) shows the each individual vection magnitude data. These vection magnitude were normalized by the data of the control (NoVib-NoOsc)

condition. Plus and minus values correspond to the vection facilitation and inhibition, respectively.

The visual oscillation (NoVib-Osc condition) hardly facilitated vection. This is inconsistent with previous studies showing that the visual oscillation facilitates the vection (Palmisano, Gillam, & Blackburn, 2000; Palmisano, Bonato, Bubka, & Folder, 2007; Palmisano, Allison, & Pekin, 2008; Nakamura, 2010; Nakamura, 2013). The difference between our experiment and previous studies was the amplitude and frequency of the visual oscillation. Previous studies used the visual oscillation with relatively lower frequency and larger amplitude ([Palmisano et al. (2007), 1.8–7.4 Hz, 4.5 deg], [Palmisano et al. (2008), 1/7 Hz, 37 deg], [Nakamura (2010), 1 Hz, 12 deg], [Nakamura (2013), 1 Hz, 7.5 deg]). The visual oscillation we used was relatively higher frequency (12.5 Hz) and smaller amplitude (2.9 deg at maximum). These parameters of the oscillation might be not effective for vection facilitation.

The foot vibration (Vib-NoOsc condition) inhibited vection for six observers (#4, 6, 11, 14, 15). This is inconsistent with previous studies showing that the vibration stimulus facilitates the vection (Farkhatdinov, Ouarti, & Heyward, 2013; Riecke, Schulte-Pelkum, Cainard, & Bülthoff, 2005). While previous studies used the vibration with the higher frequencies ([Farkhatdinov et al. (2013), 90 Hz (sinusoidal) and 70–110 Hz (chirp)], [Riecke et al. (2005), 15–90 Hz (the broad-band vibration of the seat and floor)], the frequency we used was very low (12.5 Hz). It may need the vibration with the higher frequency to facilitate vection. On the other hand, after the experiment, some observers reported that they had to pay attention to the sounds that the foot massager emitted. The foot device generating sounds might decrease the observers' immersion to the visual stimuli and inhibit the vection.

The simultaneous presentation of foot vibration and visual oscillation (Vib-Osc condition) had different effects on each observer. The foot vibration and visual oscillation facilitated vection for four observers (#1, 2, 4, 6) but inhibited vection for two observers (#17, 18). In the third experiment of Riecke et al. (2005), three out of twenty-four observers reported that the vibration did not match the velocity profile of the visual motion. For these observers, vection was inhibited. Although our result is consistent with that of Riecke et al. (2005) in that the ways to associate the vibration and visual motion differs in individuals, there were few observers who showed the vection facilitation in our experiment. The difference between two studies might be due to the difference of visual stimulus. Riecke et al. used the photorealistic image of the Tübingen market place including a cobbled pathway. It seemed relatively easy for their observers to imagine that the vibration occurs when the vehicle she/he ride run on the cobbled pathway. However, it was difficult for our observers to evoke that the vibration occurs when observer's body translation with the randomly-distributed discs we used. This discrepancy should give rise to the difference between two studies.

In the foot vibration experiment, it is revealed that simply adding the foot vibration or equalizing the frequencies of the foot vibration and the visual oscillation cannot facilitate the vection.

Foot Water-Flow

The results for the three vection indices in the foot water-flow experiment are shown in Figure 3 and Table 2. Figure 3 (A) shows the vection magnitude. Under the control (without foot water-flow and visual oscillation, NoWF-NoOsc for short) condition,

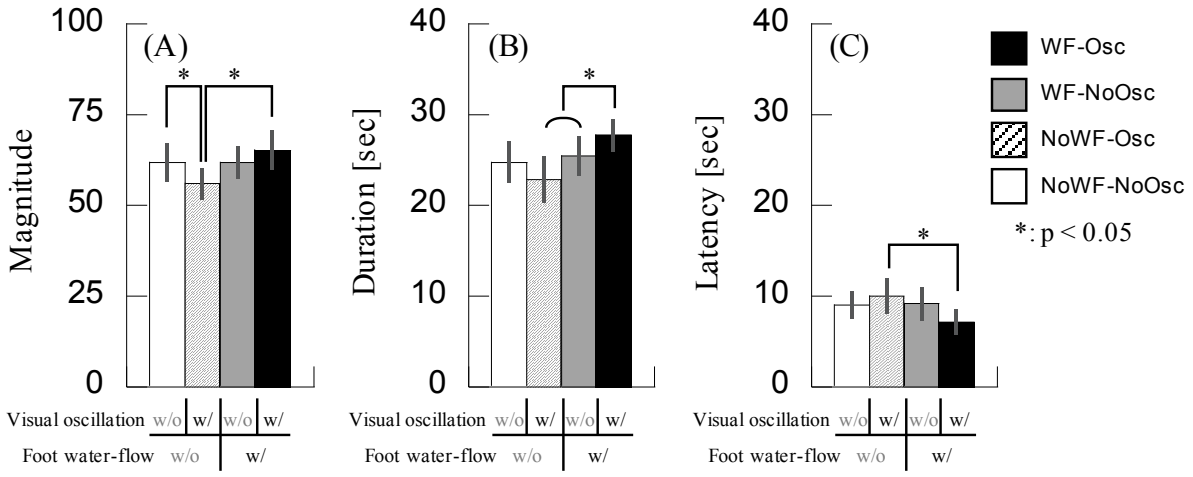

Fig. 3. Three vection indices in foot water-flow experiment. (A) Magnitude, (B) Duration, (C) Latency.

Table 2. 3-way ANOVA results in foot water-flow experiment.

		Magnitude		Duration		Latency	
	df	F	p	F	p	F	p
A: Individuals	15	8.189	****	22.685	****	13.152	****
B: Foot water-flow	1	4.681	*	13.618	****	3.397	+
C: Visual oscillation	1	0.357		0.059		0.465	
A*B	15	3.753	****	2.195	**	1.101	
A*C	15	3.915	****	2.475	***	1.44	
B*C	1	4.810	*	7.921	**	4.216	*
A*B*C	15	1.828	*	2.091	*	1.701	+

+: p<0.1, *: p<0.05, **: p<0.01, ***: p<0.005, ****: p<0.001

middle-magnitude vection occurred. When visual oscillation was presented (NoWF-Osc), vection was inhibited. When both foot water-flow was presented (WF-Osc), vection magnitude was as much as that for NoWF-NoOsc condition. When both foot vibration and visual oscillation were simultaneously presented (WF-Osc), largest magnitude vection occurred. Three-way ANOVAs for vection magnitude confirmed a significant main effect of 'Individuals' ($P < 0.0001$) and 'Foot water-flow' ($P < 0.01$) but not 'Visual oscillation' (respectively, $P > 0.1$). The interactions among 'Individuals', 'Foot water-flow', and 'Visual oscillation' were significant ($P < 0.05$).

Figure 3 (B) shows the vection duration. The longest was WF-Osc condition, followed in order by WF-NoOsc, NoWF-NoOsc, and WF-NoOsc condition. The results of three-way ANOVAs were similar to that for vection magnitude.

Figure 3 (C) shows the vection latency. The shortest was Vib-Osc condition, followed in order by WF-NoOsc, NoWF-NoOsc, and WF-NoOsc condition. Three-way

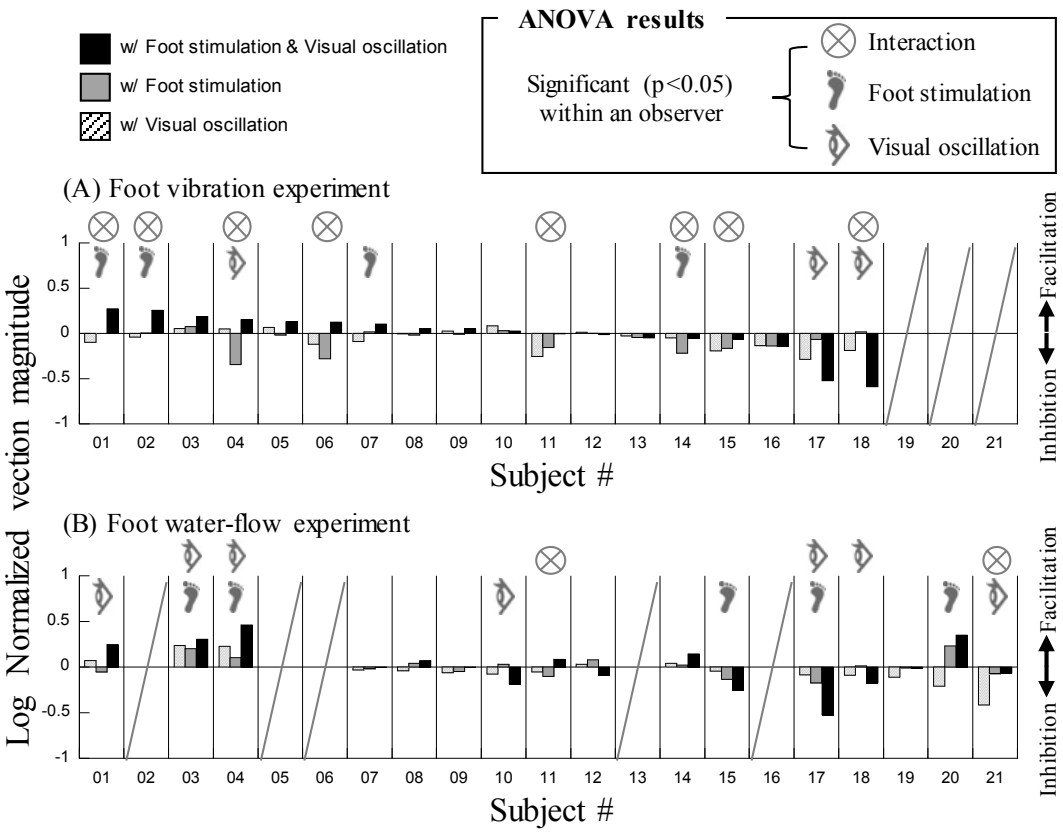

Fig. 4. Three vection indices in foot water-flow experiment. (A) Magnitude, (B) Duration, (C) Latency.

ANOVAs for vection latency confirmed a significant main effect of 'Individuals' ($P < 0.0001$) only.

The water-flow slightly enhanced vection magnitude and elongated vection duration on the whole data of the all observers. However, the effect of foot water-flow and visual oscillation differed greatly in individuals as well as the foot vibration experiment. To focus the individual differences, Figure 4 (B) shows the each individual vection magnitude data.

The visual oscillation (NoWF-Osc condition) hardly facilitated vection except for two observers (#3, 4). This is inconsistent with the foot vibration experiment.

The foot water-flow (WF-NoOsc condition) inhibited vection for three observers (#3, 4, 20). As well as the foot vibration experiment, since the foot bath machine generated relatively loud sounds, this might decrease the observers' immersion to the visual stimuli and inhibit the vection. On the other hand, while the water-flow's strength was constant, the simulated forward translation speed was changed. Due to this discrepancy, vection might be not facilitated.

The simultaneous presentation of foot water-flow and visual oscillation (WF-Osc condition) had different effects on each observer. The foot water-flow and visual oscillation facilitated vection for four observers (#1, 2, 4, 20) but inhibited vection for four observers (#10, 15, 17, 18). The observers that the vection was facilitated or inhibited were roughly consistent with the foot vibration and water-flow experiment. The way in which observers integrate the foot and visual stimulation may not depend on the type of foot stimulus.

Summary

The effects of foot-stimulation (vibrations and a water-flow) on the visually induced self-motion perception (vection) were examined. The strengths of vection were measured when foot stimulation and/or visual oscillation were added to the visual optic flow simulating a forward self-motion. In Experiment 1, the vibrations were presented to observer's sole. It was very large individual differences in the effects of foot-vibration on vection. In some observers, vection could be facilitated by the foot-vibrations, in others it was inhibited. In Experiment 2, a water-flow from the front was presented to observer's feet. Although the foot-water-flow made the vection duration longer in all observers, the foot-water-flow facilitated or inhibited vection dependently on each observer's characteristics. These results suggest that the integration process between visual inputs and foot-stimulations might vary among individuals.

References

Farkhatdinov, I, Ouarti, N., & Hayward, V. (2013). Vibrotactile inputs to the feet can modulate vection. *Proceedings of the World Haptics Conferences 2013,* 677–681.

Nakamura, S. (2010). Additional oscillation can facilitate visually induced self-motion perception: The effects of its coherence and amplitude gradient. *Perception,* 39, 320–329.

Nakamura, S. (2013). Effects of additional visual oscillation on vection under voluntary eye movement conditions—retinal image motion is critical in vection facillitation. *Perception,* 42, 529–536.

Palmisano, S., Gillam, B., & Blackburn, S. (2000). Effects of additional visual oscillation on vection under voluntary eye movement conditions—retinal image motion is critical in vection facilitation. *Perception, 42,* 529–536.

Palmisano, S., Bonato, F., Bubka, A., & Folder, J. (2007). Vertical display oscillation effects on forward vection and simulator sickness. *Aviation, Space, and Environmental Medicine,* 78, 951–956.

Palmisano, S., Allison, R. S., & Pekin, F. (2008). Accelerating self-motion displays produce more compelling vection in depth. *Perception,* 37, 22–33.

Palmisano, S., Allison, R. S., Schira, M. M. & Barry, R. J. (2015). Future challenges for vection research: definitions, functional significance, measures, and neural bases. *Frontiers in Psychology,* 6, 193, 1–15.

Riecke, B. E., Schulte-Pelkum, J., Caniard, F., & Bülthoff, H. H. (2005). Towards lean and elegant self-motion simulation in virtual reality. *Proceedings of IEEE Virtual Reality 2005,* 131–138.

Riecke, B. E., Väljamäe, A., & Schulte-Pelkum, J. (2009). Moving sounds enhance the visually-induced self-motion illusion (circular vection) in virtual reality. *ACM Transactions on Applied Perception,* 6, 1–27.

Seno, T., Ogawa, M., Ito, H., & Sunaga, S. (2011). Consistent air flow to the face facilitates vection. *Perception,* 40, 1237–1240.

Schulte-Pelkum, J., Riecke, B. E., & Bülthoff, H. H. (2004). Vibrational cues enhance believability of ego-motion simulation. *Proceeding of the fifth International Multisensory Research Forum* (IMRF 2004).

Part XVI
Free Talk Session 9

ADAPTIVE FUNCTION OF COLOR VISION IN PRIMATES

Chihiro Hiramatsu
Department of Human Science, Faculty of Design, Kyushu University, 815-8540 Fukuoka, Japan

Trichromatic color vision in primates is unique among mammals whose color vision is normally dichromatic. The adaptive functions of color vision during the course of primate evolution have been debated for decades and are still under active discussion. The most popular hypothesis posits that detecting reddish fruits and/or young leaves from green foliage background is the primary function and driving force of the evolution of trichromacy. Another hypothesis argues that detecting social signals such as skin color changes is one of the important functions acquired by primates with trichromatic vision. Alternatively, some consider that functions of trichromacy might be more general and useful for various tasks. In this talk, I will review recent studies that investigated various functions of color vision in primates from the evolutionary viewpoint, with special emphasis on: 1) unique spectral tuning of primate trichromacy, and 2) polymorphic color vision in neotropical primates and humans.

PERCEPTUAL ORGANIZATION FROM VISUAL POSITIONS DISTORTED BY MOTION SIGNALS IN DRIFTING GABOR PATCHES

Hoko Nakada, Daisuke Hayashi, and Ikuya Murakami
Department of Psychology, The University of Tokyo, Tokyo, Japan

It is well known that visual motion processing has important roles in localizing objects, as demonstrated by robust illusions of positional distortion by visual motion. For example, De Valois & De Valois (1991) demonstrated that a stationary patch containing a drifting grating appears spatially shifted in the direction of motion. However, it is yet to be clarified how these local distortions in perceptual position might influence global perceptual organization. We arranged these drifting stimuli to form a shape with various configurations, and investigated whether the locally distorted positions influenced the global form solution. The experimental results indicated that spatially distorted perceptual interpretations of the local patches caused illusory formation of global shapes, perceptual grouping, and motion correspondence, and that the global perceptual organization was determined not only by local illusory positional shifts but also by the observer's perceptual set.

REDUCING BETWEEN-SUBJECT VARIATION IN MOTION-INDUCED BLINDNESS USING THE METHOD OF CONSTANT STIMULI

Amanda I. LeBel, Hanne K. Hansen, Nicholas C. Duggan, Alison Meurer, Emma G. DePierro, Stephen Z. Zhang, Andrew J. Kitt, & Wm Wren Stine*
Department of Psychology, University of New Hampshire, Durham, NH, USA
*<bill.stine@unh.edu>

Abstract

Motion-induced blindness (MIB) describes the disappearance of targets presented in the near periphery of the visual field when a moving mask is presented behind the targets. The targets typically vanish within ten seconds. Eye-movements refresh their appearance. Most studies of MIB have measured the total time of disappearance, asking subjects to press a button when the target is invisible and release the button when the target is visible. Empirically, very large individual differences in total disappearance time occur, which probably arise from differences in subjects' fixation abilities while targets transition from visible to invisible. We describe a procedure, akin to the method of constant stimuli, where subjects merely report at the end of a trial whether or not the targets vanished, with trial duration varying randomly across trials. The resulting psychometric functions show relatively little individual variation, and have proven sensitive to the manipulation of several independent variables.

Motion-induced blindness (MIB) describes the disappearance of static elements of a viewed stimulus, known as targets, in the presence of a moving array of elements, the mask. The phenomenon was noted by Breese (1899), where the target and the motion mask were presented to different eyes, and explored by Grindley and Townsend (1965; 1966), which they called movement masking. In the early 1990s, several authors explored perceptual filling-in (e.g., Anstis, 1989; Ramachandran and Gregory, 1991; Ramachandran, Gregory, and Aiken, 1993; and Spillmann and Kurtenbach, 1992, etc.), which seem to reflect the same mechanisms as MIB (Devyatko, Appelbaum, and Mitroff, 2017; Hsu, Yeh, and Kramer, 2004, 2006). Bonneh, Cooperman, and Sagi (2001) coined the term motion-induced blindness, presenting both the target and a coherently-moving mask binocularly.

Disappearance reflects both contrast adaptation (e.g., Troxler, 1804, fading) and neural inhibition (Bonneh, Donner, Cooperman, Heeger, and Sagi, 2014; Gorea and Caetta, 2009), with an upward shift in criterion (Caetta et al., 2007). Processing decreases in V4 while increasing in the intraparietal sulcus just prior to disappearance (Donner, Sagi, Bonneh, and Heeger, 2008), with the rate of disappearance related to V4 and the duration to V1 (Donner, Sagi, Bonneh, and Heeger, 2013). Single-pulse TMS of left posterior parietal cortex shortens disappearance time in phase with the disappearance cycle and lengthened duration out of phase, the right cortex yielding opposite effects (Funk and Pettigrew, 2003).

Random noise, motion, and then flickering masks are decreasingly effective (Spillmann and Kurtenbach, 1992; cf., Welchman and Harris, 2001). Disappearance increases with target and mask contrast, mask velocity, and mask density, and decreases with mask protection zone size, target size, and target rotational velocity, and aligned Gabor stimuli and close-proximity dot targets disappear together while orthogonal Gabor stimuli and

widely-separated dots disappear separately (Bonneh, et al., 2001). Decrement masks are more effective than increment masks with increment targets, and increment targets are easier to mask than decrement targets (Stine, Levesque, Lusignan, and Kitt, In press). Attention to the target increases disappearance (Grindley and Townsend, 1965, 1966; Schölvinck and Rees, 2009). The depth-plane of the mask and surface completion influence disappearance (Graf, Adams, and Lages, 2002). When a target in a grid disappears, the grid fills in the target's location (New and Scholl, 2008). Coherent motion is less effective than random motion masks during extended trials, perhaps due to motion adaptation (Wells, Sparrow, and Leber, 2011). Finally, color and texture may fade separately, and the direction of motion of a vanished target can be reported, implying separate mechanisms for color, texture, form, and motion (Ramachandran and Gregory, 1991). Clearly, both local and global processing are involved in MIB (e.g., Spillmann and Kurtenbach, 1992), as are early and late processing.

One issue that researchers confront while studying MIB are the large individual differences reflected in the dependent measures that are typically used (e.g., Graf et al., 2002; Figure 3; Spillmann & Kurtenbach, 1992, Figure 2 caption). Most often, experimenters ask subjects to indicate when a target is visible during a trial of constant duration by, for example, pressing a button when the target is not visible and releasing that button when the target becomes visible. From these data one often calculates total disappearance time (e.g., Bonneh et al., 2001; Bonneh Donner, Sagi, Fried, Cooperman, Heeger, and Arieli, 2010, Experiment 2; Bonneh et al., 2014; Devyatko, et al., 2017; Donner et al., 2008; Donner et al., 2013; Funk & Pettigrew, 2003; Gorea & Caetta, 2009; Graf et al., 2002; Grindley & Townsend, 1965; Hsu et al. 2006; New & Scholl, 2008; Schölvinck, & Rees, 2009, Experiment 2; Spillmann & Kurtenbach, 1992; Wells et al., 2011). Given that microsaccades modulate MIB (but do not account for MIB; Bonneh et al., 2010), vary with stimulus onsets (Valsecchi, Betta, and Turatto, 2007), and influence Troxler fading (Martinez-Conde, Macknik, and Troncoso, 2006), one might speculate that subjects vary in their ability to suppress eye movements when the target transitions. A few studies have asked subjects to simply indicate whether or not the stimulus vanishes (e.g., Grindley & Townsend, 1966; Ramachandran & Gregory, 1991; Ramachandran et al., 1993; Schölvinck, & Rees, 2009, Experiment 1; Welchman, & Harris, 2001). Building on this approach, we have used an adaptation of the method of constant stimuli (Hegelmaier, 1852; Laming and Laming, 1992; Stine et al., In press) in order to measure a psychometric function for target disappearance across trial duration. Briefly, the subject indicates whether or not one of the target stimuli disappears during an MIB stimulus interval randomly chosen from five possible values. Given the subject's task, eye movements after the first stimulus transition will have no influence on the subject's response.

Method

Our methods have been described in detail previously (Stine et al., In press). Presented are data from two female unpaid volunteers (AKS and HKH) who were naïve with respect to our hypotheses, had normal or corrected to normal visual acuity, and signed informed consent with debriefing consistent with University of New Hampshire (UNH) Institutional Review Board policy. Several other subjects have run through our protocol with similar results.

All stimuli were achromatic and presented on a uniform background of 108 cd/m^2. Target dot luminance (increment—200 cd/m^2 vs decrement—15 cd/m^2), mask dot lumi-

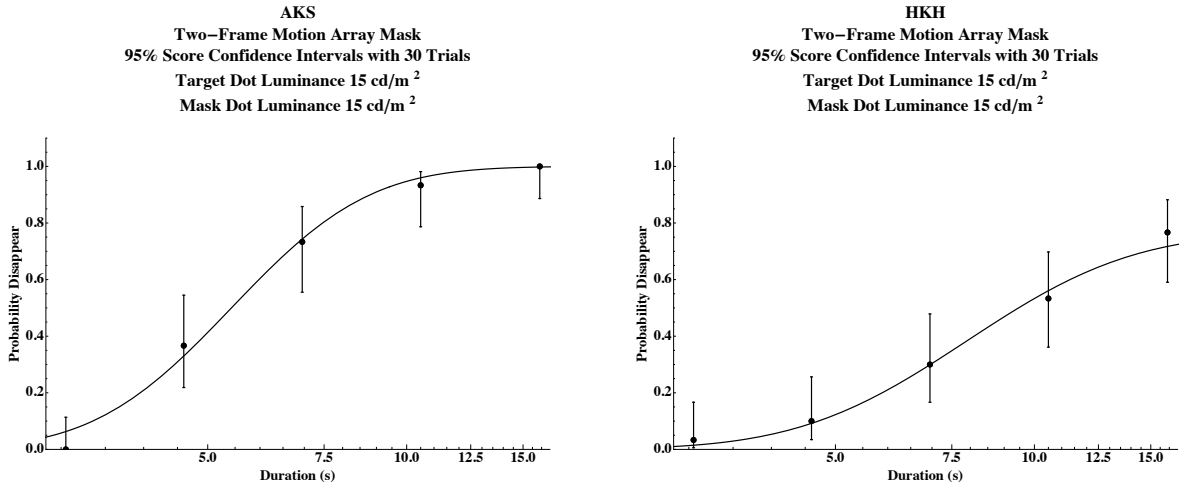

Fig. 1. Two psychometric functions with non-zero lapse rates (Klein, 2001) for decrement targets and masks and relative frequencies with 95% score confidence intervals (Agresti and Caffo, 2000; Agresti and Caffo, 1998; Wilson, 1927) as a function of trial duration on a log scale.

nance (increment—200 cd/m^2 vs decrement—15 cd/m^2), and trial duration (3.1 s, 4.6 s, 7.0 s, 11 s, or 16 s) were factorially combined, and a no-mask control condition (108 cd/m^2) for increment and decrement targets was added ($2 \times 2 \times 5 + 2 = 22$), to create 22 trial types presented in random order. Subjects indicated whether or not one of the target stimuli disappeared. Each session began with a 5 min adaptation to the uniform background and trials were separated by the background presentation for the previous trial's duration plus 2 s. Gaussian psychometric functions were fit as a function of trial duration on logarithmic coordinates (Klein, 2001). Relative frequencies were plotted with 95% score confidence intervals based on 30 trials (Agresti and Caffo, 2000; Agresti and Caffo, 1998; Wilson, 1927).

Results and Discussion

Using our analog to the method of constant stimuli, single psychometric functions from two subjects in the same condition show that the Gaussian cumulative distribution with a non-zero lapse rate approximates our data well (Figure 1). In particular, threshold trial durations for disappearance are well defined.

Across different combinations of increments and decrements, all of the functions fit the data well, with well-defined thresholds (Figure 2). Note that for two conditions, those without a mask (2 and 5 from top to bottom), there was little or no target disappearance. Decrement mask with an increment target yields the strongest effect (4), followed by a decrement mask with a decrement target and an increment mask with an increment target (1 & 6). An increment mask showed the weakest effect with a decrement target (3).

That decrements suppress increments maximally is consistent with the 'stronger' input of OFF cells relative to ON cells (Stine et al., In press). Evidence suggests that such increments and decrements are initially processed by ON and OFF ganglion cells (e.g., Dolan & Schiller, 1994; Schiller, 1992; Schiller, Sandell, and Maunsell, 1986), representing channels preserved through to cortex, and maintained as a distinction to higher levels of cortex (Dacey, 2004; Xing, Yeh, and Shapley, 2010). OFF processing provides faster

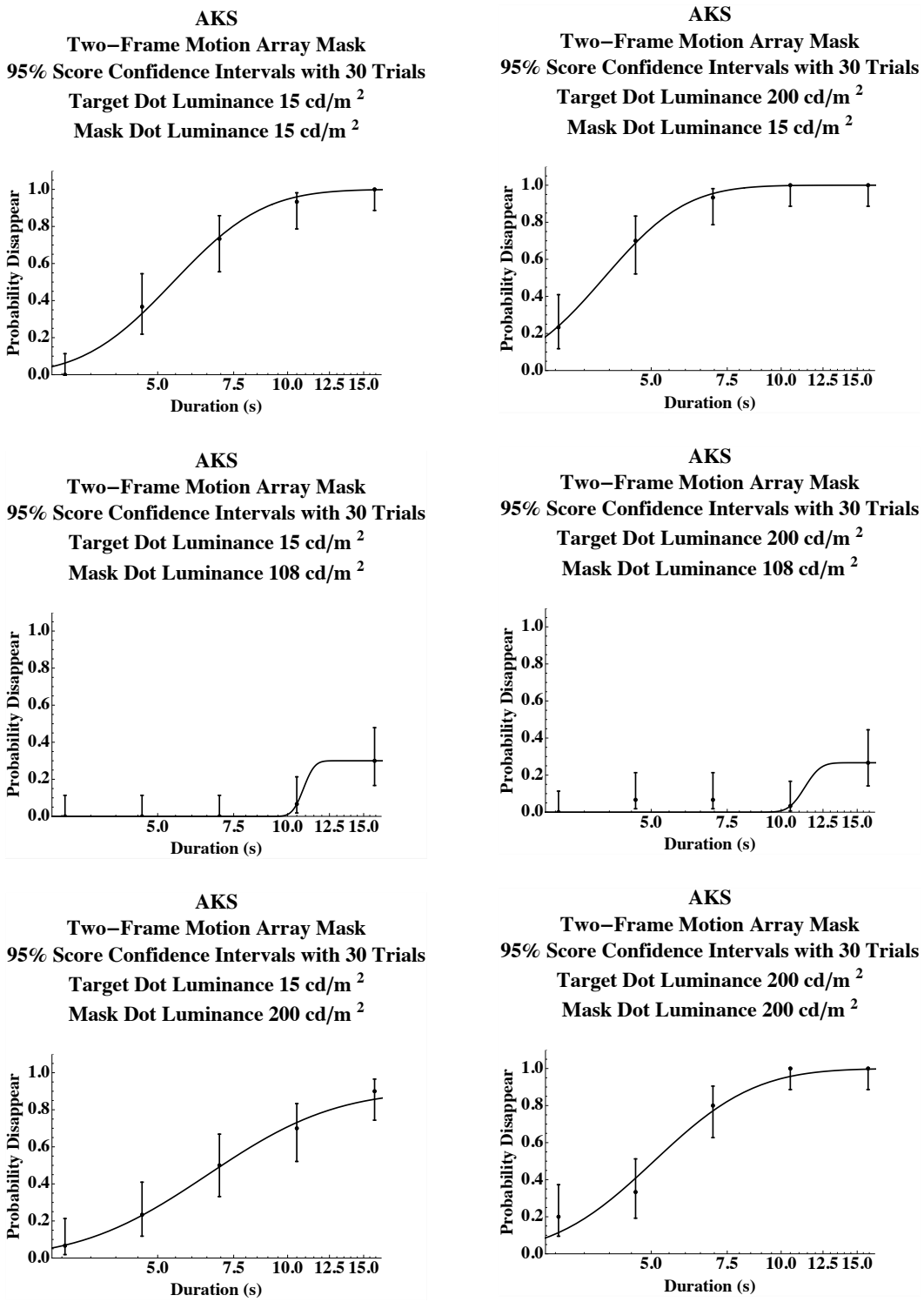

Fig. 2. From left-top to right-bottom are psychometric similar to those of Figure 1 for a single subject, AKS, across six conditions: 1—decrement target and mask, 2—decrement target and no mask, 3—decrement target and increment mask, 4—increment target and decrement mask, 5—increment target and no mask, 6—increment target and increment mask.

response times and lower thresholds than ON processing (e.g., Balasubramanian and Sterling, 2009; DeMarco, Hughes, and Purkiss, 2000; Jin, Wang, Lashgari, Swadlow, and Alonso, 2011; Komban, Alonso, and Zaidi, 2011; see Westheimer, 2007).

The result also highlights, probably at a relative high level of processing, the interdependence of OFF and ON cell inputs to higher cortex (e.g., toward V4 and the intraparietal sulcus). That decrements suppressing decrements and increments suppressing increments are roughly equivalent, and less effective than decrements suppressing increments, might suggest a relatively even balance between the role of target and mask with respect to increments and decrements. Finally, as one might expect, increments are least effective in masking decrements.

Our analogue to the method of constant stimuli would seem to provide an approach that yields robust results. Of course, it is well-known that such an approach is laborious. The degree to which the technique of presenting varying trial durations with the subject indicating simply whether or not a component of the stimulus disappeared during the trial could be applied to efficient non-parametric or parametric procedures (e.g., stochastic approximation, Robins and Monroe, 1951, or QUEST, Watson and Pelli, 1983) is an open, though interesting, question.

Using our constant-stimuli approach to measuring MIB enhances one's ability to observe the influence of subtle factors.

Acknowledgements

We gratefully acknowledged the UNH Undergraduate Research Office, Honors Program, and College of Liberal Arts.

References

Agresti, A., & Caffo, B. (2000). Simple and effective confidence intervals for proportions and differences of proportions result from adding two successes and two failures. *The American Statistician,* 54, 280-288.

Agresti, A., & Coull, B. A. (1998). Approximate is better than "exact" for interval estimation of binomial proportions. *The American Statistician,* 52, 119-126.

Anstis, S. (1989). Kinetic edges become displaced, segregated and invisible. In D. Man-Kit Lam, & C. D. Gilbert (ed.), *Neural mechanisms of visual perception* (pp. 247–260). Houston, TX: Gulf Publishing.

Balasubramanian, V., & Sterling, P. (2009). Receptive fields and functional architecture of the retina. *Journal of Physiology,* 12, 2753-2767.

Bonneh, Y. S., Cooperman, A., & Sagi, D. (2001). Motion-induced blindness in normal observers. *Nature,* 411, 797-801.

Bonneh Y. S., Donner, T.H., Cooperman, A., Heeger, D. J., Sagi, D. (2014). Motion-induced blindness and Troxler fading: Common and different mechanisms. *PLoS ONE,* 9, e92894. doi:10.1371/journal.pone.0092894

Bonneh, Y. S., Donner, T. H., Sagi, D., Fried, M., Cooperman, A., Heeger, D. J., & Arieli, A. (2010). Motion-induced blindness and microsaccades: Cause and effect. *Journal of Vision,* 10, 1–15. doi:10.1167/10.14.22.

Breese, B. B. (1899). On inhibition. *The Psychological Review: Series of Monograph Supplements,* 3, 1-65.

Caetta, F., Gorea, A., & Bonneh, Y. S. (2007). Sensory and decisional factors in motion-induced blindness. *Journal of Vision,* 7, 1–12.

Dacey, D. M. (2004). Origins of perception: Retinal ganglion cell diversity and the creation of parallel visual pathways. In M. S. Gazzaniga, (Ed.). *The cognitive neurosciences,* 3rd Ed. Cambridge, MA: MIT Press.

DeMarco, P. J., Hughes, A., & Purkiss, T. J. (2000). Increment and decrement detection on temporally modulated fields. *Vision Research,* 40, 1907-1919.

Devyatko, D., Appelbaum, L. G., & Mitroff, S. R. (2017). A common mechanism for perceptual reversals in motion-induced blindness, the Troxler effect, and perceptual filling-in. *Perception,* 46, 50-77.

Dolan, R. P. & Schiller, P. H. (1994). Effects of ON channel blockade with 2-amino-4-phosphonobutyrate (APB) on brightness and contrast perception in monkeys. *Visual Neuroscience,* 11, 23–32.

Donner, T. H., Sagi, D., Bonneh, Y. S., & Heeger, D. J. (2008). Opposite neural signatures of motion-induced blindness in human dorsal and ventral visual cortex. *The Journal of Neuroscience,* 28, 10298 –10310. doi:10.1523/JNEUROSCI.2371-08.2008

Donner, T. H., Sagi, D., Bonneh, Y. S., & Heeger, D. J. (2013). Retinotopic patterns of correlated fluctuations in visual cortex reflect the dynamics of spontaneous perceptual suppression. *The Journal of Neuroscience,* 33, 2188–2198. doi:10.1523/JNEUROSCI.3388-12.2013

Funk, A. P., & Pettigrew, J. D. (2003). Does interhemispheric competition mediate motion-induced blindness? A transcranial magnetic stimulation study. *Perception,* 32, 1325–1338.

Gorea, A., & Caetta, F. (2009). Adaptation and prolonged inhibition as a main cause of motion-induced blindness. *Journal of Vision,* 9, 1–17. doi:10.1167/9.6.16.

Graf, E. W., Adams, W. J., & Lages, M. (2002). Modulating motion induced blindness with depth ordering and surface completion. *Vision Research,* 42, 2731–2735.

Grindley, G. C., & Townsend, V. (1965). Binocular masking induced by a moving object, *Quarterly Journal of Experimental Psychology,* 17, 97-109. doi:10.1080/17470216508416418

Grindley, G. C., & Townsend, V. (1966). Further experiments on movement masking, *Quarterly Journal of Experimental Psychology,* 18, 319-326. doi:10.1080/14640746608400049

Hegelmaier, F. (1852). Ueber das Gedächtniss für Linearanschauungen. [On memory for the length of a line.] *Archiv für physiologische Heilkunde,* 11, 844-853.

Hsu, L. C., Yeh, S. L., & Kramer, P. (2004). Linking motion-induced blindness to perceptual filling-in. *Vision Research,* 44, 2857–2866. doi:10.1016/j.visres.2003.10.029

Hsu, L. C., Yeh, S. L., & Kramer, P. (2006). A common mechanism for perceptual filling-in and motion-induced blindness. *Vision Research* 46, 1973–1981. doi:10.1016/j.visres.2005.11.004

Jin, J., Wang, Y., Lashgari, R., Swadlow, H. A., & Alonso, J.-M. (2011). Faster thalamocortical processing for dark than light visual targets. *The Journal of Neuroscience,* 31, 17471-17479.

Klein, S. A. (2001). Measuring, estimating, and understanding the psychometric function: A commentary. *Perception & Psychophysics,* 63, 1421-1455.

Komban, S. J., Alonso, J.-M., & Zaidi, Q. (2011). Darks are processed faster than lights.

The Journal of Neuroscience, 31, 8654-8658.

Laming, D., & Laming, J. (1992). F. Hegelmaier: On memory for the length of a line. *Psychological Research,* 54, 233-239. doi:10.1007/BF01358261

Martinez-Conde, S., Macknik, S. L., Troncoso, X. G., & Dyar, T. A. (2006). Microsaccades counteract visual fading during fixation. *Neuron,* 49, 297–305. doi:10.1016/j.neuron.2005.11.033

New, J. J., & Scholl, B. J. (2008). "Perceptual scotomas": A functional account of motion-induced blindness. *Psychological Science,* 19, 653–659.

Ramachandran, V. S., & Gregory, R. L. (1991). Perceptual filling in of artificial scotomas in human vision. *Nature,* 350, 699-702.

Ramachandran, V. S., Gregory, R. L., & Aiken, W. (1993). Perceptual fading of visual texture borders. *Vision Research,* 33, 717-721.

Robbins, H., & Monro, S., (1951). A stochastic approximation method. *Annals of Mathematical Statistics,* 22, 400-407.

Schiller, P. H. (1992). The ON and OFF channels of the visual system. *Trends in Neurosciences,* 15, 86-92.

Schiller, P. H., Sandell, J. H., & Maunsell, J. H. R. (1986). Functions of the ON and OFF channels of the visual system. *Nature,* 322, 824-825.

Schölvinck, M. L., & Rees, G. (2009). Attentional influences on the dynamics of motion-induced blindness. *Journal of Vision,* 9, 1–38. doi:10.1167/9.1.38.

Spillmann, L., & Kurtenbach, A. (1992). Dynamic noise backgrounds facilitate target fading. *Vision Research,* 32, 1941-1946.

Stine, W. W., Levesque, P. A., Lusignan, M. E., & Kitt, A. J. (In press). Motion induced blindness using increments and decrements of luminance. *Proceedings of the Latvian Academy of Sciences. Section B. Natural, Exact, and Applied Sciences.*

Troxler, D. (1804). Über das Verschwinden gegebener Gegenstände innerhalb unseres Gesichtskreises [On the disappearance of given objects from our visual field]. In Himly, K. & Schmidt, A. (Eds), *Ophthalmologic Bibliothek,* Vol. 2, (pp. 431-573). Jena: Springer.

Valsecchi, M., Betta, E., & Turatto, M. (2007). Visual oddballs induce prolonged microsaccadic inhibition. *Experimental Brain Research,* 177, 196–208.

Watson, A. B., & Pelli, D. G. (1983). QUEST: A Bayesian adaptive psychometric method. *Perception & Psychophysics,* 33, 113-120.

Welchman, A. E., & Harris, J. M. (2001). Filling-in the details on perceptual fading. *Vision Research,* 41, 2107–2117.

Wells, E. T., Leber, A. B., & Sparrow, J. E. (2011). The role of mask coherence in motion-induced blindness. *Perception,* 40, 1503-1518.

Wilson, E. B. (1927). Probable inference, the law of succession, and statistical inference. *Journal of the American Statistical Association,* 22, 209-212.

Xing, D., Yeh, C.-I. & Shapley, R. M. (2010). Generation of black-dominant responses in V1 cortex. *Journal of Neuroscience,* 30, 13504-13512.

Part XVII
Free Talk Session 10

BUKIMI NO TANI: THE EFFECTS OF REGULTORY FOCI ON RESPONSE THRESHOLD AND ITS EFFECTS ON COGNITIVE AND AFFECTIVE UNCERTAINTY

Jordan Richard Schoenherr[1] and Tyler Burleigh[2]
[1]*Department of Psychology, Carleton University*
[2]*Institute for the Study of Decision Making, New York University*
<Jordan.Schoenherr@Carleton.ca, TylerBurleigh@gmail.com>

Abstract

The uncanny valley (UCV) reflects a region along the perceptual continuum used to discriminate human and nonhuman objects and entities associated with uncertainty and negative affect. Recent studies have explored cognitive and affective components of UCV phenomenon. While cognitive uncertainty appears to be a function of categorical representations, stimulus training frequency appears to be the main determinant of affective uncertainty. Studies have also observed that discrimination performance can be changed by manipulating participants' regulatory foci. For instance, whereas promotion focus emphasizes gains (attain 95% accuracy), prevention focus emphasizes losses (avoid 5% errors). These studies have demonstrated that participants with a promotion focus outperform those with a prevention focus. In the current study, we manipulated stimulus training frequency along a continuum following promotion- or prevention-focus instructions. We found that the instructional manipulation altered participants' response threshold such that a promotion focus increased stimulus identification accuracy across the stimulus continuum.

Recently, researchers have begun to explore the possible bases for phenomena referred to as the Uncanny Valley, or bukimi no tani (UCV; Mori, 1970). Some researchers have suggested that there might be specialized cognitive mechanisms that are responsible for these effects (e.g., Macdorman, 2005). Alternative, general learning mechanisms (e.g., categorization; e.g., Cheetham, Suter, & Jancke, 2014) and frequency-based sensitization (e.g., Burliegh & Schoenherr, 2015) might offer a more parsimonious alternative.

The present study investigates whether knowledge of the internal structure of a category is related to affective responses associated with uncertainty and can instead offer a more general account of UCV. Specifically, we examine whether novel face-like category exemplars (i.e., extrapolation items) are associated with greater negative affect, supporting familiarity-based preference (Park et al., 2010). We additionally examined whether these effects were stimulus-specific or were instead the result of a shift in participants' response threshold. We explored this possibility by presenting participants with promotion or prevention processing instructions (e.g., Higgins, 1997) as previous studies have suggested that these instruction change a participants response threshold.

Perceptual Sensitization, Category Learning, and Uncertainty

Categorization research has focused on a number of different learning mechanisms and representations. A broad class of models assumes that individuals use the similarity of old and new exemplars to determine the category membership of novel items (for a review see, Goldstone et al., 2012). When presented with a novel stimulus, participants compare it to existing prototypes (averages), exemplars (instances), or category boundaries (deci-

sion criterion) stored in memory. Importantly, all of these models assume that the region between categories is associated with uncertainty due to the similarity of a stimulus with neighboring prototypes, exemplars, or category boundaries. However, participants likely maintain multiple representations (e.g., category boundary and exemplars). This assumption is supported by numerous studies (e.g., Pisoni & Tash, 1974; Paul et al., 2011) with subjective ratings of exemplar typicality (Miller & Volatis, 1989), certainty (Paul et al., 2011), or both (Schoenherr & Logan, 2013) revealing dissociable knowledge of category structure and category members.

Alternative models have examined factors that affect the inclusion of novel exemplars within an existing category. Drawing from the literature on Regulatory Focus Theory (RFT; Higgins, 1997) and loss and gain framing (Tversky & Kahneman, 1981), Novelty Categorization Theory (NCT; Förster et al., 2010) predicts that participants are more likely to include a new item in an old category when it is processed in the context of a promotion focus (i.e., emphasising accuracy) rather than a prevention focus (i.e., emphasising error avoidance) by changing the response threshold. For instance, participants should be more accurate when told to be correct (promote the inclusion of novel items) rather than to avoid errors (prevent the inclusion of novel items) due to general desire to explore novel features of our environment and tendency toward loss aversion, respectively. Moreover, as NCT suggests that processing focus affects the inclusion or exclusion of novel exemplars, it predicts item-specific effects rather than overall changes in preference and performance.

While NCT finds some empirical support (Gillebaart et al., 2012) there are several issues. First, in contrast to category learning paradigms wherein participants are presented with feedback to determine category membership, participants in Gillebaart et al. (2012) were presented with a single set of stimuli without feedback. While this does conform to a mere exposure paradigm (Bornstein, 1989), it only requires that participants encode individual exemplars (e.g., absolute identification) rather than acquire the relational structure of a category, thereby implicitly assuming participants acquire exemplar-based representations. Second, NCT does not distinguish between response uncertainty due to category membership and uncertainty associated with affect or preference. Yet there is evidence that individuals have access to both stimulus-based and category-based information (Miller & Volatis, 1989) and can retain multiple kinds of representations (Smith & Minda, 1999), which suggests that categorization and affective responses are determined by dissociable mechanisms (Burleigh & Schoenherr, 2015).

Categorization models can be used to understand and predict affective responses to stimuli. For instance, the ease with which a stimulus can be categorized predicts positive affect (Reber, Winkielman & Schwarz, 1998), and conversely that a lack of processing fluency predicts negative affect (Yamada, Kawabe & Ihaya, 2013). Negative affect might also occur when stimuli activate multiple, competing stimulus representations (e.g., Burleigh, Schoenherr, & Lacroix, 2013). Thus, stimuli located at the category boundary where there is the greatest uncertainty and categorization difficulty might be associated with more negative affect than more prototypical stimuli. Several recent studies have investigated this possibility, finding mixed results (Burleigh & Schoenherr, 2015; Cheetham, Suter & Jancke, 2015). Further examination is required to determine the relationship between cognitive and affective uncertainty responses.

Thus, in contrast to NCT, affective responses might reflect a different set of processes outside of categorization (Burleigh & Schoenherr, 2015). In addition to categorization processes, Burleigh and Schoenherr (2015) suggest that participants' affective re-

sponses are determined by stimulus frequency independently of category structure. While affective responses can become associated with categorical knowledge, during early stages of learning this can lead to dissociations. Thus, by manipulating participants' processing foci, we should observe a general increase in categorization performance when participants employ a promotion (vs. prevention) focus, as a result of observing the similarity between a novel item and the category representation stored in long-term memory. In contrast, early stages of processing that are dependent on frequency which determine affect should be unaffected by processing foci.

The present study examines whether basic category learning processes can account for the results of experiments examining UCV. We additionally sought to examine claims made by researchers that regulatory foci could alter the response threshold. However, in contrast to other studies (Gillebaart et al., 2012), we used a categorization paradigm. Participants were also required to rate exemplar eeriness (i.e., negative affect) and exemplar typicality.

Method

Participants. Participants were 116 undergraduate students ($M_{age} = 20.16$). They received 0.5% credit toward their final grade.

Stimuli. There were 15 creature stimuli, 7 for each creature category, and 1 at the boundary. Creatures were nonhuman entities with humanoid properties selected from a larger stimulus set used in a previous study (Figure 1; see also, Burleigh & Schoenherr, 2015).

Procedure. Participants first received an instructional manipulation. They were instructed to maintain a 95% level of accuracy (promotion focus) or to avoid making 5% errors (prevention focus). Following the instruction, they began the experimental phase, which consisted of 8 blocks of training, 2 transfer blocks, and 1 typicality rating task. Presentation frequencies for each three training set in training and transfer phases are presented in Table 1.

During training, participants were first presented with a screen with the word 'Ready?' After pressing the spacebar, a screen with a fixation point (+) was presented

Fig. 1. Sample stimuli from two graded categories used in the study.

Table 1. Stimulus presentation frequency for equal frequency distribution (EFD) and unequal frequency distributions (UFD) used in training and the equal frequency transfer blocks.

	Stimulus															Total
	1	2	3	4	5	6	7	8	9	10	11	12	13	14	15	
EFD	0	0	4	4	4	4	4	0	4	4	4	4	4	0	0	40
UFD	0	0	8	6	4	2	0	0	0	2	4	6	8	0	0	40
Transfer	2	2	2	2	2	2	2	2	2	2	2	2	2	2	2	30

for 500 ms. The fixation screen was replaced by a randomly selected stimulus for 750 ms. The stimulus was then replaced with a prompt that indicate the response keys ('C-species' (C) or 'M-Species' (M)), which remained on the screen until the participant selected a response. As previous studies (Burleigh & Schoenherr, 2015) revealed that participants quickly reached asymptote, participants received feedback on only 50% of the trials to increase presentation frequency while allowing for learning of the category structure (for a similar method in a categorization task, see Ziori & Dienes, 2008).

During transfer, participants did not receive any feedback. Participants categorized the stimulus (old items from training and new extrapolations or boundary-adjacent items), and then rated its eeriness on a scale of 1 "not at all" to 7 "extremely". After two transfer blocks, participants completed a final block wherein they rated stimulus typicality, on a scale of 1 (highly typical of the category) to 5 (highly atypical of the category). Typicality values were reverse coded for analyses. As we did not want to increase frequency of extrapolation items, thereby affecting eeriness ratings, all participants were presented with affective ratings first followed by typicality ratings.

Results and Discussion

Repeated measures analyses of variance (ANOVA) were conducted after collapsing across response key counter-balancing and category set (e.g., alien or reptile). Adjacent blocks were grouped together (e.g., Block 1 and 2). Analyses included between-subjects measures of Regulatory Focus (Promotion/ Prevention) and Training Frequency (Equal/ Unequal) as well as within-subjects measures of Training Phase (1-4) and stimulus (8). Analyses of transfer stimuli were also collapsed, but included the complete stimulus continuum (15).

Training Categorization Accuracy. With categorization performance, there was a significant main effect of Training Phase, $F(3, 336) = 48.87, MSE = .060, p < .001, \eta_p^2 = .030$, indicating that performance improved over the course of training. We also observed a significant effect of stimulus location, $F(7, 784) = 4.82, MSE = .066, p = .004, \eta_p^2 = .041$, replicating past findings that performance increased monotonically with distance from the category boundary.

Transfer Categorization Accuracy. While the effect of regulatory focus was absent in our analysis of training accuracy, we observed a main effect of regulatory focus in the analysis of transfer categorization accuracy, $F(14, 1302) = 6.93, MSE = .090, p < .001, \eta_p^2 = .70$. A main effect of stimulus was also obtained, $F(1, 93) = 212.48, MSE = .073, p = .010, \eta_p^2 = .069$. Figure 2 indicates transfer accuracy was lowest around the cat-

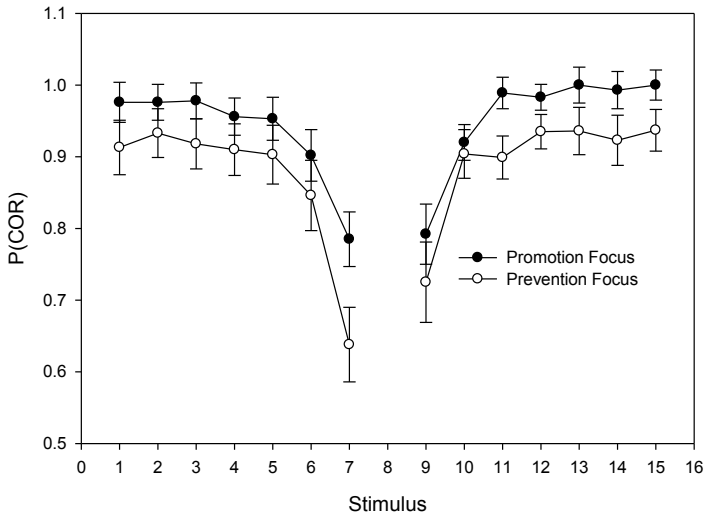

Fig. 2. Transfer block categorization accuracy in equal- and unequal-frequency conditions. Error bars represent standard error of the mean.

egory boundary but increased as a function of distance away from the category boundary. Contrary to NCT, performance in the promotion focus condition ($M = .88, SE = .017$) was generally higher than in the prevention focus condition ($M = .81, SE = .019$) with no stimulus-specific effects evidenced.

Affective and Typicality Ratings. Within affective ratings, there were significant main effects of Training Frequency, $F(1, 109) = 7.51, MSE = 20.51, p = .007, \eta_p^2 = .064$, and Stimulus Location, $F(14, 1526) = 4.26, MSE = 14.14, p = .024, \eta_p^2 = .038$. These findings are inconsistent with NCT. Figure 3 indicates that eeriness was highest for stimuli located at the extremes of the continuum, and did not increase for boundary-adjacent stimuli. Given the assumptions of NCT, differences in affect for stimuli near the boundary in the Unequal Frequency condition would be expected (cf. Burliegh & Schoenherr, 2015). Moreover, Regulatory Focus did not change affective ratings, $F(1, 109) = .153, p = .70$.

With typicality, there was only a significant effect of stimulus location, $F(14, 1484) = 7.13, MSE = 3.11, p < .001, \eta_p^2 = .063$. Figure 3 suggests that participants have knowledge of exemplars that define the category structure: exemplars located at the category boundary were rated least typical, and typicality increased with distance from the boundary. A correlational analaysis revealed that eeriness ratings were neither strongly correlated with accuracy ($r = -.034, p > .05$) nor with typicality ($r = .118, p > .05$), while typicality was negatively correlated with accuracy ($r = -.445, p < .01$).

Conclusions

The results of our experiment support the assertion that instructional manipulations can change regulatory foci and alter response accuracy by changing participant's response threshold. Specifically, we observed that participants performed better in the promotion focus condition (95% correct) relative to the prevention focus condition (avoidance of 5% errors). This suggests that the instructional manipulations changed their response

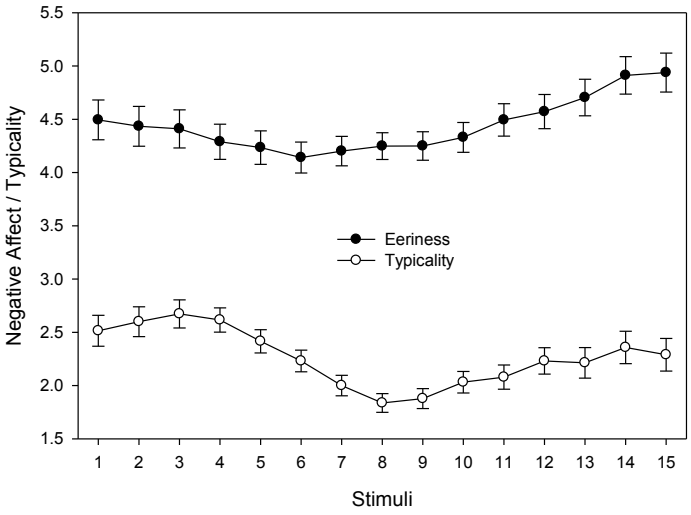

Fig. 3. Transfer block categorization accuracy in equal- and unequal-frequency conditions. Error bars represent standard error of the mean.

threshold. However, unlike the prediction of NCT, we did not observe item-specific effects. Namely, regulatory foci did not affect identification of individual exemplars or ratings of affect or typicality. However, exemplar training frequency altered affective responses, with the greatest negative affect observed for novel extrapolation stimuli. Importantly, these items were also assigned high typicality ratings and were responded to accurately. This suggests that affective ratings and categorical knowledge were dissociable. Consequently, while the Uncanny-Valley-like phenomena (bukimi no tani) appear to exist, general categorization mechanisms offer a more parsimonious explanation.

References

Ashby, F. G., & Gott, R. E. (1988). Decision rules in the perception and categorization of multidimensional stimuli. *Journal of Experimental Psychology: Leaning, Memory, and Cognition,* 14, 33–53.

Blair, M., & Homa, D. L. (2001). Expanding the search for a linear separability constraint on category learning. *Memory & Cognition,* 29,1153–1164.

Bornstein, R. F. (1989). Exposure and affect: overview and meta-analysis of research, 1968-1987. *Psychoogical Bulletin,* 106, 265–289. doi: 10.1037//0033- 2909.106.2.265

Burleigh, T. J., & Schoenherr, J. R. (2015). A reappraisal of the uncanny valley: Categorical perception or frequency-based sensitization? *Frontiers in Psychology,* 5:1488.

Burleigh, T. J., Schoenherr, J. R., and Lacroix, G. L. (2013). Does the uncanny valley exist? an empirical test of the relationship between eeriness and the human likeness of digitally created faces. *Computers and Human Behaviour,* 29, 759–771. doi: 10.1016/j.chb.2012.11.021

Cheetham, M., Suter, P., & Jancke, L. (2014). Perceptual discrimination difficulty and familiarity in the Uncanny Valley: more like a "Happy Valley". *Frontiers in Psychology,* 5:1219.

Förster, J., Marguc, J., & Gillebaart, M. (2010). Novelty categorization theory. *Social*

Psychology and Personality Compass, 4, 736–755. doi:10.1111/j.1751-9004.2010.00289.x

Gillebaart, M., Förster, J., & Rotteveel, M. (2006). Mere exposure revisited: The influence of growth versus security cues on evaluations of novel and familiar stimuli. *Journal of Experimental Psychology: General,* 141, 699–714. doi:10.1037/a0027612

Goldstone, R. L., Kersten, A., & Carvalho, P. F. (2012). Concepts and Categorization. In Weiner, I.B, Healey, A.J., & Proctor, R.W. (Eds.) *Handbook of Psychology,* Volume 4, Experimental Psychology, 2nd Edition (pp. 607–630). New York, NY: Wiley.

Higgins, E. T. (1997). Beyond pleasure and pain. *American Psychologist,* 52, 1280–1300. doi:10.1037/0003-066X.52.12.1280

MacDorman, K. (2005). "Androids as an experimental apparatus: why is there an uncanny valley and can we exploit it?" in Toward Social Mechanisms of Android Science: A CogSci 2005 Workshop (Stresa), 106–118.

Miller, J. L., & Volaitis, L. E. (1989). Effect of speaking rate on the perceptual structure of a phonetic category. *Perception & Psychophysics,* 46, 505–512.

Mori, (1970). Bukimi no tani [The uncanny valley]. *Energy,* 7, 33–35.

Park, J., Shimojo, E., & Shimojo, S. (2010). Roles of familiarity and novelty in visual preference judgments are segregated across object categories. *Proceedings of the National Academy of Science,* 107, 14552–14555., doi:10.1073/pnas.1004374107

Paul, E. J., Boomer, J., Smith, J. D., & Ashby, F. G. (2011). Information-integration category learning and the human uncertainty response. *Memory Cognition,* 39, 536–554.

Reber, R., Winkielman, P., & Schwarz, N. (1998). Effects of perceptual fluency on affective judgments. *Psychological Science,* 9(1), 45–48.

Schoenherr, J. R., & Logan, J. (2013). Subjective awareness during cross-language speech perception: Attending unattended regions of an acoustic continuum. *Proceedings of the 34th Annual Meeting of the Cognitive Science Society,* Berlin, Germany.

Smith, J. D., & Minda, J. P. (1998). Prototypes in the mist: The early epochs of category learning. *Journal of Experimental Psychology: Learning, Memory, and Cognition,* 24, 1411–1436.

Yamada, Y., Kawabe, T., & Ihaya, K. (2013). Categorization difficulty is associated with negative evaluation in the "uncanny valley" phenomenon. *Japanese Psychological Research,* 55(1), 20–32.

Ziori, E., & Dienes, Z. (2008). How does prior knowledge affect implicit and explicit concept learning? *The Quarterly Journal of Experimental Psychology,* 61, 601–624.

THE EFFECT OF FACIAL ATTRACTIVENESS ON FACE PERCEPTION UNDER BINOCULAR RIVALRY

Hidetoshi Kanaya[1], Takeharu Seno[2], Masayoshi Nagai[3], and Takao Sato[3]
[1]*Faculty of Human Informatics, Aichi Shukutoku University, 2-9 Katahira Nagakute-shi Aichi, Japan*
[2]*Faculty of Design, Kyushu University, 4-9-1 Shiobaru Minami-ku Fukuoka, Japan*
[3]*College of Comprehensive Psychology, Ritsumeikan University, 2-150 Iwakura-cho Ibaraki Osaka, Japan*

In the present study, the effect of facial attractiveness on face perception under binocular rivalry was examined. Two male or two female faces, which had different attractiveness, were simultaneously presented on a display and fused by a mirror stereoscope. Ten female participants observed two male faces (male-face group) and the other ten females observed two female faces (female-face group). The participants kept pressing a key corresponding to each face while they were perceiving one of the two for ten seconds. Results showed that, in male-face condition, the more attractive faces were perceived much longer and dominant in perception rather than the less attractive faces. In female-face condition, the less attractive faces were perceived much longer and dominant in perception rather than the more attractive faces. These results suggest that facial attractiveness affects the face perception of the same and opposite sex.

Author Index


FECHNER DAY 2017
IN FUKUOKA
THE 33RD ANNUAL MEETING
OF THE INTERNATIONAL SOCIETY
FOR PSYCHOPHYSICS
22-26 OCTOBER 2017
DEADLINE FOR SYMPOSIUM PROPOSALS:
7 APRIL 2017
ABSTRACT DEADLINE: 5 MAY 2017
DENKI BUILDING
(KYOSOKAN & HONKAN)
FUKUOKA, JAPAN
KEYNOTE SPEAKERS:
ISAMU MOTOYOSHI &
ROBERT HARTSUIKER
MAIL:
fd2017@design.kyushu-u.ac.jp
HP:
http://fechnerday.com/fd2017/
FECHNER DAY 2017
SPONSORED BY
ReCAPS
RESEARCH CENTER FOR APPLIED PERCEPTUAL SCIENCE
KYUSHU UNIVERSITY
ORGANIZING COMMITTEE:
YOSHITAKA NAKAJIMA, KAZUO UEDA, & GERARD B. REMIJN
提供：福岡市